A Comparative Study of the Extraction, Transport and Coordination Chemistry of Novel Monotopic and Ditopic Salen-type Ligands

by

Joshua Craig Hensberg

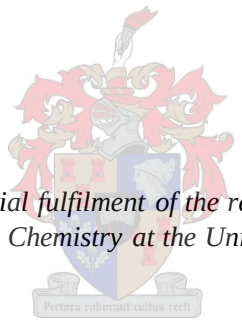

Thesis presented in partial fulfilment of the requirements for the degree Master of Science in Chemistry at the University of Stellenbosch

Supervisor: Dr. R. C. Luckay
Faculty of Science
Department of Chemistry and Polymer Science

March 2017

DECLARATION

By submitting this thesis/dissertation electronically, I declare that the entirety of the work contained therein is my own, original work, that I am the sole author thereof (save to the extent explicitly otherwise stated), that reproduction and publication thereof by Stellenbosch University will not infringe any third party rights and that I have not previously in its entirety or in part submitted it for obtaining any qualification.

March 2017

ACKNOWLEDGEMENTS

Firstly, I would like to express my sincere gratitude to my supervisor, Dr. R.C. Luckay, for accommodating me in his research group, displaying patience and providing necessary encouragement, assistance and guidance throughout this investigation. On this note, I would also like to give thanks to Dr. R. Malgas-Enus, for taking the time to sit down with me and share valuable suggestions so as to approach certain problems which arose during the course of this study. Furthermore, to all research group members of Inorganic Chemistry at Stellenbosch University, acknowledgements must be made for the assistance that was given in any way during progress meetings as well as general conversation.

Secondly, to my parents, to whom I owe all that I am, thank you for heartening me in my every pursuit. I appreciate the support you both have given to me during the course of my academic career. The thoughtful words of wisdom and encouragement which were provided, assisted me in completing this research project.

Thirdly, to my friends and to the rest of my family for sustained words of consolation and assurance especially at the times I was unable to see the light at the end of the tunnel. Jaques Buys and Elaine Barnard, I have been considerably fortunate to have had such good friends and fellow postgraduates to have worked with during these past few years. I am indebted to you both for the sense of comradery we shared during this grueling challenge, which certainly made this project more sufferable. Scott Kriel, Fred Lubbe, Andrew Adie, Robey Beswick and Giles Maybery, I appreciate our respective friendships and the genuine interest you all showed in my work. My honours mentee, Thalia Carstens, I admire your work ethic which kept me motivated and I am grateful for your assistance in refining X-ray data as well as your contribution towards producing **L6** and **L10** which are included in this work. Hezron Ogutu thank you for your presence in the lab, it certainly made it a more pleasant experience. Furthermore, thank you for aiding my project particularly with your help refining crystal structures.

Last but not least, I would like to express thanks to Stellenbosch University, CAF for analytical results, NRF for funding. In addition, I am thankful to all the staff of the Inorganic Chemistry department for all their friendly conversations and their general company which made this investigation more tolerable.

ABSTRACT

This dissertation reports the synthesis and full characterisation of a series of novel monotopic and ditopic Schiff base salen-type ligands. The monotopic and ditopic ligands were assessed in competitive extraction and competitive bulk liquid membrane transport experiments for the recovery of the metal ions; Cu(II), Ni(II), Co(II), Zn(II), Cd(II) and Pb(II). Additionally, the ditopic ligands were assessed in competitive extraction and competitive bulk liquid membrane transport experiments involving anions; Cl^-, NO_3^- and SO_4^{2-}.

Monotopic ligands, **L1**-**L6**, were designed with varying structural modifications focused on affecting the disposition of the donor atoms in these ligands. This was accomplished by reacting two equivalents of 5-tert-butyl-2-hydroxybenzaldehyde with one equivalent of different diamines. **L1**-**L6** were successfully synthesised and fully characterised using ^1H and ^{13}C NMR spectroscopy, FT-IR (ATR) spectroscopy, melting point determination, mass spectrometry, micro-elemental analysis as well as SCD analysis (in all cases except **L5**). Single crystals of two complexes were attained, **Ni[L4-2H]** and **Cu[L6-2H]**, respectively. The solid-state structures of the free ligand and corresponding metal complex were compared and it was observed that ensuing conformational changes are evident upon coordination to the metal ion.

Ditopic ligands **L7**-**L10** were designed with varying structural modifications to the diamine group and to the incorporated dialkylamino methyl pendant arms. They were synthesised by way of a four-step convergent synthesis and fully characterised using a range of analytical techniques including FT-IR (ATR) spectroscopy, ^1H and ^{13}C NMR spectroscopy, mass spectrometry, melting point determination (in the cases of **L7** and **L9)** and elemental analysis.

In the competitive metal ion extraction experiments, all ligands displayed an exceptional selectivity towards Cu(II) over the other metal ions. There was a slight increase in the uptake of Cu(II) by the ditopic ligands in comparison to the corresponding monotopic ligands and was justified by the incorporation of the dialkylaminomethyl groups which promoted their solubility in the organic phase. In the competitive bulk liquid membrane transport studies, all ligands continued their preference for Cu(II) ions. The cation flux rates ($molh^{-1}$) for Cu(II) under the experimental conditions employed, was low despite being transported effectively into the organic membrane

ABSTRACT

phase. This suggested a high formation constant for Cu(II). Ditopic ligands showed a surprising potential for the transport of Zn(II) under the experimental conditions employed. The ditopic ligands presented herein show potential to effectively separate Cu(II) ions from Zn(II) ions.

Lastly, "copper-only" complexes of ditopic ligands **L7**-**L10** were subjected to competitive anion extraction and bulk liquid membrane transport tests with the anions Cl^-, NO_3^- and SO_4^-. In both tests, the ligands showed selectivity in the increasing order: $SO_4^{2-} < Cl^- < NO_3^-$, indicating the prevalence of the Hoffmeister bias.

OPSOMMING

Hierdie werkstuk handel oor die sintese en volle karakterisering van ‘n reeks nuwe monotopiese en ditopiese Schiff basis salen-tipe ligande. Die monotopiese en ditopiese ligande was geevalueer in mededingende ontginning en mededingende vloeistof membraan vervoer eksperimente vir die isolering van metaalione; Cu(II), Ni(II), Zn(II), Co(II), Cd(II) en Pb(II). Die ditopiese ligande was ook geevalueer in mededingende ontginning en mededingende vloeistof membraan vervoer experimente van verskeie anione; Cl^-, NO_3^- en SO_4^{2-}.

Tydens die ontwerp van die monotopiese ligande **L1**-**L6**, word daar ondersoek ingestel oor hoe die skenker atome beinvloed word deur spesifieke strukturele eienskappe. Dit word bewerkstellig deur verskillende diamine groepe te inkorporeer met 5-tersiêre-butyl-2-hydroxybenzaldehyde in ‘n 1:2 mol verhouding. **L1**-**L6** is suksesvol gesintetiseer en ten volle gekarakteriseer met behulp van ^{1}H en ^{13}C-KMR-spektroskopie, FT-IR (ATR) spektroskopie, smeltpunt bepaling, massaspektrometrie, elementele analise asook SCD analise (in alle gevalle behalwe **L5**). Enkelkristalle van twee komplekse was geisoleer, **Ni[L4-2H]** en **Cu[L6-2H]**, onderskeidelik. Die vaste-toestand strukture van die vrye ligand en ooreenstemmende metaal komplekse dui aan dat ‘n konformasie verandering wel plaasvind tydens koördinasie vam die metaalioon aan die onderskeilike ligand.

Die variasie van die oorbrugende diamine groepe geinkorporeer by die monotopiese ligande was weereens gebruik vir die ditopiese ligande **L7**-**L10**, asook die ïnkorporeering van dialkielamino metiel arms. Die ligande is gesintetiseer deur middel van 'n vier-stap konvergente sintese en ten volle gekarakteriseer deur 'n verskeidenheid analitiese tegnieke, insluitende FT-IR (ATR) spektroskopie, ^{1}H en ^{13}C-KMR-spektroskopie, massaspektrometrie, smeltpunt bepaling (in die geval van **L7** en **L9**) en elementele analise.

Na aanleiding van die mededingende metaalioon onttrekking eksperimente, was dit duidelik dat beide reekse ligande 'n uitsonderlike selektiwiteit vir Cu(II) vertoon teenoor die ander metaalione. Daar was 'n effense toename in die opname van Cu(II) vir die ditopiese ligande in vergelyking met die ooreenstemmende monotopiese ligande. Hierdie was geregverdig deur die ïnkorporeering van die dialkielamino metiel groepe wat die oplosbaarheid van die ligande/komplekse in die organiese fase bevorder. Tydens die mededingende vloeistof membraan vervoer

OPSOMMING

studies het beide reekse ligande weereens ‘n voorkeur vir Cu(II) ione getoon. Die katioon vloed tempo ($molh^{-1}$) vir Cu(II) onder die eksperimentele toestande was laag ten spyte van die effektiewe vervoer na die organiese membraan fase. Dit voorspel dat die ligande 'n hoë vorming konstante vir Cu(II) toon. Verbasend genoeg toon die ditopiese ligande potensiaal om Zn(II) ook te vervoer onder die eksperimentele toestande. Dus, die ditopiese ligande bied potensiaal om Cu(II) ione van Zn(II) ione selektief te skei.

Laastens, slegs die Cu(II) komplekse van ditopiese ligande **L7**-**L10** was ondersoek vir die mededingende ontginning en mededingende vloeistof membraan vervoer toetse met die anione Cl^-, NO_3^- en SO_4^{2-}. In beide toetse het die ligande selektiwiteit vir die anione in die toenemende volgorde van $SO_4^{2-} < Cl < NO_3^-$ getoon wat aandui die Hoffmeister bias word volhou.

TABLE OF CONTENTS

A COMPARATIVE STUDY OF THE EXTRACTION, TRANSPORT AND COORDINATION CHEMISTRY OF NOVEL MONOTOPIC AND DITOPIC SALEN-TYPE LIGANDS

TABLE OF CONTENTS

TABLE OF CONTENTS

TABLE OF CONTENTS

TABLE OF CONTENTS

LIST OF FIGURES

CHAPTER 1

CHAPTER 2

LIST OF FIGURES

CHAPTER 3

CHAPTER 4

LIST OF SCHEMES

CHAPTER 1

CHAPTER 2

CHAPTER 3

LIST OF TABLES

CHAPTER 2

CHAPTER 3

LIST OF TABLES

CHAPTER 4

LIST OF ABBREVIATIONS & SYMBOLS

[M]	concentration of metals
[L]	concentration of ligand
ΔG°	change in Gibbs free energy
ΔH°	enthalpy change of reaction
ΔS°	entropy change of reaction
°C	degrees celsius
δ	chemical shift
Å	Angstrom
Anal.	analytically
Ar	aryl
ATR	Attenuated total reflectance
aq.	aqueous
cm^{-1}	wavenumber
cm^3	cubic centimetres
conc.	concentrated
$CDCl_3$	deuterated chloroform
CFSE	Crystal Field Stabilisation Energy
d	doublet
DCM	dichloromethane
dd	doublet of doublets
ddd	doublet of doublet of doublets
dt	doublet of triplets
EA	elemental analysis
eq.	equivalents
ESI-MS	Electrospray Ionisation Mass Spectrometry
FT-IR	Fourier transform infrared
g	grams

h	hours
HBD	H-bond-donating
HMPA	hexamethylphosphoramide
HSAB	Hard-soft acid-base
Hz	hertz
ICP	Inductively Coupled Plasma
J	coupling constant
J (mol/h)	cation flux rate
K	equilibrium constant
L	litres
m	multiplet
M	molar concentration
mbar	millibar
mg	milligrams
min	minutes
m/z	mass-to-charge ratio
mL	millilitres
mol	moles
mmol	millimoles
MHz	megahertz
M_r	molar mass
nm	nanometres
NMR	Nuclear Magnetic Resonance
OAc	acetate
OES	Optical Emission Spectroscopy
org.	organic
p	pentet

LIST OF ABBREVIATIONS & SYMBOLS

ppm	parts per million
q	quartet
R	ideal gas constant
rpm	revolutions per minute
rt	room temperature
s	singlet
SCD	Single-crystal X-ray Diffraction
T	temperature
t	triplet
t	time
TMS	tetramethylsilane
v	frequency

CHAPTER 1: INTRODUCTION AND OBJECTIVES

1.1. Extractive metallurgy

1.1.1. Introduction

Extractive metallurgy encompasses a broad range of mechanical and chemical processes, some of which date back several thousand years.[1] The term *extractive metallurgy* refers to the process by which a specific element contained in an ore is effectively separated from other components present in the ore to ultimately yield the desired element, usually a metal, in high purity.[2]

Most metallic elements occur naturally as minerals or ores, which are compounds that result from a reaction between metallic and non-metallic atoms.[3] Most copper, zinc and lead ores exist as sulfides while iron and aluminium are generally present in oxide ores.[4] The extraction of metals from their respective ores requires energy to separate the metal from sulfur or oxygen. This energy can be supplied in the form of heat and was realised in ancient times when people discovered melting of ores to acquire metals.[4, 5] This subsequently led to the first of three typical approaches practiced in extractive metallurgy termed *pyrometallurgy*. Pyrometallurgy employs older technology to attain metals from ores and accomplishes this by chemical reaction at high temperatures in fuel-fired furnaces. The technique may involve melting the ores to extract the metals they contain (smelting) and/or additional purification through roasting which involves gas-solid reactions at elevated temperatures. Although this technology is useful, it is a serious source of air pollution.

The use of pyrometallurgy is most applicable for the reduction of high-grade oxide ores. However, owing to the absence of other technology at the time, thermal methods were similarly applied for the treatment of massive sulfides.[6] Although the sulfides did not produce a metal directly on smelting, as in the case of copper and lead sulfides, roasting was devised to expose the ore to air or oxygen at elevated temperatures to transform the sulfide to oxide which was then reduced to metal.

Other more modern methods of extraction and refinement include hydrometallurgy and more recently, electrometallurgy. *Hydrometallurgy* “involves the processing of an ore by the dissolution, separation, purification, and precipitation of the dissolved metal by the use of aqueous solutions”.[1] Since the discovery of

the cyanidation and Bayer's processes' in 1887[5], this practice has become increasingly popular over pyrometallurgical methodologies due to further developments being made in the field and because of its focus on green chemistry.

The use of electric current in extractive metallurgy became possible when the dynamo was invented in the nineteenth century which eliminated the need for bulky and expensive batteries. Hence it was used immediately in the refining of copper needed for the growing electrical industry. This established the extractive metallurgical practice known as electrometallurgy. *Electrometallurgy* is generally employed in the processes that purify extracted metal (refining) through the application of large amounts of electrical energy.

Refining of metals, like the extraction of metals from ores, includes many ancient practices and more modern technology. Extremely high-purity metals are habitually too soft for any sort of structural application. A prime example is gold, which at a purity of 99.999+ % is not useful for any structural purpose even for use as pins or chains in jewellery. On the other hand, numerous modern materials require excellent refining techniques. Copper, used for its conductivity in electric wires and silicon (as well as germanium and other metalloids), used in the semiconductor industry, must be generated at strictly monitored purity levels equal to and not more than one impurity atom for every million atoms of the pure element. This extremely high-purity is required when structural strength is less essential than other properties such as electrical conductivity.

The introduction of new hydrometallurgical techniques at the end of the nineteenth century has gradually displaced some of the polluting or energy-intensive pyrometallurgical processes. With growing environmental concerns in the modern era, emphasis has been placed on developing greener extractive metallurgical methods. For this reason, research has been directed towards hydrometallurgical processes to separate metals from their ores which embrace greener technology to accomplish this.

1.2. Hydrometallurgy

1.2.1. Introduction

Hydrometallurgy entails separating the desired metal from other metals contained in an ore while in aqueous solutions. This is achieved by exploiting solubility differences and/or electrochemical properties of the

respective metals. The foundation of modern hydrometallurgy dates back to 1887 when two vital processes were developed. The first, the cyanidation process for treating gold and silver ores, and the second, the Bayer process for refining alumina.[5, 7, 8]

1.2.1.1. Cyanidation Process

One of the reasons for the high value placed on gold is its resistance to attack by most chemical reagents. One exception is cyanide, or more specifically, a cyanide-containing solution, which dissolves the precious metal.[9] The earliest, well-documented work describing the action of cyanide solution on metallic gold dates back as early as 1783, to the Swedish chemist, Scheele.

In 1846, Elsner in Germany studied this phenomenon further and found that atmospheric oxygen played a crucial role in the dissolution process. The application of this knowledge to extract gold from its ores was proposed and patented much later by the Scottish chemist John Stewart MacArthur in 1887, and in 1888, effectively established the current cyanidation process ie: the employment of cyanide in dissolution and precipitation using zinc.

The first commercial-scale cyanidation plant began operating at the Crown Mine in New Zealand in 1889, and by 1904 cyanidation processes were also in place in South Africa, Australia, United States, Mexico and France. Therefore, by the turn of the century, the use of cyanide to extract gold from low-grade ores was a fully established metallurgical technology. The impact of this process on hydrometallurgy has been tremendous.

1.2.1.2. Bayer Process

The second major hydrometallurgical process of this era was the process invented by Karl Josef Bayer in 1887 for the preparation of pure Al_2O_3 (alumina) and is known as the Bayer process.[7] This process was concerned with leaching bauxite with sodium hydroxide solution at temperatures above boiling point in a pressure reactor. After separating the insoluble material, the pure solution was then seeded to precipitate pure crystalline aluminium hydroxide, which was filtered, washed, dried, and underwent calcination (thermal treatment process in the absence or limited supply of oxygen) to yield the alumina product suitable for application in the electrolytic reduction cell invented two years later.

The process began to increase in popularity and importance within the discipline of extractive metallurgy and still remains practically unchanged. Furthermore, it is now responsible for most of the world's alumina supply as an intermediate step in aluminium production.

1.2.2. Developments within hydrometallurgy

At the beginning of the 1900s, numerous leaching and metal recovery processes were proposed. Some of these proposals were put into practice, while others were not applied for about fifty years. Moreover, some never developed beyond a preliminary/trial plant.

Between the years 1904 and 1920, Ipatieff, a Russian scientist, treated hydrogen under pressure to precipitate metals from solution. However, it was only until 1953 before this technique was practiced commercially. This was due to the high cost of hydrogen gas before that time. It only became inexpensive once the reforming processes for petroleum gases had been developed.

World War I brought with it a high demand for zinc for the production of brass (an alloy of copper and zinc) to be used in the manufacturing of cartridges. Zinc, for this intention, was previously acquired through the distillation of commercially available metal which was supplied by Belgium and Germany, who in turn, were supplied with the ore by Australia. This predicament motivated industry to introduce cheaper and more efficient methodologies to obtain zinc. This led to the innovation of the process for electrolytic zinc. An additional outcome of this was the investigation into, and implementation of leaching of zinc oxide ores using sulfuric acid as a leaching agent. Cadmium progressively emerged as a valuable by-product of this process.

During the 1940s, there was an intensive exploration into methods aimed at the extraction of uranium from their ores. This exploration was accelerated by the Manhattan project, a United States program aimed at creating an atomic bomb. A variety of new techniques for metal recovery were implemented on a large scale as a result. These techniques include the use of Na_2CO_3 as a leaching agent, ion exchange, solvent extraction and numerous methods of metal precipitation from aqueous solution. Furthermore, the demand for uranium drove industry to manufacture a large number of synthetic resins for application as ion exchangers. Similarly, a wide variety of organic solvents were synthesised for use as extractants for the preparation of uranium.

In the 1950s it was acknowledged that hydrometallurgy could overcome the pollution issues arising in smelters through the production of sulfuric acid using the sulfur oxides derived from smelting.[9, 10] This led to zinc metal production becoming an entirely hydrometallurgical operation.[11] Furthermore, developments were made in the isolation of rare earth metals, where separation using ion exchange resins replaced the tedious fractional crystallisation methods which were previously being employed. Subsequently, solvent extraction processes replaced ion exchange and industries began using mixer-settlers to produce high-purity precious metals.

During the 1960s, the function of bacteria in leaching was recognised and the wide-spread use of heap and *in situ* leaching for the extraction of copper was employed on a large scale. The same technique was later adopted for leaching low-grade uranium and gold ores. During the same period, organic solvents (mainly oximes) were applied for the extraction of copper. In the 1980s, the hydrometallurgical processes pertaining to gold conquered the scene. The use of activated charcoal for gold adsorption as well as the aqueous oxidation of gold refractory ores was industrialised.

1.2.3. Mineral processing in base metal recovery

1.2.3.1. Introduction

In terms of recovery from primary sources (metal ores), the processing steps prior to the isolation of a pure metal are often broken up into the unit operations; mineral processing, leaching, separation and concentration, reduction, and when a high-purity product is required, additionally refining.[2, 12, 13] These major steps for a typical hydrometallurgical flowsheet can be seen in Fig. 1.1 below:

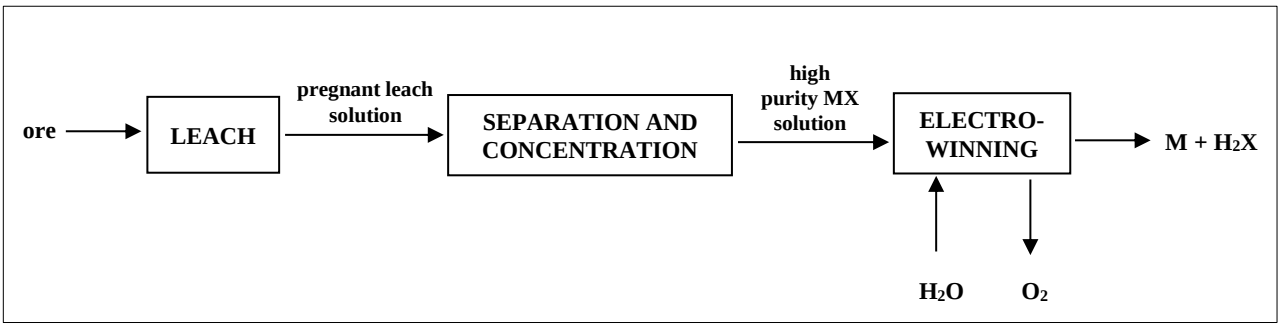

FIGURE 1.1 The key steps in a hydrometallurgical flow sheet for recovery of base metals using metal sequestering agents

1.2.3.2. Mineral processing

The history of mineral processing dates back to the origin of mankind. Severing stones, sharpening flint stones and categorisation methods were one of the first mineral processing activities practiced by humans. Extensive development has been made to the division of mineral processing and its physicochemical foundation over the last century. Processing of valuable minerals has established a branch of science and technology which is in close cooperation with mining and chemical industries as well as other branches of industry.[14]

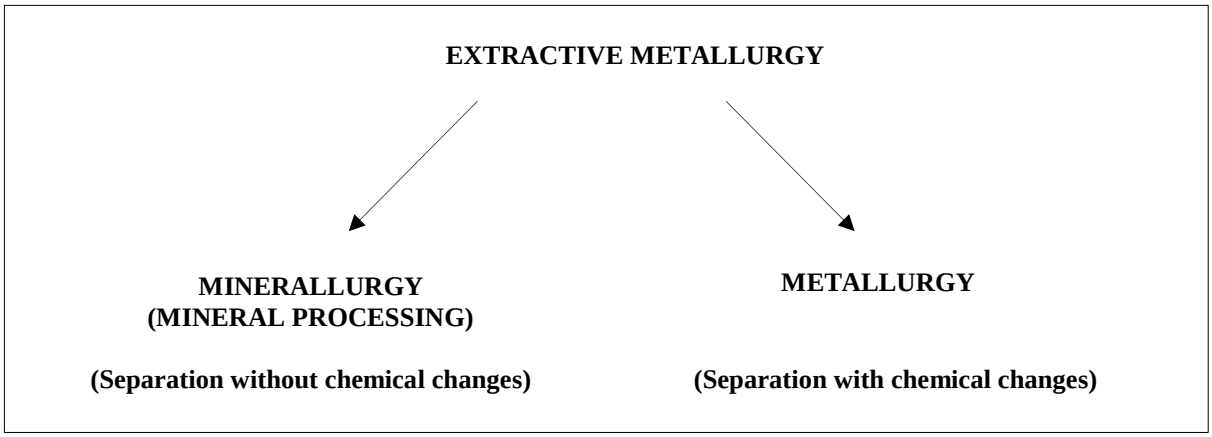

FIGURE 1.2 Schematic diagram showing the disciplines of extractive metallurgy

Mineral processing, together with metallurgy, constitutes the divisions within the discipline of extractive metallurgy (Fig. 1.2). Since natural mineral deposits are mostly heterogeneous mixtures of solid materials, they require physical processes such as crushing and grinding to liberate the minerals containing the metal of value. Such processing methodologies often represent a significant fraction of the total capital and energy costs of metal recovery. One of the potential advantages of hydrometallurgical pathways for metal recovery is that it is sometimes possible to conduct heap leaching on ores which have not had to be physically processed through milling or crushing, for example in the recovery of copper from oxidic or transition ores.

The separation of crushed solid components is typically achieved by exploiting differences in their respective physical properties. Of the numerous techniques to obtain ore “concentrates,” those of froth flotation and agglomeration take advantage of differences in surface activities, which in many instances, seem to involve the formation of complexes at the surface of the mineral particles. Separation by means of froth flotation (Fig 1.3) is dependent on the conversion of hydrophilic (water-wetted) solids to hydrophobic (non-wetted) solids

which are carried in an oil-based froth leaving behind the undesired materials, also known as gangue (an aqueous slurry), which is drained from the bottom of the separator. The selective conversion of the ore particles to hydrophobic material involves the adsorption of chemical species which are commonly referred to as "collectors".

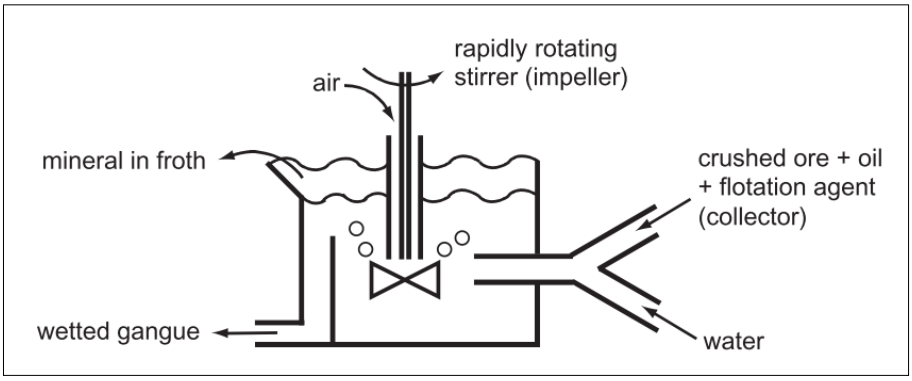

FIGURE 1.3 Schematic representation of a froth flotation separator

1.2.3.3. Leaching

Hydrometallurgical extraction is often referred to as *leaching*, which constitutes the second step in a typical hydrometallurgical flowsheet subsequent to mineral processing. A variety of leaching processes exist with the intent of converting the metal contained in an ore to a water-soluble metal salt using an appropriate leaching agent (also referred to as a lixiviant).[1] Ore particles house natural pores through which these leaching agents can slowly penetrate. This delivers aqueous solutions of metal cations for separation and concentration. It has been found in practice, that chloride leaching is preferred for precious metal refining[15], whilst for f-block elements, recovery is also commonly achieved from nitrate solutions.

The main modes of leaching are *in situ*, dump, heap, atmospheric pressure, tank, concentrate and pressure leaching. All serve the purpose of extracting as much of the desired metal from the mineral deposit as possible. Often, leaching operations take advantage of oxygen as an oxidant. Even though this is the case, many leaching processes are hindered by the delivery of oxygen into their systems. Leaching under ambient conditions in heaps and dumps is generally less expensive in contrast to the other leaching techniques, and is accelerated by bacteria. This leaching strategy is performed using particles with varying sizes that are placed in piles and the

rate of this mode of leaching is often influenced significantly by the permeability of the leaching agent. *In situ* and pressure leaching, on the other hand, are typically accelerated by the improved activity of oxygen at higher pressures.

Hydrometallurgical extraction is only achievable under appropriate solution conditions and the circumstances that are needed for leaching to occur are determined by means of thermodynamics. Consequently, phase diagrams are commonly employed to ascertain the solution environment that will be crucial for successful leaching procedures.

1.2.3.4. Separation and concentration

Since mineral deposits or ores comprise of a mixture of metals, after leaching, an aqueous solution containing a mixture of metals usually results. The next step in accordance with a typical hydrometallurgical flowsheet is to separate the desired metal from the other metals present in the leach solution. Once this is achieved, the desired metal can be concentrated into a separate aqueous solution resulting in a pure solution of the desired metal. This is a prerequisite for effective electrowinning downstream. The most convenient technology to achieve the separation and concentration of metals from such aqueous streams is solvent extraction using organic extractants or selective chelating agents. Such processes can operate continuously and on large scales.[1]

Liquid-liquid or solvent extraction is a common process for selectively concentrating metals. The chemical mechanisms within solvent extraction pertaining to metal extraction are discussed later in this chapter (**1.3. Coordination chemistry of metal solvent extraction**). The technique as applied to metal extraction is performed using an organic extractant which is dissolved in an organic phase. The organic phase is brought into contact with an aqueous phase containing the dissolved metals or metal ion complexes. For this reason, it is called *liquid-liquid extraction* as two immiscible liquids are used; these include the organic and aqueous phase. There is, however, some loss of organic phase during the process, but this is usually only a minuscule amount (less than 15ppm).[16]

The organic phase contains some kind of extractant or extractants as well as a diluent. The role of the diluent is to effectively dilute the extractant and usually includes paraffin, alkyl aromatics or various other water-immiscible solvents. Diluents are necessary to facilitate the pumping, processing, and settling of the extractant

species, which is often viscous and challenging to deal with in the absence of a diluent. Furthermore, the diluent also aids in the effective distribution of the extractant within organic phase droplets and promotes the presence of extractant at the liquid-liquid interface.

Solvent extraction loading involves thorough mixing of organic and aqueous phases during which metal ions are selectively extracted into the organic medium. This process is executed using mixers which assist in dispersing the organic phase within the aqueous phase in the form of small droplets. These small droplets improve extraction kinetics. A schematic representation of a solvent extraction system is exemplified in Fig. 1.4.

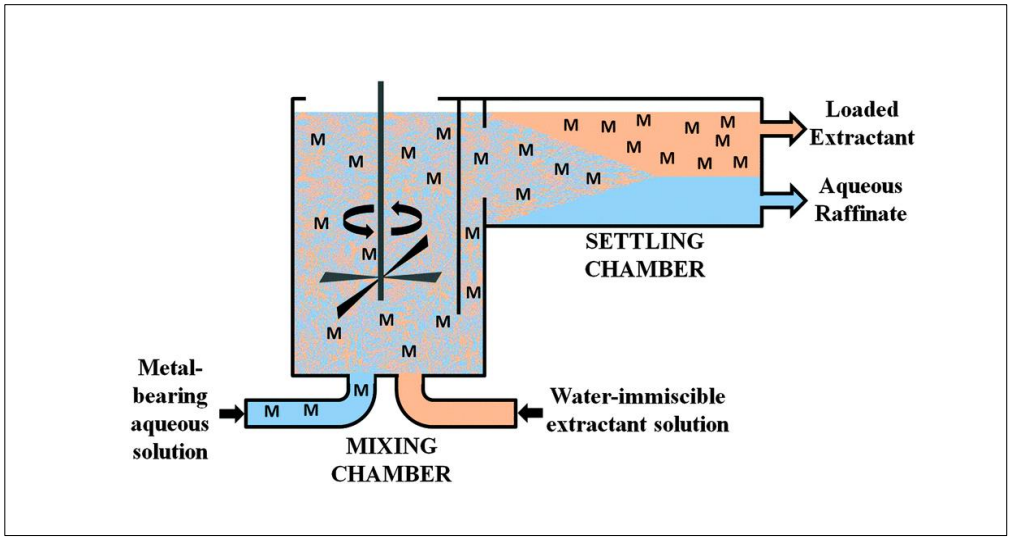

FIGURE 1.4 Schematic diagram of a solvent extraction mixer and settler in the loading stage

The mixing stage is interfaced with a settling stage as illustrated in Fig 1.4. The settling stage allows for the phase disengagement (separation of phases). After loading, the organic phase is scrubbed to get rid of undesired metal ions. The loaded organic phase is then stripped into a separate aqueous solution.

The aqueous phase often requires some conditioning. These conditioning steps often entail the application of refining processes to remove particulate matter and residual solvent, when necessary. Additional conditioning includes the removal of crud, which is typically comprised of a mixture of aqueous, organic, and solid matter. Crud removal can develop into a crucial maintenance issue and must therefore be strictly addressed.

1.2.3.5. Electrowinning & electrorefining

Electrometallurgy typically entails the employment of electricity to refine metal values. In essence, an electric current is used to bring about chemical changes that assist in the processes of extraction (electrowinning) or purification (electrorefining) of the desired metal.[17] There are alternative names for each of these techniques; electrowinning is also called electrolytic extraction, while electrorefining is also referred to as electrolytic refining. Both serve the purpose of purifying metals to an extreme degree. As mentioned previously, some metals are required to be of high purity in order to carry out their chosen application, a major example of this is the use of pure copper for its high conductivity. These processes are practiced extensively in the metal industry and make up the last unit operation in a typical hydrometallurgical flowsheet.

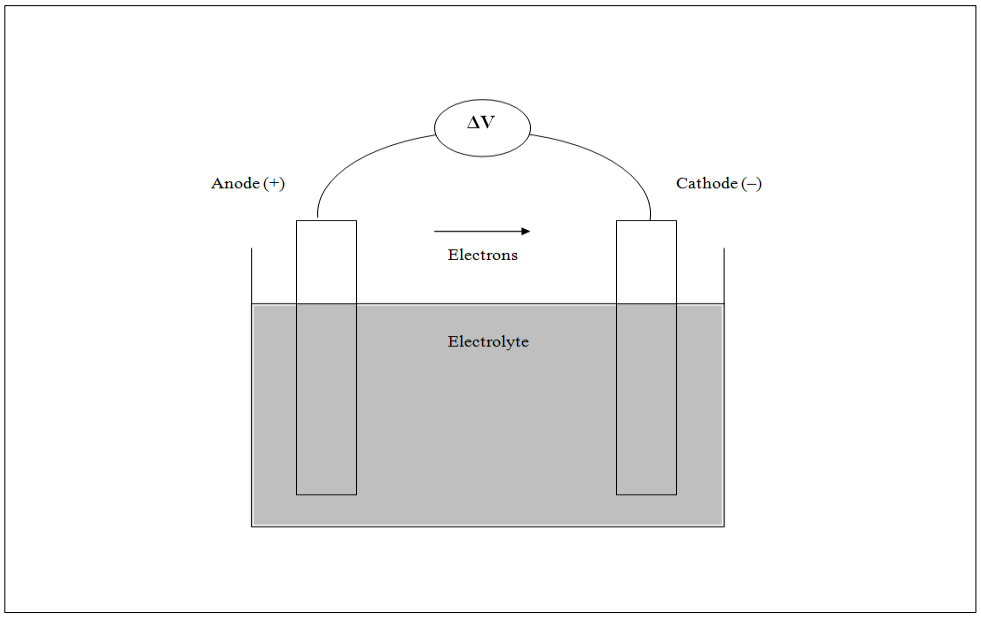

FIGURE 1.5 A simplistic diagram of a typical electrolytic process[9]

During the electrowinning process depicted in Fig 1.5, a potential difference is applied across two electrodes, an inert positive anode and a negative cathode submerged in an electrolyte solution which contains the target metal ions. This solution, which is usually the acidic metal salt solution obtained from stripping, allows for the flow of electrons, via ions, from the cathode to the anode to maintain charge neutrality within the system. The metal ions in the solution are reduced at the cathode resulting in the deposition of the desired metal onto the cathode. The associated anions (usually sulfate) and/or water molecules are usually oxidised at the anode

producing sulfuric acid and/or oxygen, respectively. Electrowinning is not a viable recovery method for all metals. While the process works effectively for metals with high electro-potentials such as gold, silver, copper and zinc, it does not work as effectively on others such as chromium and nickel.

Electrorefining is usually an additional process with the aim of achieving greater metal purity and utilises the desired metal of intermediate purity (95-99.5 %) as the anode. In this process, the metal anode is oxidised, delivering the desired metal ions into an acidic electrolyte solution which are then reduced and deposited onto the cathode. Electrorefining consumes a fraction of the energy needed for electrowinning because the required cell voltage is lower.

These two techniques are currently the most economical and effective means of purifying non-ferrous metals in aqueous solutions derived from hydrometallurgical operations, and together, they play a principal role in the process of metal recovery.

1.2.3.6. Role of coordination chemistry in base metal recovery

The extensive range of technologies applied in hydrometallurgy is to some extent a consequence of the variety of challenges presented by the separation and concentration operations. This problem needs to account for precious metals which are often present at trace levels (< 10^{-3} %) in natural deposits. Moreover, it needs to address the more abundant metals such as aluminium and iron, which can approach up to half the metal content. The base metals fall between these extremes; production of 1 tonne of electrical grade copper typically requires movement of 800 tonnes of rock[1] (Fig. 1.6).

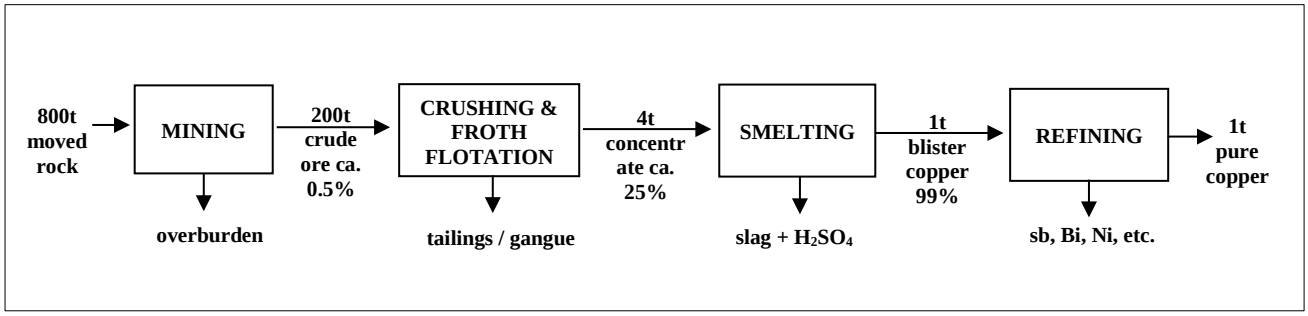

FIGURE 1.6 Schematic diagram of the quantity of pure copper derived from its respective ore[1]

In the broadest sense, coordination chemistry is involved in almost all of the steps prior to the isolation of a pure metal because the physical properties and relative stabilities of metal compounds relate to the nature and disposition of ligands in the metal coordination spheres. This applies both to pyrometallurgy and hydrometallurgy.

One of the most imperative roles of coordination chemistry in hydrometallurgical processes is to bring about the effective and efficient separation and concentration of the target metal. The design of metal extractants with the necessary 'strength' and selectivity to meet the requirements of the front-end of the flowsheet, leaching, and the back-end, reduction to generate pure metal (see Fig 1.6), presents challenging targets for the coordination chemist.

1.3. Coordination chemistry of metal solvent extraction

1.3.1. Introduction

Solvent extraction provides a very efficient way to achieve *separation* and *concentration* in extractive hydrometallurgy.[18] It consists of contacting an organic phase containing an extractant or chelating agent, with an aqueous phase containing the metal of interest. The extractant chemically reacts with the metal to form an organic-metal complex that is soluble in the organic phase. Impurities normally do not react with the extractant and remain in the aqueous phase. The organic phase, containing the organic-metal complex, is separated from the aqueous phase. The metal is recovered and concentrated into another aqueous phase by reversing the chemical reaction.[18]

Solvent extraction was first applied to higher value metals, but now due to the availability of new extractants with improved selectivity, faster kinetics and phase disengagement times, and recent developments in efficient equipment with less area and reagent inventory, the technology is now applicable to lower value metals.

The past decade has witnessed unprecedented growth in the development and implementation of solvent extraction technology in the extractive metallurgy of nickel and cobalt.[19] Solvent extraction is proving to be a powerful tool, opening new opportunities for simpler, more cost-efficient and environmentally sound metal

refining processes. To improve on current technology, the design of ligands or extractants is usually steered towards generating stable metal complexes.

1.3.2. Stability of metal complexes

1.3.2.1. Introduction

The chemistry of metal ions in solution is, in essence, the chemistry of their respective complexes. Transition metal ions, in particular, form many stable complexes. Some of the factors that favour the formation of a metal complex includes;

- Small and highly charged metal ions possessing suitable vacant orbitals of the correct geometry and sufficient energy.
- The acquisition of a noble gas electron configuration.
- The attainment of a structure of high symmetry and a high crystal field splitting energy (CFSE).

1.3.2.2. Irving-Williams series

In 1953, Harry Irving and Robert Williams postulated a spectrochemical series indicating the relative stabilities of metal complexes formed by metal cations of the first row of transition metals depicted in the periodic table. It showed that for the high-spin divalent ions of the first-row transition metals, the stability of complexes formed with these cations increase across the period to a maximum stability at copper:

$$Mn(II) < Fe(II) < Co(II) < Ni(II) < Cu(II) > Zn(II)$$ [20]

There are three main reasons which have been proposed which are generally used to account for the order of the relative stabilities exemplified by the above series. The first explanation concerns itself with the ionic radius of the metal ion which is expected to decrease regularly across the period from Mn(II) to Zn(II). This is the typical periodic trend and would account for the general increase in stability of complexes formed with these divalent metal ions. If the increase were smooth, then it alone would give the stability sequence Mn < Fe < Co < Ni < Cu < Zn and generate the Irving-Williams order in all but the last step. The second explanation

makes use of crystal field theory, where the Crystal Field Stabilisation Energy (CFSE) justifies the increase in stability from Mn(II) (which has a CFSE = 0) to a maximum at Ni(II) and back to a minimum at zero for Zn(II). The final explanation elucidates that although the CFSE of Cu(II) is less than that of Ni(II), octahedral Cu(II) complexes are subject to the Jahn-Teller effect, which affords octahedral Cu(II) complexes additional stability.

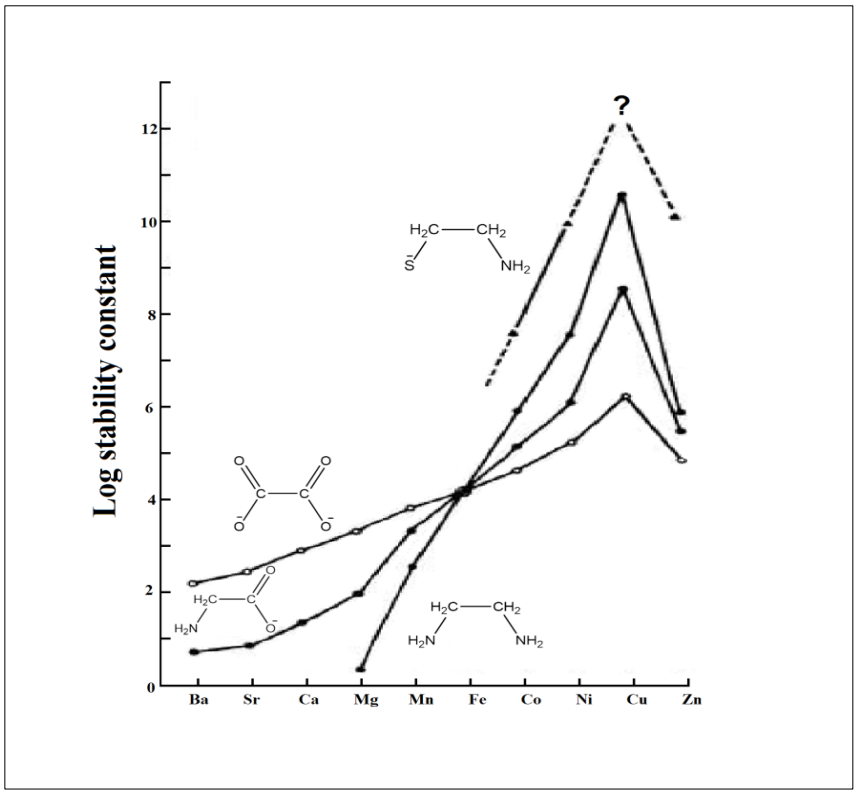

FIGURE 1.7 The Irving-Williams effect: The stability increases in the series Mn-Cu and decreases with Zn[20]

1.3.2.3. Hard-soft-acid-base (HSAB) principle

In 1963, Ralph Pearson introduced the hard-soft-acid-base (HSAB) principle.[21] This very simple concept was used to rationalise a large collection of chemical data. Using two Lewis acids of different properties as references, Pearson and co-workers tested various bases to identify which they preferred to bind to CH_3Hg^+ or H^+. The group compiled tables from their results and classed them based on their affinity for either the methylmercury species or the proton. Those which preferred to bind to methylmercury were considered soft bases and those which preferred to bind to the proton were classed as hard bases. An important feature the

group noticed was that bases in which the donor atom is N, O, or F prefer to coordinate to the proton. While bases in which the donor atom is P, S, I, Br, Cl, or C prefer to coordinate to the methyl mercury. From this information, they recognised that the donor atoms in the first group (preferring binding to the H^+) were highly electronegative, of low polarisability, and difficult to oxidise. They termed this collection of bases, comprising these donor atoms, "hard" bases making reference to the fact that they hold onto their electrons tightly. The donor atoms in the second group (preferring to bind to CH_3Hg^+) were of low electronegativity, of high polarisability, and easy to oxidise. They termed this group of bases "soft", to effectively describe the 'looseness' by which these donor atoms hold onto their valence electrons. Owing to this discovery, it is now viable to classify every possible base into one of three categories, hard, soft, or borderline. Fig. 1.8 and Fig. 1.9 below illustrate this categorisation by Pearson and co-workers.[21, 22, 23]

Hard	Soft
H_2O, OH^-, F^-	R_2S, RSH, RS^-
$CH_3CO_2^-$, PO_4^{3-}, SO_4^{2-}	I^-, SCN^-, $S_2O_3^{2-}$
Cl^-, CO_3^{2-}, ClO_4^-, NO_3^-	R_3P, R_3As, $(RO)_3P$
ROH, RO^-, R_2O	CN^-, RNC, CO
NH_3, RNH_2, N_2H_4	C_2H_4, C_6H_6
	H^-, R^-
Borderline	
$C_6H_5NH_2$, C_5H_5N, N_3^-, Br^-, NO_2^-, SO_3^{2-}, N_2	

FIGURE 1.8 Classification of hard-soft bases

Class (a)/Hard	Class (b)/Soft
H^+, Li^+, Na^+, K^+	Cu^+, Ag^+, Au^+, Tl^+, Hg^+, Cs^+
Be^{2+}, Mg^{2+}, Ca^{2+}, Sr^{2+}, Sn^{2+}	Pd^{2+}, Cd^{2+}, Pt^{2+}, Hg^{2+}
Al^{3+}, Se^{3+}, Ga^{3+}, In^{3+}, La^{3+}	CH_3Hg^+
Cr^{3+}, Co^{3+}, Fe^{3+}, As^{3+}, Ir^{3+}	Tl^{3+}, $Tl(CH_3)_3$, RH_3
Si^{4+}, Ti^{4+}, Zr^{4+}, Th^{4+}, Pu^{4+}, VO^{2+}	RS^+, RSe^+, RTe^+
UO_2^{2+}, $(CH_3)_2Sn^{2+}$	I^+, Br^+, HO^+, RO^+
$BeMe_2$, BF_3, BCl_3, $B(OR)_3$	I_2, Br_2, INC, etc.
$Al(CH_3)_3$, $Ga(CH_3)_3$, $In(CH_3)_3$	Trinitrobenzene, etc.
RPO_2^+,$ROPO_2^+$	Chloranil, quinones, etc.
RSO_2^+, $ROSO_2^+$, SO_3	Tetracyanoethylene, etc.
I^{7+}, I^{5+}, Cl^{7+}	O, Cl, Br, I, R_3C
R_3C^+, RCO^+, CO_2, NC^+	M^0 (metal atoms)
	Bulk metals
HX (hydrogen-bonding molelcules)	
Borderline	
Fe^{2+}, Co^{2+}, Ni^{2+}, Cu^{2+}, Zn^{2+}, Pb^{2+}	
$B(CH_3)_3$, SO_2, NO^+	

FIGURE 1.9 Classification of hard-soft Lewis acids

Pearson's principle regarding the HSAB concept indicates that hard-hard and soft-soft interactions are more likely to occur in comparison to hard-soft interactions. In other words, hard acids prefer to bind to hard bases and soft acids prefer to bind to soft bases. The rule is a concise statement which sums up the experimental information used to compile the tables of these acids and bases. It is not to be regarded as a theory or a hypothesis. Nevertheless, it is a useful tool enabling one to predict favoured interactions between Lewis acids and bases and rationalise the stability of metal complexes.

1.3.2.4. The chelate effect

There are a number of complexes that exist in which a ligand occupies more than one coordination position. In other words, more than one atom in a particular ligand is bonded to the central metal atom. For example, ethylenediamine produces a chelate complex (Scheme 1.1) in the presence of a metal ion. In this complex, the ethylenediamine molecule is coordinated to the metal ion in two separate places. For this reason, ethylenediamine is called a bidentate ligand. As a result, a ring structure is generated (in this case a five-membered ring) and such ring structures are referred to as chelates. Chelating complexes have a greater stability over similar complexes formed with unidentate ligands (Scheme 1.2). This additional stability is termed the chelate effect.[24, 25]

SCHEME 1.1 Metal complex formation with bidentate ethylenediamine ligand

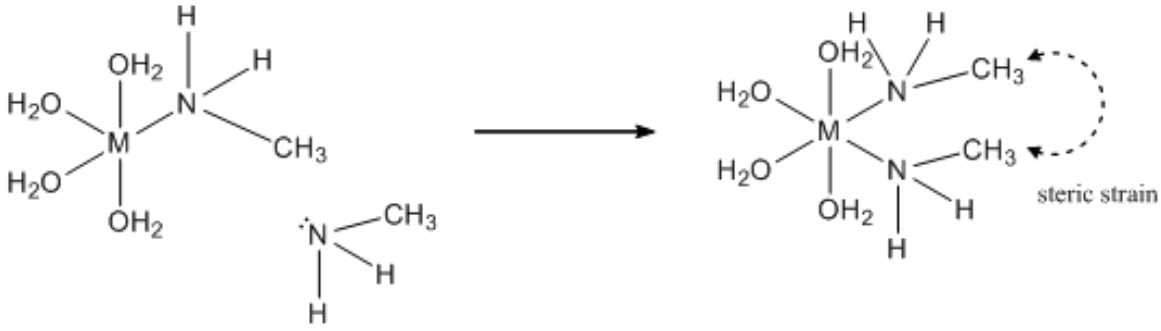

SCHEME 1.2 Metal complex formation with unidentate methylamine ligand

The enhanced stability of chelating complexes can be justified in terms of effective concentrations and entropy considerations.[25, 26] The first explanation is illustrated by comparing Scheme 1.1 and Scheme 1.2. As seen in Scheme 1.1, the second nitrogen is held in close proximity to the metal by the ethyl backbone of the bidentate ligand, allowing the second bond to form easily. However, in the case of the monodentate analogue (Scheme 1.2), the second nitrogen species must remain in motion until it comes within close proximity of a metal to initiate bonding hence it is less likely to form the second bond with the metal center. Furthermore, there is less steric strain in the chelate complex in comparison to that which forms with the monodentate analogues.

The second explanation for the chelate effect is the role of entropy. As seen in Scheme 1.3, for the formation of the chelate complex, there is a change in the number of particles (two particles produce three particles) and for the monodentate analogue, there is no change in the number of particles. So for the complex illustrated in Scheme 1.4, there is no entropy change, whereas the chelate complex (Scheme 1.3) shows a positive change in entropy.

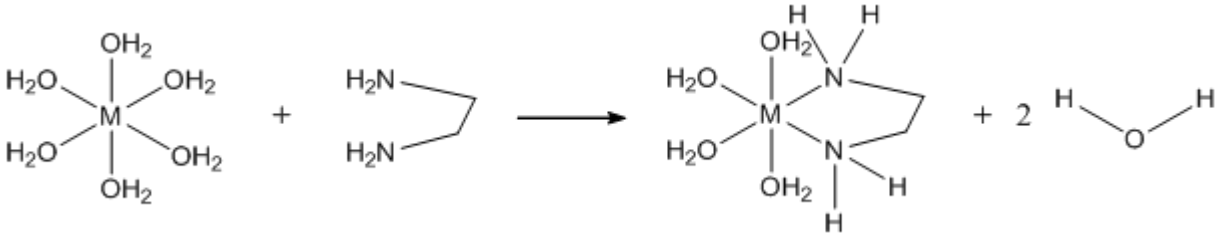

SCHEME 1.3 Chelate ring formation displacing two water molecules (increase in entropy term)

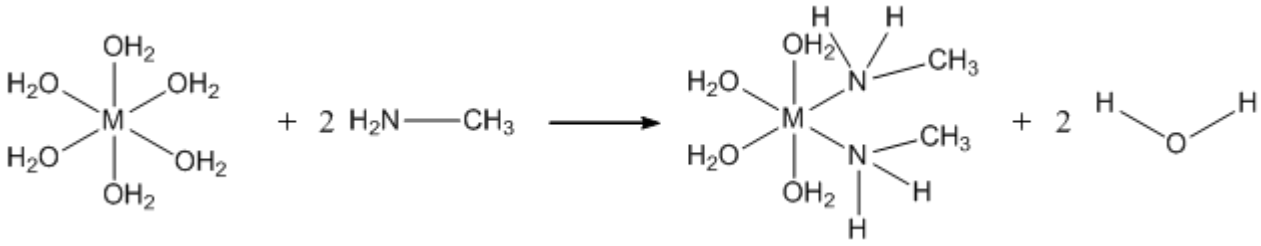

SCHEME 1.4 Substitution of water molecules by monodentate methylamine ligands (no change in entropy)

The larger the number of particles distributed randomly, the higher the entropy of the reaction. According to the Gibbs free energy equation (Eq. 1.1):

$$\Delta G^0 = \Delta H^0 - T\Delta S^0 \qquad \text{(Eq. 1.1)}$$

A large increase in ΔS^0 will result in a more negative ΔG^0 and according to Eq. 1.2, a more negative ΔG^0 leads to a more positive equilibrium (formation) constant.

$$\Delta G^0 = -RT\ln K \qquad \text{(Eq. 1.2)}$$

1.3.2.5. Chelate ring size

The size and shape of chelate rings are crucial to their stability as various limitations are imposed on bond angles and bond lengths by the presence of a metal ion. Five- and six-membered chelate rings are the most common chelate ring size formed and are typically the most stable. Five-membered chelate rings are generally more stable than six-membered rings since the bond strain is less and the ligand permits an increase in bonding ability to the metal centre. Four-membered rings are much less common as they tend to suffer from bond strain.[24, 25] The order of stability is depicted in Fig 1.10.

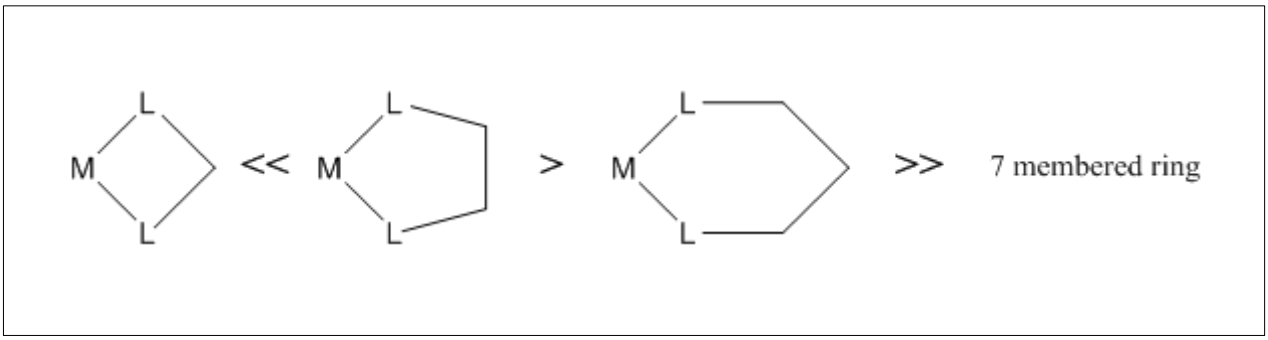

FIGURE 1.10 Relative stabilities of different chelate ring sizes

The number of chelate rings is also important in terms of complex stability and for two similar metal chelates that which contains the greater number of stable chelate rings will generally be the more stable. Their impact on the stability of a complex is also influenced by the flexibility of the ring and the presence of other chelate rings. It should be established that large chelate rings are not necessarily detrimental to the stability of metal complexes, but usually, form part of a highly stable polydentate chelate structure or macrocycle. This additional stability observed in these systems is the result of a phenomenon known as the macrocyclic effect.[25]

1.3.3. Design of metal extractants/chelating agents

1.3.3.1. Introduction

Extractant properties play a basic role in the selective separation and concentration of solutes from dilute solutions. Many synthetic extractants have been developed during the past few decades. As an example, crown ether macrocycles, which selectively bind alkali and some other metal ions, have been synthesised and used

as extractants for the selective recognition of neutral, charged, or zwitterionic species. There are numerous methodologies which have been adopted, specifically within solvent extraction, to achieve the selective extraction of desired metals from pregnant leach solutions and were mentioned earlier in this chapter.

1.3.3.2. Parameters to be considered

Extraction performance is strongly related to the characteristics of an extractant.[27, 28] The main parameters involved in the design of an extractant are as follows:

1. High selectivity towards species to be separated.
2. High capacity of the species that has to be extracted.
3. High ability of an extractant to complexate a solute of interest from an aqueous feed phase into an organic phase – high extraction, or distribution, or partition constant, $E_{F/E.}$
4. High ability of an extractant-solute complex to be decomplexed and stripped from loaded organic to an aqueous strip phase - high decomplexation, or stripping constant, $E_{E/R.}$
5. Rapid kinetics of formation (complexation) and destruction (decomplexation) of the complex.
6. Rapid kinetics of diffusion of the extractant-solute complex through the interface organic layer (a high diffusion coefficient, D_{LM}).
7. Stability of the extractant.
8. No side reactions.
9. No irreversible or degradation reactions.
10. Low solubility of the extractant in the aqueous phase.
11. Low co-extraction of water.
12. Extractant should be easily regenerated.
13. Extractant should have suitable physical properties, such as density, viscosity, and surface tension.
14. Low toxicity for biological systems and low corrosivity.
15. Reasonable price at industrial applications.

For the majority of large-scale operations, relatively high boiling point hydrocarbons are the preferred choice of water-immiscible solvents due to their lower cost and the general safety surrounding them. Furthermore, their exceptionally low solubility in water lowers the threat of pollution and promotes phase disengagement. Additionally, the very low polarity of these solvents favours the formation of secondary bonds, particularly hydrogen bonds (H-bonds) between the ligands used as metal extractants.[27, 28] The formation of supramolecular assemblies arising from such secondary bonding is very important in defining the modes of action and thermodynamic stability of such extractants. It is only recently that attempts have been made to design extractants for the purpose of controlling the stability and geometries of assemblies of ligands and thus to tune the strength and selectivity of metal extraction.[29] Another important consideration to note is that the transfer of a metal value from a pregnant leach solution to a water-immiscible solvent can be affected by a number of mechanisms, which depend on whether the extractant operates on the inner or outer coordination sphere of the metal ion and how the loading/stripping equilibria are controlled.[29]

1.3.4. Metal extraction mechanisms via solvent extraction

1.3.4.1. Extraction of metal cations (via ion-exchange)

Ion exchange is one of the extraction mechanisms pertaining to solvent extraction. This mechanism proceeds when an ion is transferred from the aqueous phase to the organic phase. Specifically focusing on metal extraction, the transport of metal cations into a water-immiscible solvent without anion co-extraction requires an exchange with another cation to ensure the establishment of charge neutrality within the system. Most often, the exchanged cations are protons, and the extractants are organic acids, LH, which partition according to the equilibria revealed in Eq. 1.3, where metal loading and stripping are dependent on pH.[29, 30]

$$nLH_{(org)} + M^{n+} \rightleftharpoons [ML_n]_{(org)} + nH^+ \qquad \text{(Eq. 1.3)}$$

Cation exchange reagents produce neutral, organic-soluble metal complexes [ML_n] by providing anionic donors (L^-) to the inner coordination sphere (directly attached to metal ion). In most cases, the anion is generated by deprotonation of an acidic ligand (LH). In terms of metal extraction, a “strong” reagent is one

which has a low $pH_{1/2}$ value (the pH at which 50 % of the extractant is loaded with metal). Therefore, strong extractants are capable of recovering metals from highly acidic feed solutions. On the contrary, weak extractants for metal cations only have the ability to recover metals at high pH values. As mentioned earlier, metal stripping and loading are pH dependent, this makes it possible to control the loading and stripping of the metal in the organic phase by adjusting the pH of the aqueous solution which is in contact with it. The loaded organic phase is then stripped by contacting with a strongly acidic solution, thus generating a pure aqueous electrolyte that is suitable for reduction. In this way, the extractant is regenerated, providing a good materials balance.

One of the most commercially successful processes of this type is the recovery of copper from sulfate streams using phenolic oxime reagents. These types of extractant are currently used in solvent extraction plants worldwide, producing over 2.3 million tonnes of copper per annum, around one-fifth of the total world production [16, 31] The strength and selectivity of these reagents for copper arises from the 'goodness-of-fit' of the cavity formed by two deprotonated ligands which generate a 14-membered pseudo-macrocycle by means of strong hydrogen bonding interactions between the phenolic and oxime groups[32, 33] (Scheme 1.5)[34]

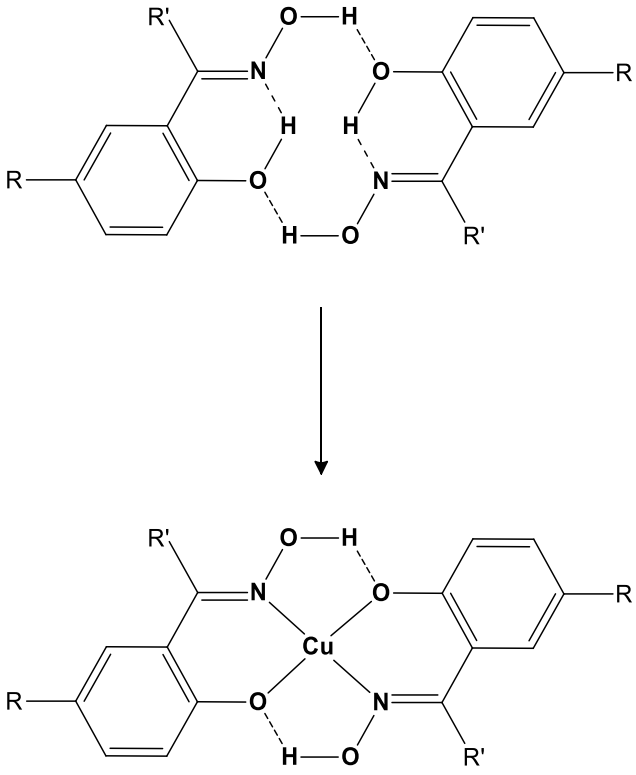

SCHEME 1.5 The 14-membered pseudo-macrocyclic structures formed by the phenolic oxime reactants[34]

The pH dependency of extraction can be studied by conducting pH isotherm experiments. The pH isotherm, also referred to as an "S" curve, provides useful information as it relates the extent of metal ion extraction with the solution pH for a given solution composition.[28] This information can be employed to establish the most suitable pH of the aqueous feed solution to ensure selective transport of the desired metal cation to the organic phase. Moreover, it provides insight into deciding on an appropriately strong acidic solution to strip the metal from the organic phase into an isolated aqueous solution. Fig. 1.11 (top) shows the "S-curves" associated with the pH-dependence metal loading by the commercial phenolic oxime reagent "Acorga P50" whose generic structure can be seen in Fig. 1.11 (bottom).

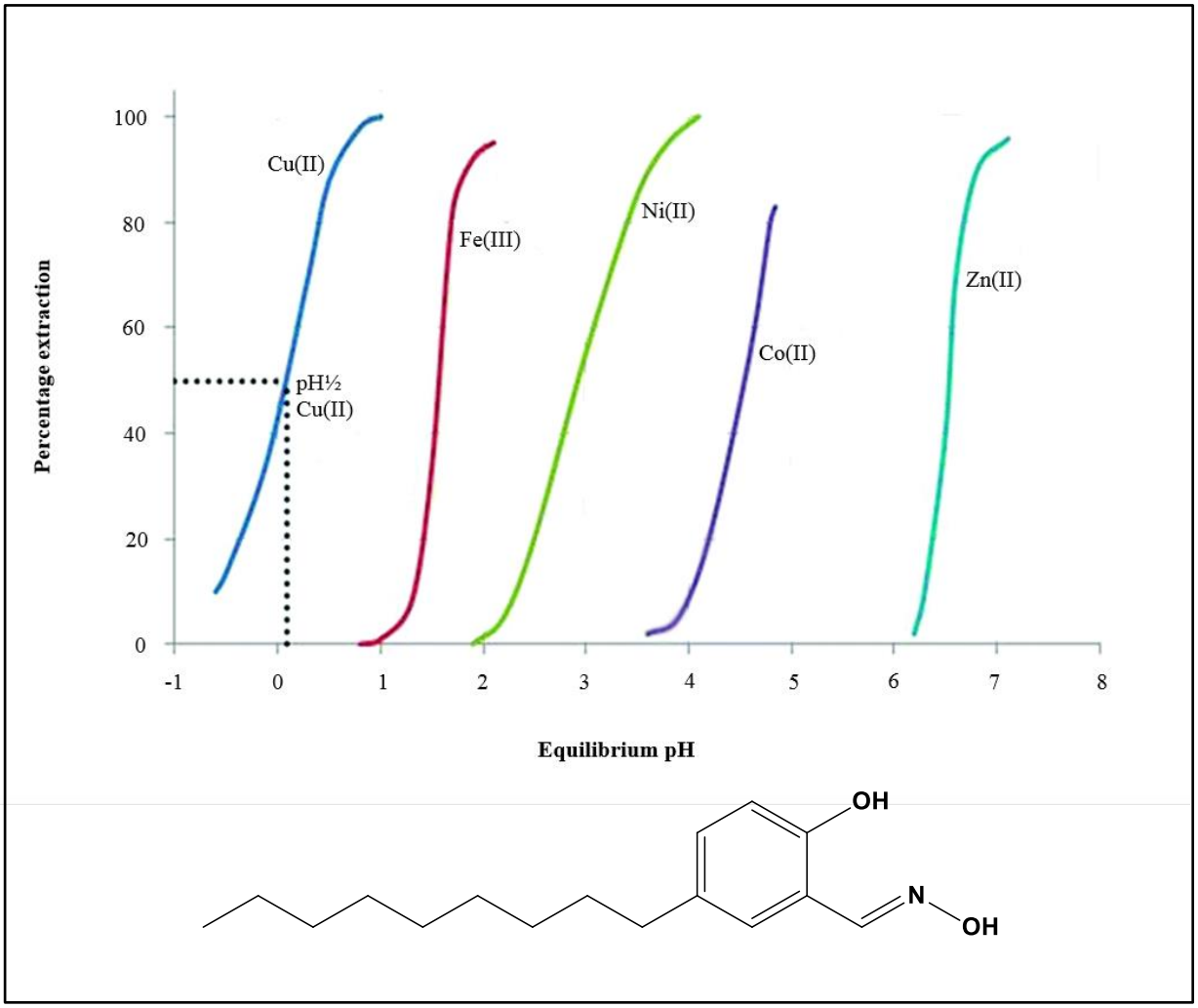

FIGURE 1.11 pH isotherm plots of Acorga P50 reagent (top) and the chemical structure of Acorga P50 (bottom)[39]

It is clear from the pH isotherm plots for the Acorga P50 reagent illustrated in Fig. 1.11, that this extractant will reject Ni(II) and Zn(II) at a pH < 2 when Cu(II) is present. The efficacy of extraction of the metals shown

in Fig.1.11 (top), is roughly that which would be predicted by the Irving–Williams order but with those metals which have a preference for the planar geometry of the pseudo-macrocyclic donor set, Ni(II), and Cu(II), being favoured.[34]

Moreover, for a reagent to be a successful extractant of copper, it must favour complex formation of Cu(II) over other metals in the pregnant leach solution, notably over ferric iron which is usually present at comparable or higher concentrations. Also, complex formation must be favourable at relatively low pH values (< 2.0) required to ensure that ferric iron remains in solution. On the contrary, the efficiency of these cation-exchange reagents is reduced when dealing with high tenor feeds since the transfer of copper to the organic phase results in a build-up of protons in the aqueous phase since for every metal(II) ion extracted into the organic phase, two protons are transferred to the aqueous phase (Eq. 3). This is particularly problematic with chloride streams because high concentrations of chloride ions boost proton activity.[35] The build-up of protons in the aqueous phase affects the extraction process since in the case of the phenolic oxime reagents, the phenolate oxygen atoms remain protonated and the imine moiety becomes more susceptible to hydrolysis at low pH values. Furthermore, inter-stage neutralisation must be executed which involves the addition of base to the aqueous solution – this further complicates circuit operation and affects material balances.[36]

1.3.4.2. Extraction of anions and metallate anions (ion-pair formation)

Anion binding is essential in processes which require anion extraction (with or without an attached metal) and the removal of anions where they are unwanted. The defining characteristic of an anion is its negative charge and therefore electrostatic interactions play an important role in these binding mechanisms. Anions are larger than their respective isoelectronic cations and thus recognition cavities have to be comparatively larger. Furthermore, the geometry of the anionic species is an important parameter to be considered as anions exhibit a range of geometries which require complementary binding sites.

Many anionic species such as COO^-, PO_4^{3-} and SO_4^{2-} only exist over a limited pH range (high pH values) because at low pH values; these anions become protonated and lose their negative charge. Another crucial concept when dealing with anion extraction is that of solvation. The extent of aqueous solvation is reflected

by the Hoffmeister bias which states that larger and more highly charged anionic species tend to be more hydrated in aqueous solution and therefore more difficult to extract. The ease of which an anion can be extracted from aqueous solutions follows the spectrochemical series also referred to as the Hoffmeister series below:

$ClO_4^- > I^- > Cr_2O_7^{2-} > Br^- > NO_3^- > CO_3^{2-} > CH_3COO^- = HCO_3^- > C_2O_4^{2-} = NO_2^- > Cl^- > S_2O_3^{2-} > SO_4^{2-} > CN^- > PO_4^{3-}$

The extraction of metallate anions follows a similar trend to the extraction of typical anions. It concerns itself with a metal extraction mechanism within the process of solvent extraction. Anion-exchange reagents complex metallate anions and transport them into water-immiscible solvents usually by a mechanism known as ion pair formation. This technique exploits outer-sphere coordination to recover metals. In other words, the metal is covalently bonded to an anionic ligand or ligands producing an anionic metal complex which interacts with an extractant by means of electrostatic interactions. In this process, the metal itself does not interact directly with the extractant but rather through an attached ligand group or groups.[1]

Using hydrophobic cations and exploiting outer-sphere coordination, it is possible to extract metallate anions from aqueous solutions by forming assemblies, conventionally referred to as ion pairs. For example, the uptake of $FeCl_4^-$ from an aqueous solution using trialkylamines (Eq. 1.4):

$$R_3N_{(org)} + H^+ + FeCl_4^- \rightleftharpoons [R_3NH][FeCl_4]_{(org)} \qquad \text{(Eq. 1.4)}$$

The electrostatic attraction between the anion and trialkylammonium ion is assumed to be complemented by hydrogen-bonding in extractions from acidic chloride solutions.[1] Trialkylammonium reagents are used in commercial processes to recover kinetically inert precious metals as their chlorometallate complexes from acidic media.[15] Selective transfer of the desired metal value remains a challenge in designing these anion-exchange reagents.

1.3.4.3. Extraction of metal salts

While the above-mentioned mechanisms are well-suited for a variety of flowsheets used to recover metals from both primary and secondary sources, there are situations when a much more efficient approach would be to extract and transport metal salts. Such an approach requires complexing agents which accommodate both the metal cation and its attendant anion or anions. The benefit of such a system lies in the fact that the transfer of metal values to an organic phase using metal salt extractants is not associated with a change in proton concentration in the aqueous phase (Eq. 1.5), as in the case of typical cation-exchange reagents.

$$\bar{L} + M^{n+} + X^{n-} \rightleftharpoons \overline{MLX} \qquad \text{(Eq. 1.5)}$$

The application of water-immiscible reagents to extract a metal salt brings about the question as to whether the attendant anion (X) exists in the inner or outer coordination sphere, or both. The arrangement which dominates is in essence dependent on the degree as to which the counter anion X is a good inner-sphere ligand, and on the nature of the bonds which are preferentially formed by the cation.

The successful development of selective anion receptors[37, 38] often exploit ion-pairing in which an electrostatic interaction between the anion and a positively charged metal in the anion receptor is used to improve the strength and selectivity of binding (Fig. 1.12).[39]

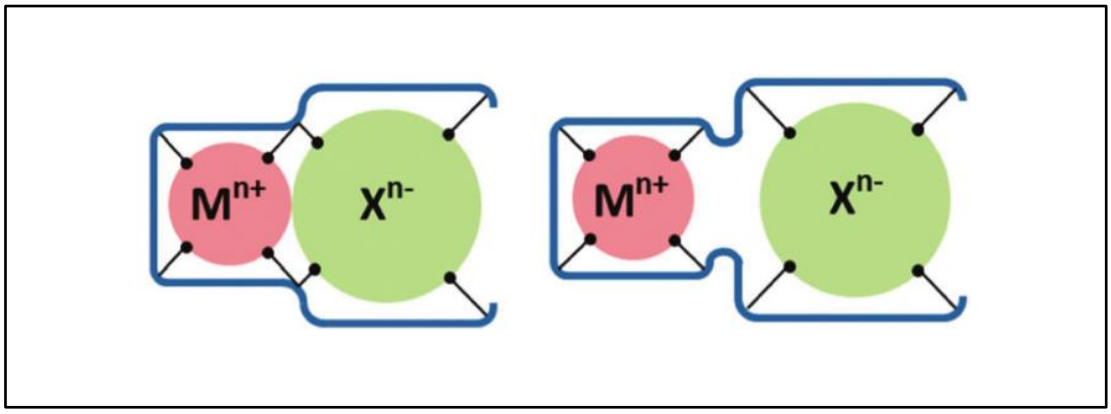

FIGURE 1.12 Ditopic extractants of metal salts (MX) to accommodate contact ion pairs (left) and separated ion pairs (right)[39]

Systems in which the anion can be considered to be present in the outer coordination sphere of the metal can be used as anion sensors since the presence of X often significantly changes the spectroscopic or electrochemical properties of the metal center. However, the development of polytopic solvent extractants which contain sites to bind both cations and anions as a metal salt (Fig. 1.12) is much less common.[39,40] When reagents are targeted to recover alkali metal salts, emphasis must be placed on incorporating a strong and selective binding site for the metal cation.

Although various strategies have been developed for processing metal complexes with anions such as chloride and nitrate, a greater focus has been directed towards extracting metal sulfates from pregnant leach solutions, as sulfate is derived from the commonly used leaching agent sulfuric acid. Sulfate is a weaker inner-sphere ligand for d- and f-block cations in comparison to chloride and nitrate.[41] Consequently, strategies have been developed to extract sulfate salts using ditopic ligands either as ion pairs (left in Fig. 1.12) or as well-separated cations and anions in strong and selective binding sites (right in Fig. 1.12).

Recently, White and co-workers[42] described a synthetic method to generate a new class of ditopic ligand designed to provide separate dianionic and dicationic binding sites (Scheme 1.6). These sites are derived from the zwitterionic form of the ligand formed by transferring the phenolic protons to the nitrogen atoms of the integrated dialkylamino methyl pendant groups. These salen-based reagents possessing these unique characteristics provide for efficient stripping of the desired metal cation and anion at different pH values into separate aqueous solutions. This is essential since the extractant is successfully recycled and additionally, the selective transport of anions allows for a pure metal salt solution to be produced. This is a prerequisite for downstream electrowinning of the metal which requires electrolytes of high purity in order to control over-potentials at cathodes and to ensure that single reactions occur at anodes.

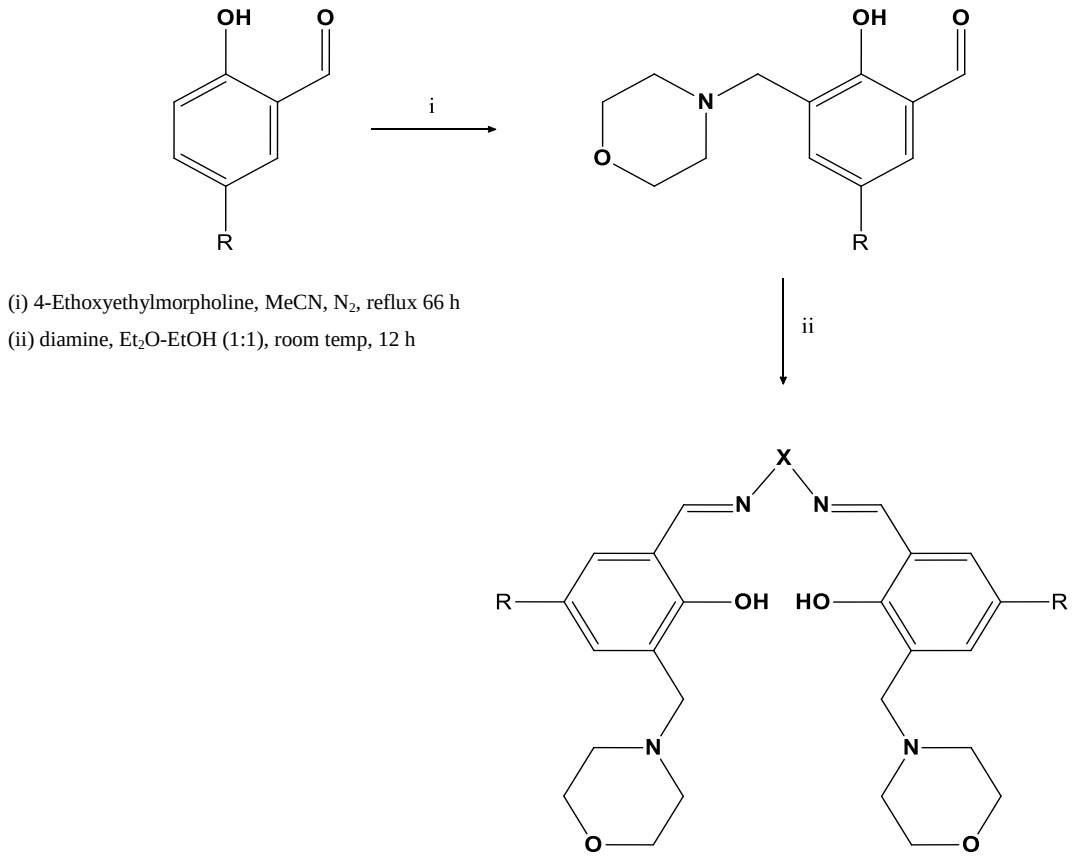

SCHEME 1.6 Synthetic route proposed by White and co-workers generating a salen-type ditopic ligand providing separate dianionic and dicationic binding sites[42]

1.4. Objectives of research

The chemistry of salen ligands in the presence of transition metals has been extensively researched.[43] Moreover, multidentate Schiff base ligands have the ability to form complexes with certain transition metal ions which can exhibit extraordinary coordination, high thermodynamic stability, biological activities and various other interesting attributes. Simultaneously, owing to their facile preparation, structural varieties and diverse chemical properties, these multidentate Schiff base ligands are widely applied in the construction of metal-organic complexes[44], with this precedent in mind, the objectives of the study were two-fold.

Firstly, the research entails: (i) the design of six salen-type, monotopic ligands boasting unique molecular symmetries and electronic characteristics. These modifications will be focused on affecting the disposition of the donor atoms in the ligands by making use of different linker diamine moieties. This will be executed in

order to get an insight into the factors which influence the selectivity of these types of ligands for specific metals.

(ii) The synthesis and full characterisation of the monotopic ligands by ^{1}H and ^{13}C NMR spectroscopy, FT-IR (ATR) spectroscopy, melting point determination, mass spectrometry, micro-elemental analysis and, where possible, by SCD analysis.

(iii) The evaluation of these monotopic ligands as extractants for metal recovery processes (via solvent extraction) for the recovery of base metals and some post-transition metals. This will be assessed through metal extraction and transport studies in addition to pH isotherm experiments. The metal cations which are examined in this investigation include; Cu(II), Ni(II), Zn(II), Co(II), Cd(II) and Pb(II).

(iv) Crystal growth of the free monotopic ligands and respective metal complexes suitable for SCD studies in the solid-state. Analysis using SCD will divulge information pertaining to metal-ligand coordination namely bond lengths, bond angles, torsion angles, probable stoichiometry of metal-ligand complexation and a few other important coordinative and structural characteristics. Further details regarding the importance of SCD and its role in elucidating chemical information in such systems will be disclosed in Chapter 2.

Secondly, the study involves: (i) the design of six salen-type, ditopic ligands (housing both a cation and anion binding site), incorporating anion-binding sites of varying geometric structure and electronic nature into their scaffold. These modifications will be aimed towards altering the chemical environment of the individual anion-binding receptors in an attempt to attain a deeper understanding of variables responsible for anion selectivity, and in effect, attempt to surmount the Hoffmeister bias.

(ii) The synthesis and full characterisation of the ditopic ligands by ^{1}H and ^{13}C NMR spectroscopy, FT-IR (ATR) spectroscopy, melting point determination (where applicable), mass spectrometry and micro-elemental analysis.

(iii) The evaluation of these ditopic ligands as extractants for metal salt recovery processes (via solvent extraction) for the recovery of base metals and some post-transition metals as well as various anions. This will be exercised through metal extraction and transport studies. The metal cations which are assessed in this

investigation include; Cu(II), Ni(II), Zn(II), Co(II), Cd(II) and Pb(II), and the particular anions of interest in this study are Cl^-, NO_3^- and SO_4^- (derived from the most widely-used leaching agents).

1.5. References

1. Tasker, P. A., Plieger, P. G., West, L. C. *Compr. Coord. Chem. II*. **2004**, *9*, 759–808.
2. Habashi, F. *Handbook of extractive metallurgy, Volume 2*; Wiley-VCH, 1997.
3. Chang, J. Y. C.; Parsons, S.; Pieger, P. G.; Tasker, P. A. *J. Incl. Phenom. Macrocycl. Chem.* **2011**, *71* (3–4), 529–536.
4. Reardon, A. C. *Metall. non-metallurgist.* **2011**, *36* (2).
5. Own, S. Y.; Me, N. **2014**, No. February.
6. Forgan, R. S.; Davidson, J. E.; Fabbiani, F. P. A; Galbraith, S. G.; Henderson, D. K.; Moggach, S. A.; Parsons, S.; Tasker, P. A.; White, F. J. *Dalton Trans.* **2010**, *39* (7), 1763–1770.
7. Habashi, F. *Hydrometallurgy*. **2005**, *79* (1–2), 15–22.
8. Habashi, F. *Principles of Extractive Metallurgy, Volume 1*; CRC Press, 1969.
9. Free, M. L. *Hydrometallurgy: Fundamentals and Applications*; Wiley, 2013.
10. Habashi, F. *Miner. Process. Extr. Metall. Rev.* **2007**, *15* (1–4), 5–12.
11. Peters, E. *Hydrometallurgy*. **1992**, *29* (1–3), 431–459.
12. Burkin, A. R. *Chemical Hydrometallurgy: Theory and Principles*; World Scientific, 2001.
13. Swaddle, T. W. *Inorganic Chemistry: An Industrial and Environmental Perspective*; Academic Press, 1997.
14. Drzymala, J. *Mineral Processing, Foundations of theory and practice of minerallurgy*; 2007.
15. Bernardis, F. L.; Grant, R. A.; Sherrington, D. C. *React. Funct. Polym.* **2005**, *65* (3), 205–217.
16. Ritcey, G. M. *Tsinghua Sci. Technol.* **2006**, *11* (2), 137–152.
17. Kislik, V. S. *Solvent Extraction: Classical and Novel Approaches*; Elsevier, 2011.

18. Forgan, R. S.; Roach, B. D.; Wood, P. A.; White, F. J.; Campbell, J.; Henderson, D. K.; Kamenetzky, E.; McAllister, F. E.; Parsons, S.; Pidcock, E.; Richardson, P.; Swart, R. M.; Tasker, P. A. *Inorg. Chem.* **2011**, *50* (10), 4515–4522.

19. Bacon, G.; Mihaylov, I. *J. South African Inst. Min. Metall.* **2002**, No. November, 435–444.

20. http://www.nature.com/nature/journal/v162/n4123/abs/162746a0.html (accessed Sep 15, 2015).

21. Pearson, R. G. *J. Am. Chem. Soc.* **1963**, *85* (22), 3533–3539.

22. Pearson, R. G. *J. Chem. Educ.* **1968**, *45* (9), 581.

23. Pearson, R. G. *Survey of Progress in Chemistry Volume 5*; Survey of Progress in Chemistry; Elsevier, 1969; Vol. 5.

24. Lee, J. D. *CONCISE INORGANIC CHEMISTRY, 5TH ED*; Wiley India Pvt. Limited, 2008.

25. Hancock, R. D. *J. Chem. Educ.* **1992**, *69* (8), 615.

26. Chung, C.-S. *Inorg. Chem.* **1979**, *18* (5), 1321–1324.

27. Kislik, V. S. *Modern (Classical) Fundamental Principles of Solvent Extraction*; 2012.

28. Kislik, V. S. *Solvent Extraction: Classical and Novel Approaches*; Elsevier, 2011.

29. Miller, H. A.; Laing, N.; Parsons, S.; Parkin, A.; Tasker, P. A.; White, D. J. *J. Chem. Soc. Dalt. Trans.* **2000**, No. 21, 3773–3782.

30. Kunin, R. *Science (80-.).* **1969**, *166* (3911), 1391–1392.

31. Galbraith, S. G.; Wang, Q.; Li, L.; Blake, A.; Wilson, C.; Collinson, S. R.; Lindoy, L. F.; Plieger, P. G.; Schroeder, M.; Tasker, P. A. *Chem. - A Eur. J.* **2007**, *13* (21), 6090–6107.

32. Szymanowski, J. *Hydroxyoximes and Copper Hydrometallurgy*; CRC Press, 1993.

33. Elizalde, M. P.; Castresana, J. M.; Aguilar, M.; Cox, M. *Solvent Extr. Ion Exch.* **2007**, *3* (3), 251–266.

34. Smith, A. G.; Tasker, P. A.; White, D. J. *Coord. Chem. Rev.* **2003**, *241* (1–2), 61–85.

35. Senanayake, G. *Miner. Eng.* **2007**, *20* (1), 1–15.

36. Tasker, P. A.; Tong, C. C.; Westra, A. N. *Coord. Chem. Rev.* **2007**, *251* (13–14 SPEC. ISS.), 1868–

1877.

37. Sessler, J. L.; Cai, J.; Gong, H.-Y.; Yang, X.; Arambula, J. F.; Hay, B. P. *J. Am. Chem. Soc.* **2010**, *132* (40), 14058–14060.

38. Kilah, N. L.; Wise, M. D.; Serpell, C. J.; Thompson, A. L.; White, N. G.; Christensen, K. E.; Beer, P. D. *J. Am. Chem. Soc.* **2010**, *132* (34), 11893–11895.

39. Turkington, J. R.; Bailey, P. J.; Love, J. B.; Wilson, A. M.; Tasker, P. A. *Chem. Commun. (Camb).* **2013**, *49* (19), 1891–1899.

40. Moyer, B. A; Bonnesen, P. V; Custelcean, R.; Delmau, L. H.; Hay, B. P. *Alcohol* **2008**, *54* (2), 65–87.

41. Martell, A. E.; Smith, R. M. *Critical Stability Constants*; Springer US: Boston, MA, 1982.

42. White, D. J.; Laing, N.; Miller, H.; Parsons, S.; Tasker, P. A. *Chem. Commun.* **1999**, 2077–2078.

43. Sánchez, M.; Harvey, M. J.; Nordstrom, F.; Parkin, S.; Atwood, D. A. *Inorg. Chem.* **2002**, *41* (21), 5397–5402.

44. Gong, X.; Ge, Y.-Y.; Fang, M.; Gu, Z.-G.; Zheng, S.-R.; Li, W.-S.; Hu, S.-J.; Li, S.-B.; Cai, Y.-P. *CrystEngComm.* **2011**, *13* (23), 6911.

CHAPTER 2: SYNTHESIS & CHARACTERISATION OF MONOTOPIC LIGANDS & RESPECTIVE METAL COMPLEXES

2.1. Introduction

2.1.1. Schiff base ligands

Schiff bases are chemical compounds which are derived from the condensation reaction of a primary amine and an active carbonyl group (Scheme 2.1) [1].

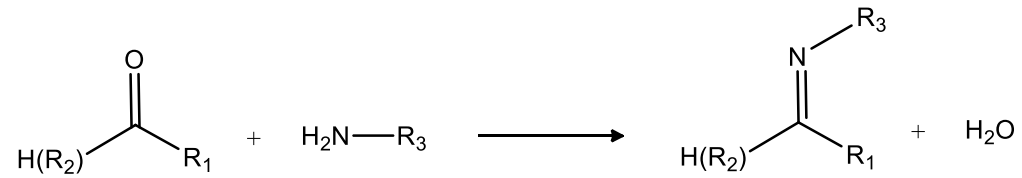

Aldehyde or ketone | Primary amine | Schiff base product

R_1, R_2, R_3 = independent alkyl groups

SCHEME 2.1 General condensation reaction producing a Schiff base product

The synthesis of Schiff bases was first reported by Hugo Schiff in 1864[2] and is accordingly named after him. They have the ability to form stable complexes with transition metal ions of varying oxidation states, especially if the amine and carbonyl compounds contain a second functional group sufficiently near the site of condensation to form five- and/or six-membered chelate rings.[3] The coordination takes place through the lone pair of electrons on the imine nitrogen, as well as a second heteroatom combined with the imine, usually nitrogen or oxygen.

Taking into consideration their facile preparation and diverse coordinative abilities they are not surprisingly employed in a range of disciplines which concern metal chelation processes. Collectively with their complexes, Schiff bases have been found increasingly advantageous in a variety of applications within biological, clinical, and analytical fields.[3] In the interest of base metal extraction, the literature is overwhelmed with findings commending the organic Schiff base salen-scaffold and its extraordinary potential in metal solvent extraction applications.[4, 5]

Mindful of the aforementioned, the current chapter serves to elaborate on all synthetic aspects pertaining to monotopic ligands **L1-L6** possessing the salen-scaffold. Firstly, we report the synthetic aspects relating to the transformation of 4-tertbutyl phenol to the ligand precursor, 5-tert-butyl-2-hydroxybenzaldehyde. Ensuing this, a discussion of the synthesis (using the ligand precursor as a reagent) and full characterisation of Schiff base ligands **L1-L6 (**Fig 2.1) by means of FT-IR (ATR) spectroscopy, ^{1}H and ^{13}C NMR spectroscopy, melting point determination, mass spectrometry, micro-elemental analysis and in the cases of **L1-L4** and **L6**, by means of single crystal X-ray diffraction (SCD).

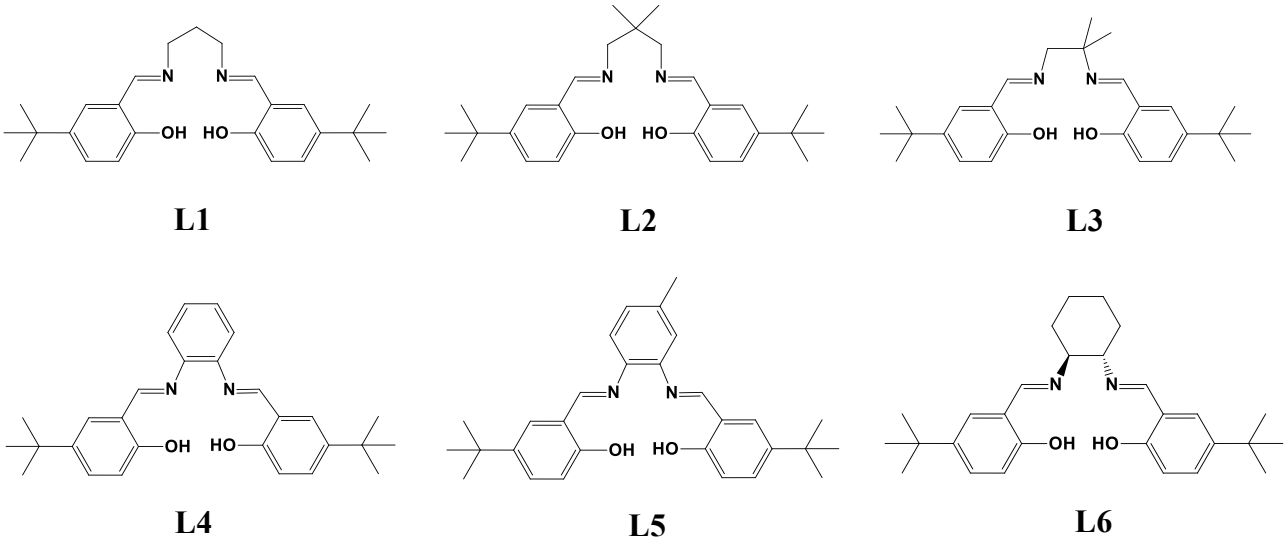

FIGURE 2.1 Structural representation of monotopic ligands **L1-L6**

2.2. Results and Discussion

2.2.1. Synthesis of ligand precursor (5-tert-butyl-2-hydroxybenzaldehyde)

The precursor aldehyde species which serves as a building block in the production of the Schiff bases **L1-L6**, was synthesised and characterised using FT-IR (ATR) spectroscopy, ^{1}H and ^{13}C NMR spectroscopy. Once it was assured that the isolated product was of sufficient purity, it was utilised as a chemical reagent in the preparation of the monotopic ligands **L1-L6** (Scheme 2.3).

The precursor, 5-tertbutyl-2-hydroxybenzaldehyde, was generated from 4-tertbutyl phenol by making use of the synthetic route offered by Aldred and co-workers.[6] This group identified that deprotonation of phenols by treatment with magnesium methoxide in conjunction with the distillative abstraction of free methanol and the addition of paraformaldehyde results in ortho-specific magnesium-mediated formylation to afford the corresponding salicylaldehyde magnesium salts, from which the salicylaldehydes can be isolated by acidic work-up (Scheme 2.2).

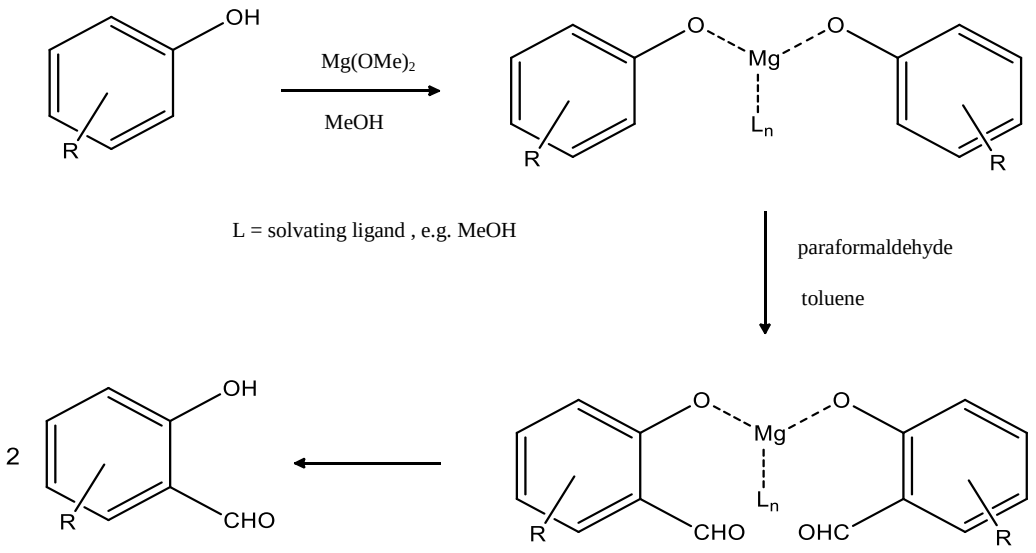

SCHEME 2.2 Formylation of phenol to corresponding salicylaldehyde devised by Aldred and co-workers[6]

This method was adopted due to reports of its triumph over conventional aromatic formylation procedures such as the known Duff, Reimer-Tiemann, Vilsmeier or Gatterman reactions.[7, 8, 9] Since for these reactions to be effective the phenol hydroxyl group should be derivatised (for example as an ether). Although other strategies exist for ortho-formylation of phenols, as with the use of metal salt catalysts[6] (eg. use of Sn, Ti, Fe, Cr and Zr salts), these necessitate the use of high pressures and bring with them additional complications. An alternative approach reported by Casiraghi, Casnati and co-workers[10], indicated successful formylation of aryloxymagnesium bromides by formaldehyde. Unfortunately, it was dismissed as having limited large-scale applicability due to the disadvantages of the conditions involving Grignard reagents and toxic hexamethylphosphoramide (HMPA). With the demand for ortho-formylated phenols for the synthesis of

various pharmaceuticals, agrochemicals, fragrance chemicals, mining chemical ligands, and other products[6], the synthetic work executed by Aldred and co-workers has proved useful.

In this synthetic procedure, methanol is produced as a formylation reaction by-product and, if it is not removed by distillation during the course of the reaction, the progress of formylation is inhibited resulting in poorer conversion of starting material to product. It was, therefore, necessary to remove free methanol via distillation and a replacement solvent added, in this case, toluene. In this investigation, the formylation reaction proceeded smoothly to ultimately afford a pale yellow oil through high vacuum distillation. Fortunately, the para-position of the starting phenol was occupied by a tert-butyl group and this thus relieved the difficulty of having to separate a mixture of ortho- and para- formylation products.

The principal characteristic peak in the FT-IR (ATR) spectrum, confirming that formylation had been effective, was the appearance of a single sharp absorption band in the carbonyl wavenumber region. It was found that the isolated product showed this sharp band at approximately 1650.56 cm^{-1} indicating that the aldehyde functionality had successfully formed. Further confirmation was achieved using ^{1}H and ^{13}C NMR spectroscopy and both assisted in verifying that the product was of adequate purity to be subjected to the final Schiff base-producing step. It was found from the ^{1}H NMR spectrum the presence of a sharp resonance at 9.89 ppm representative of the aldehyde proton. Furthermore, it was evident in the aromatic region (6.90 – 7.60 ppm in this instance) that there existed three discrete resonances implying three protons of unique chemical environments corresponding to the three protons attached directly to the aromatic ring of 5-tert-butyl-2-hydroxybenzaldehyde. In concluding characterisation by ^{1}H NMR, all resonances and integrals were accounted for and insignificant and minute traces of 4-tert-butylphenol were seen in the aromatic and aliphatic chemical shift region. ^{13}C NMR spectroscopy showed the existence of nine distinct carbon resonance peaks indicative of the structure of the desired product. The sharp resonance pertaining to the carbonyl carbon of the newly-formed aldehyde functionality was observed at 196.93 ppm.

In conclusion, it was confirmed by means of FT-IR (ATR), ^{1}H and ^{13}C NMR spectroscopy that the formylation reaction had been successful and the steps taken towards purification had resulted in the desired product, 5-tert-butyl-2-hydroxybenzaldehyde, being formed with trace impurities. It was thus applicable for use in manufacturing monotopic ligands **L1-L6**.

2.2.2. Synthesis of monotopic ligands L1-L6

The Schiff base ligands, **L1-L6**, were prepared by Schiff base condensation of two equivalents of 5-tert-butyl-2-hydroxybenzaldehyde with various electronically unique diamines (Scheme 2.3). The ligands were isolated in high yields as yellow-orange crystalline solids and showed solubility in polar organic solvents. The ligands were found to be stable both in solution and in the solid-state. **L1**, **L4** and **L6** have been reported previously[11, 12, 13] whereas **L2**, **L3,** and **L5** are novel. All the aforementioned ligands, however, have not been described in metal solvent extraction studies in known literature.

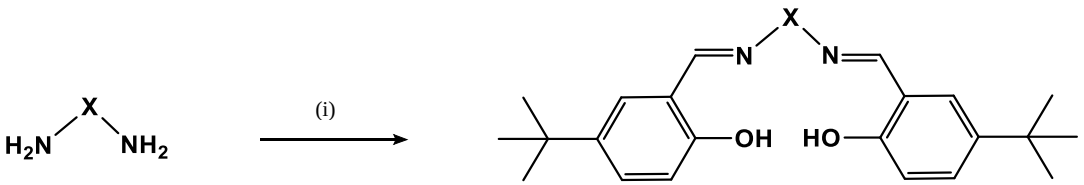

(i) 2 mol eq. 5-tertbutyl-2-hydroxybenzaldehyde, EtOH, reflux 12-18 h

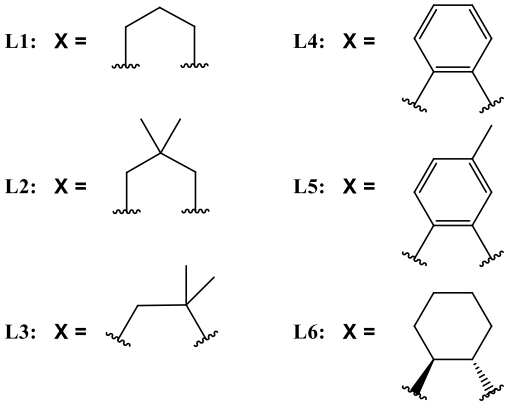

SCHEME 2.3 General reaction scheme for the synthesis of monotopic ligands **L1-L6**

Numerous characterisation techniques were employed to ascertain the purity of these chemical species before they could be thoroughly assessed as chelating agents in coordination studies. These techniques, which will be discussed in the following order, include melting point determination, mass spectrometry, FT-IR (ATR) spectroscopy, ^{1}H and ^{13}C NMR spectroscopy, elemental analysis and in most instances by use of SCD analysis.

2.2.2.1. Characterisation by melting point, mass spectrometry & FT-IR (ATR) spectroscopy

Table 2.1 below presents the important characteristic data pertaining to the synthesis of **L1-L6**. This includes the FT-IR absorption frequency for the imine C=N stretch, the proton adduct of the molecular ion in the acquired mass spectra and determined melting temperatures.

TABLE 2.1 Characteristic data applicable to the synthesis of **L1-L6**

Ligand	FT-IR[a] ($\upsilon_{C=N}$, cm^{-1})	ESI-MS[b] (*m/z*)	Melting Point[c] (°C)
L1	1632.98	395.27 (394.56)	76.0-76.9
L2	1633.20	423.30 (422.61)	111-115
L3	1635.53	409.29 (408.58)	120-122
L4	1611.88	429.25 (428.57)	176-178
L5	1615.20	443.29 (442.60)	192-194
L6	1628.00	435.30 (434.62)	165-170

[a] Recorded as neat spectra on a ZnSe crystal, using an ATR accessory. [b] Reported ion corresponds to the proton adduct of the molecular ion, [M + H]+, [c] Melting points recorded are uncorrected.

The FT-IR spectra of the Schiff base products were monitored for the disappearance of the carbonyl absorption band of 5-tert-butyl-2-hydroxybenzaldehyde at exactly 1650.56 cm^{-1} and the emergence of a sharp peak in the range of 1600-1650 cm^{-1} indicative of the imine functionality. Individually, all monotopic ligands delivered sharp peaks in the imine wavenumber region with **L4** providing this absorption peak at 1611.88 cm^{-1} lower than all the other ligands. This is due to the most electron-withdrawing diamine linker being used to produce **L4**. **L3**, on the other hand, shows its imine resonance at 1635.53 cm^{-1} being higher than the other ligands. This is justified by the shorter ethylene diamine backbone in this ligand with a carbon attached to two methyl groups in close proximity to the imine. In other words, the region of the imine peak in these ligands is dependent on the electronic nature of the diamine reacted with 5-tertbutyl-2-hydroxybenzaldehyde with increased electron density on the C=N bond of the imine resulting in its absorption at higher wavenumbers.

Electrospray Ionisation Mass Spectrometry (ESI-MS) assisted in disclosing information concerning the mass-to-charge ratio of pseudo molecular ions generated from the neutral organic ligands. The proton adduct of the singly-charged pseudo molecular ion derived from **L1**-**L6**, respectively, is exemplified in Table 2.1. These values correlate well to the calculated molecular masses (in parenthesis) of each ligand indicating that the ligands were in fact made in high yield. In each of the mass spectra, a doubly-charged molecular ion was seen which represented the base peak in each spectra having a mass-to-charge ratio equal to the value of [*m/z* $[M+H]^+ + 1] / 2$.

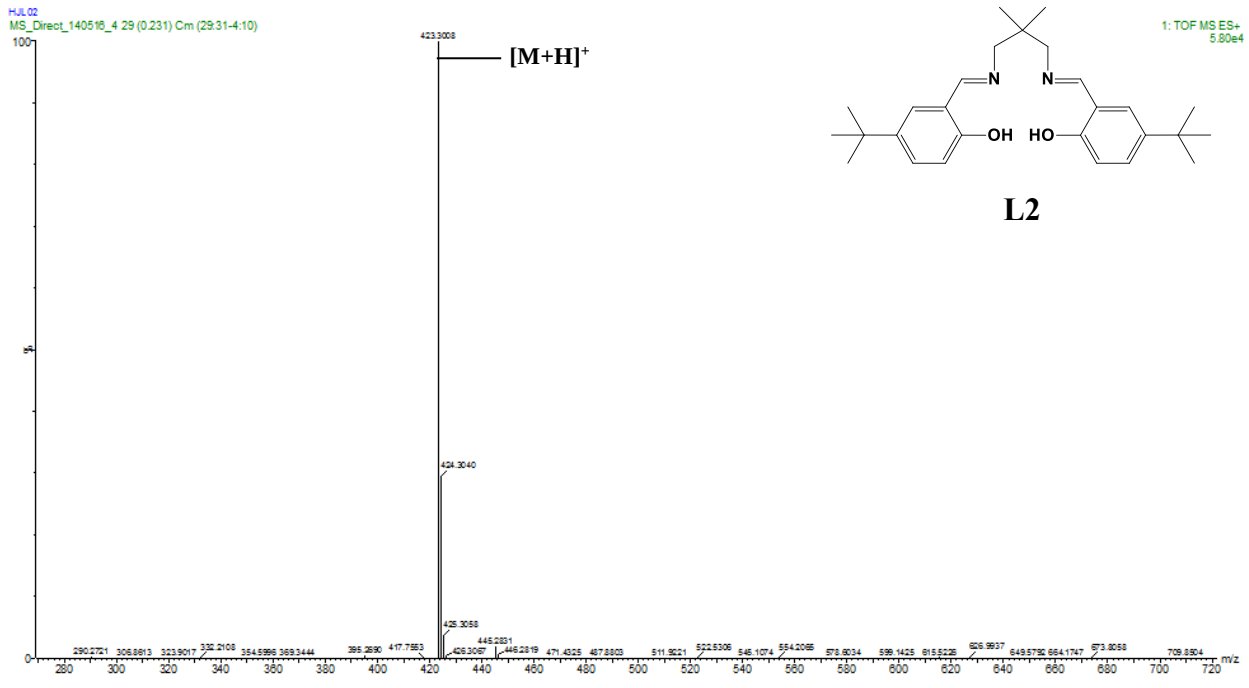

FIGURE 2.2 ESI-MS (positive mode) spectrum of **L2** with the labelled proton adduct

Lastly, since most monotopic ligands were formed as crystalline materials, an accurate melting temperature could be acquired and it was found that **L1**-**L6** showed melting in the range of 76.0-189 °C. **L1**, **L4** and **L6** exhibited melting temperatures which correlated well with those reported in literature.[11, 12, 13]

2.2.2.2. Characterisation by ^{1}H NMR spectroscopy

The numbering of protons and carbons within these molecules, and used for constructing Tables 2.2 and 2.3, is exemplified in Fig. 2.3. The phenoxy groups and linked imines on either side of the diamine moiety are labelled (i) and (ii), respectively. This is to denote the symmetry of these groups in the numbering system.

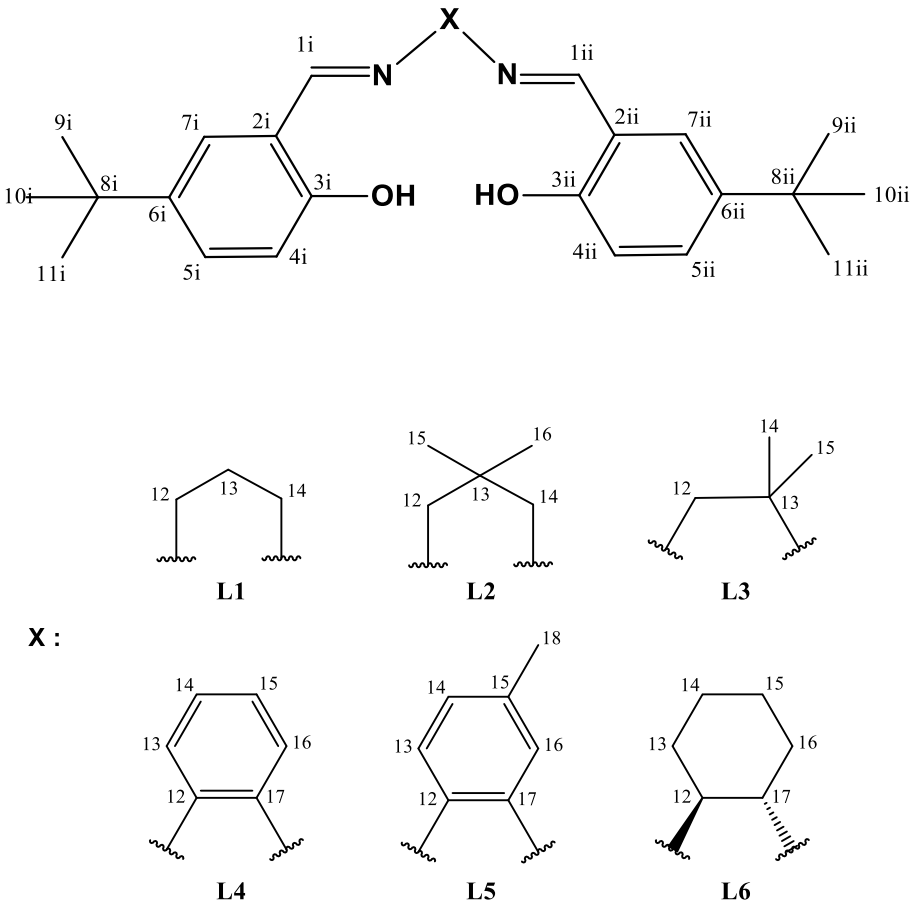

FIGURE 2.3 Numbering scheme used in the annotations of the ^{1}H and ^{13}C NMR spectra and respective tables.

Characterisation by means of ^{1}H NMR spectroscopy provided adequate evidence of the successful formation of monotopic ligands **L1-L6**. Notable peaks suggesting the efficacious production of the respective Schiff bases were observed by the disappearance of the resonance at 9.89 ppm implying the proton connected to the carbonyl carbon of 5-tert-butyl-2-hydroxybenzaldehyde and the appearance of a sharp signal in the region of roughly 8.40–8.60 ppm indicating the proton associated with the imine functionality. This was indeed observed; **L1-L6** showed characteristic peaks in the appropriate imine proton range with ligands **L1-L3** and

L6 having imine resonances more upfield (8.25-8.39 ppm) in comparison to the imines associated with more electron-withdrawing substituents as in the case of **L4** and **L5** (8.59-8.66 ppm). It was found that for **L3** and **L5**, two distinct imine proton peaks existed, this was in fact anticipated since the lower symmetry introduced by their respective diamines results in the imine protons having unique chemical environments. In closing, all proton resonances were accounted for with integral values corresponding well to the appropriate number of protons present in the desired products. For simplistic purposes, the fully annotated ^{1}H NMR spectrum of the novel ligand **L2 (**Fig 2.4) is shown as a representation of similar spectra obtained for the other monotopic ligands **L1**-**L6**.

2.2.2.3. Characterisation by ^{13}C NMR spectroscopy

The success of the Schiff base reaction generating **L1**-**L6** in high purity was further confirmed using ^{13}C NMR spectroscopy and all peaks are accounted for as expressed in the numbering system exemplified in Fig. 2.3. For **L1**, **L2** and **L4**, **L6**, the molecules are symmetrical and have a line of symmetry bisecting them providing two symmetrically-related groups,(**i**) and (**ii**) in the numbering scheme. Thus for these particular ligands, each of the carbons which are depicted by (**1**-**11**)**i** exist in the same chemical environment as their respective (**1**-**11**)**ii** counterpart as confirmed by ^{13}C NMR spectroscopy. Furthermore, it is clear that there is a break in symmetry for **L3** and **L5**, this is due to the lower symmetry introduced into the final ligand structure by the diamine group. The (**i**) section of the ligand is thus not in the same chemical environment as its (**ii**) counterpart. This is indicated by two resonance peaks appearing for the same carbon presented in the aromatic rings which contain the phenoxy oxygen atom. All ligands have imine carbon resonance peaks in the range of 162-167 ppm and due to symmetry factors, there are two resonance peaks corresponding to each of the imine carbons of **L3** and **L5**, respectively. Ultimately, all six monotopic ligands produced distinct carbon-13 resonances in the appropriate chemical shift regions of which all were accounted for as exemplified in Table 2.3 below. For simplistic purposes, the fully annotated ^{13}C NMR spectrum of the novel ligand **L2 (**Fig 2.5) is presented as a representation of similar spectra obtained for the other monotopic ligands **L1**-**L6**.

TABLE 2.2 ^{1}H NMR spectral data of **L1-L6**[a]

Compound	***CH=N***	**Aromatic region**	**Aliphatic region**		
			-CH-	***-CH$_2$-***	***-CH$_3$***
L1	8.39 (d, *J* = 1.3 Hz, 2H, H^{1})	6.92 (dd, *J* = 8.7, 0.5 Hz, 2H, H^{4}), 7.23 (d, *J* = 2.5 Hz, 2H, H^{7}), 7.36 (dd, *J* = 8.7, 2.6 Hz, 2H, H^{5})	–	2.10 (p, *J* = 6.6 Hz, 2H, H^{13}), 3.71 (td, *J* = 6.6, 1.2 Hz, 4H, H^{12,14})	1.30 (s, 18H, H$^{9-11}$)
L2	8.35 (d, *J* = 1.3 Hz, 2H, H^{1})	6.92 (dd, *J* = 8.6, 0.4 Hz, 2H, H^{4}), 7.25 (d, *J* = 2.5 Hz, 2H, H^{7}), 7.37 (dd, *J* = 8.7, 2.5 Hz, 2H, H^{5})	–	3.49 (d, *J* = 1.2 Hz, 4H, H^{12,14}),	1.08 (s, 6H, H^{15,16}), 1.31 (s, 18H, H$^{9-11}$)
L3	8.19 – 8.39 (m, 2H, H^{1})	6.89 (dd, *J* = 8.7, 2.2 Hz, 2H, H^{4}), 7.22 (dd, *J* = 5.0, 2.5 Hz, 2H, H^{7}), 7.34 (ddd, *J* = 8.7, 4.8, 2.5 Hz, 2H, H^{5})	–	3.72 (d, *J* = 1.2 Hz, 2H, H^{12})	1.29 (d, *J* = 1.8 Hz, 18H, H$^{9-11}$), 1.42 (s, 6H, H^{14,15})
L4	8.64 (s, 2H, H^{1})	6.99 (d, *J* = 8.6 Hz, 2H, H^{4}), 7.23 (dd, *J* = 5.9, 3.4 Hz, 2H, H^{13,16}), 7.33 (dd, *J* = 5.9, 3.4 Hz, 2H, H^{14,15}), 7.35 (d, *J* = 2.5 Hz, 2H, H^{7}), 7.41 (dd, *J* = 8.7, 2.6 Hz, 2H, H^{5})	–	–	1.32 (s, 18H, H$^{9-11}$)
L5	8.63 (s, 1H, H^{1}), 8.64 (s, 1H, H^{1})	6.98 (d, *J* = 4.5 Hz, 1H, H^{4}), 7.00 (d, *J* = 4.5 Hz, 1H, H^{4}), 7.04 (m, 1H, H^{14}), 7.14 (m, 2H, H^{13,16}) 7.35 (d, *J* = 5.3 Hz, 1H, H^{7}), 7.36 (d, *J* = 5.3 Hz, 1H, H^{7}), 7.41 (m, 2H, H^{5})	–	–	1.32 (s, 18H, H$^{9-11}$), 2.43 (s, 3H, H^{18})
L6	8.25 (s, 2H, H^{1})	6.82 (d, *J* = 8.7 Hz, 2H, H^{4}), 7.11 (d, *J* = 2.5 Hz, 2H, H^{7}), 7.23-7.31 (m, 2H, H^{5})	3.30 (dt, 2H, H^{12,17})	1.45-1.69 (m, 4H, H^{14,15}), 1.86 (dt, *J* = 19.9, 13.5 Hz, 4H, H^{13,16})	1.23 (s, 18H, H$^{9-11}$)

[a] Spectra run in $CDCl_3$ at 25 °C. Chemical shifts reported as δ ppm values, referenced relative to the residual solvent peak. Superscripts denote protons as per numbering scheme (Fig. 2.3)

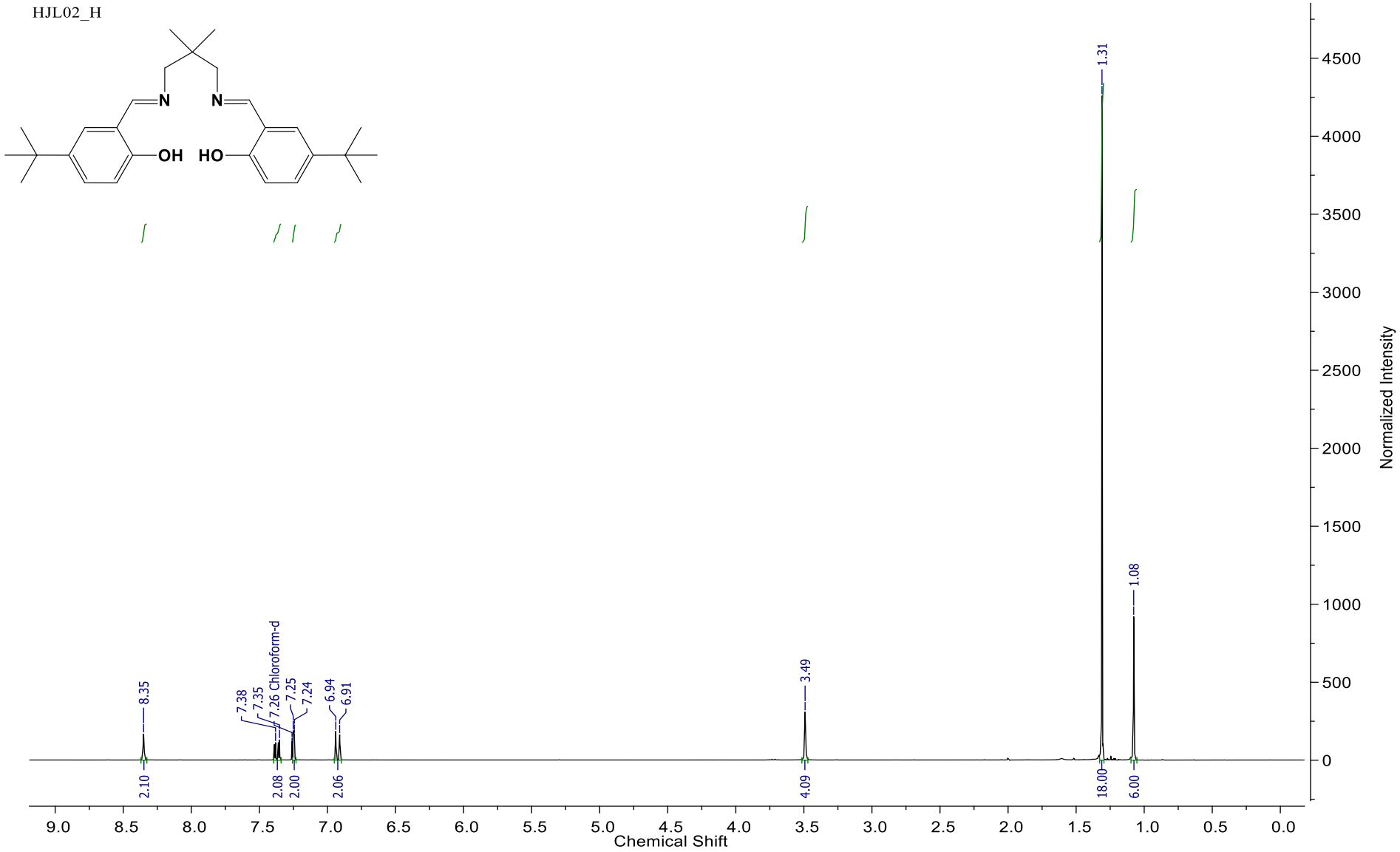

FIGURE 2.4 ^{1}H NMR spectrum of **L2** recorded in $CDCl_3$ at 25 °C

TABLE 2.3 ^{13}C NMR spectral data of **L1-L6**[a]

Compound	CH=N	Aromatic region	Aliphatic region			
			-C-	-CH-	-CH$_2$-	-CH$_3$
L1	165.91$^{(1)}$	116.63$^{(4)}$, 118.15$^{(2)}$, 127.81$^{(7)}$, 129.73$^{(5)}$, 141.48$^{(6)}$, 158.89$^{(3)}$	34.13$^{(8)}$	–	31.99$^{(13)}$, 56.97$^{(12,14)}$	31.59$^{(9-11)}$
L2	166.15$^{(1)}$	116.62$^{(4)}$, 118.13$^{(2)}$, 127.86$^{(7)}$, 129.78$^{(5)}$, 141.45$^{(6)}$, 159.01$^{(3)}$	34.13$^{(8)}$, 36.44$^{(13)}$	–	68.35$^{(12,14)}$	25.54$^{(15,16)}$, 31.59$^{(9-11)}$
L3	[161.99, 166.97]$^{(1i-ii)}$	[116.59, 116.70]$^{(4i-ii)}$, [118.07,118.19]$^{(2i-ii)}$, [128.06, 128.18]$^{(7i-ii)}$, [129.66, 129.89]$^{(5i-ii)}$, [141.27, 141.44]$^{(6i-ii)}$, [158.90, 159.12]$^{(3i-ii)}$	34.10$^{(8i-ii)}$, 60.41$^{(13)}$	–	70.88$^{(12)}$	25.54$^{(14,15)}$, [31.56, 31.58]$^{(9i-ii,10i-ii,11i-ii)}$
L4	164.17$^{(1)}$	117.26$^{(4)}$, 118.64$^{(2)}$, 119.78$^{(12,17)}$, 127.63$^{(14,15)}$, 128.76$^{(7)}$, 131.01$^{(5)}$, 141.72$^{(13,16)}$, 142.99$^{(6)}$, 159.28$^{(3)}$	34.15$^{(8)}$	–	–	31.56$^{(9-11)}$
L5	[163.31, 164.01]$^{(1i-ii)}$	[117.20, 117.23]$^{(4i-ii)}$, [118.64, 118.70]$^{(2i-ii)}$, 119.33$^{(12)}$, 128.25$^{(14)}$, [128.63, 128.74]$^{(7i-ii)}$, 129.90$^{(16)}$, 130.50$^{(13)}$, [130.77, 130.93]$^{(5i-ii)}$, 137.77$^{(15)}$, 140.30$^{(17)}$, [141.63, 141.67]$^{(6i-ii)}$ [159.22, 159.26]$^{(3i-ii)}$	[34.15, 34.18]$^{(8i-ii)}$	–	–	21.28$^{(18)}$, [31.41, 31.56]$^{(9-11)(i-ii)}$
L6	165.13$^{(1)}$	116.35$^{(4)}$, 118.09$^{(2)}$, 128.03$^{(7)}$, 129.56$^{(5)}$, 141.34$^{(6)}$, 158.73$^{(3)}$	34.03$^{(8)}$	72.94$^{(12,17)}$	24.34$^{(14,15)}$, 33.34$^{(13,16)}$	31.51$^{(9-11)}$

[a] Spectra run in $CDCl_3$ at 25 °C. Chemical shifts reported as δ ppm values, referenced relative to the residual solvent peak. Superscripts denote carbons as per numbering scheme (Fig. 2.3)

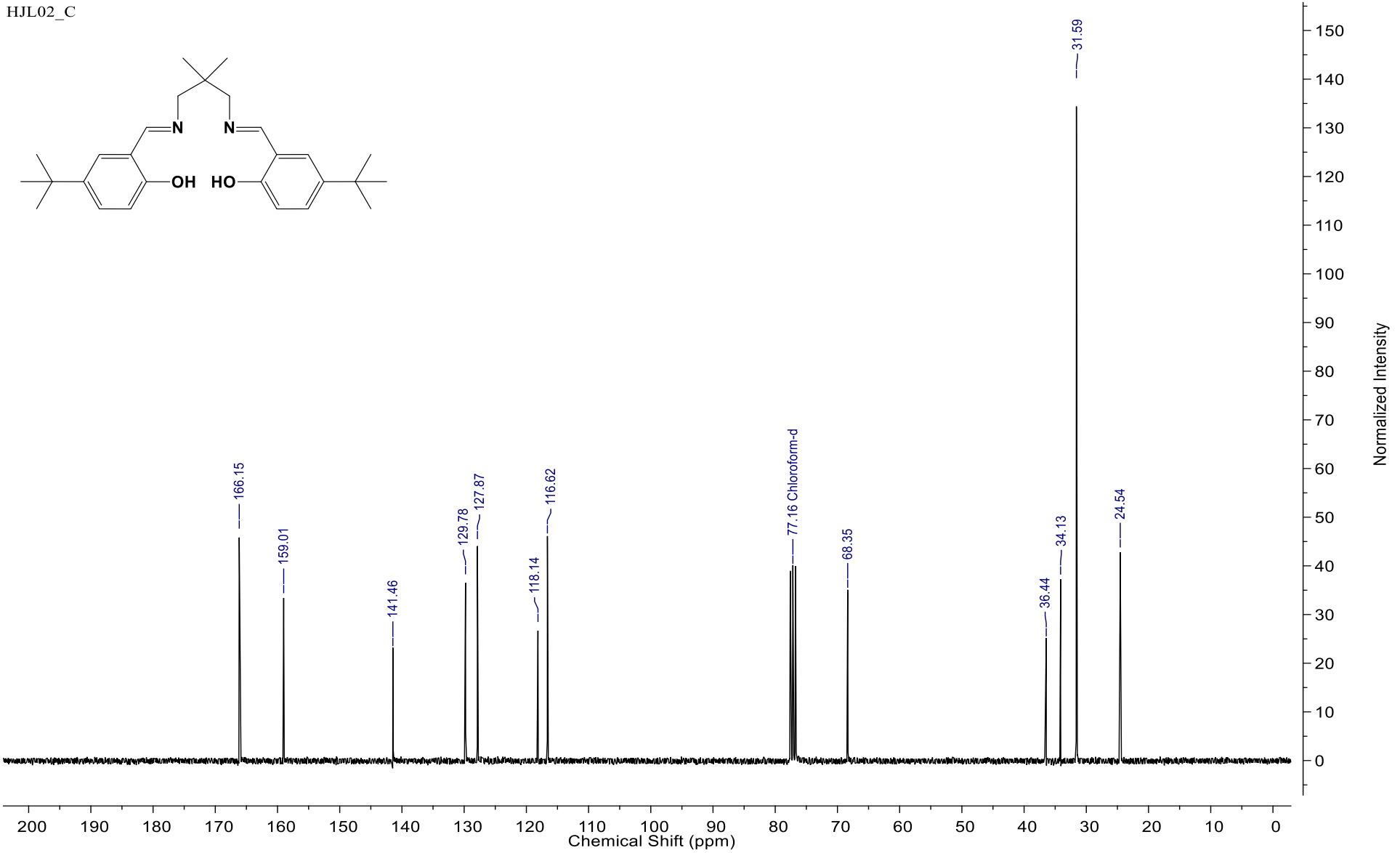

FIGURE 2.5 ^{13}C NMR spectrum of **L2** recorded in $CDCl_3$ at 25 °C

2.2.2.4. Characterisation by Elemental Analysis

Before the extraction performance of **L1**-**L6** could be evaluated, they were further characterised using micro-elemental analysis (EA). EA is considered an unambiguous and powerful characterisation technique that accounts for all analysed elements within a provided sample. The percentage carbon, hydrogen and nitrogen for each ligand product was thus assessed and a good correlation existed between experimentally-determined and calculated percentage values. These values are depicted in Table 2.4 where an average value was deduced for the experimental value since the analysis was conducted in duplicate to minimise error.

TABLE 2.4 Elemental analysis data of **L1**-**L6**

Ligand	Elemental Analysis: Found (Calculated)		
	% C	**% H**	**% N**
L1	76.05 (76.10)	8.52 (8.69)	7.12 (7.10)
L2	76.56 (76.74)	8.98 (9.06)	6.56 (6.63)
L3	76.11 (76.43)	8.33 (8.88)	6.43 (6.86)
L4	78.57 (78.47)	7.00 (7.53)	6.45 (6.54)
L5	78.35 (78.70)	7.64 (7.74)	6.30 (6.33)
L6	77.79 (77.38)	8.63 (8.81)	6.53 (6.49)

2.2.2.5. Characterisation by SCD

2.2.2.5.1. Introduction

The determination of a material's single crystal structure is debatably the most conclusive of all characterisation techniques currently available. SCD is a non-destructive technique that utilizes X-ray radiation to ultimately determine the atomic coordinates of a molecule(s) in the solid-state. Solid-state materials yield characteristic diffraction patterns with reflection intensities for the constituting atoms and analysis of these

parameters allows a 3-D structure determination from which vital information concerning chemical formula, bond lengths and angles as well as absolute configuration can be elucidated.[14]

Although these single crystals elucidate much information pertaining to these complexes in the solid-state, critical information can also be extracted which would also most likely depict what is occurring in solution. This includes information concerning the likely stoichiometry of metal and ligand, as well as prospective intermolecular interactions. For this investigation, numerous experiments were conducted with the ultimate goal of obtaining a single crystal of free ligands **L1**-**L6** and affiliated metal complexes for analysis by SCD techniques. For the majority of these trials, 20 mg of each ligand was used and dissolved in minimal solvent to achieve a supersaturated solution for crystallisation. The dissolution process was abetted with vigorous stirring and when necessary, elevated temperatures were applied. Once the supersaturated solution was attained, the growth of single crystals was promoted through either slow cooling or slow evaporation, as previously mentioned, the rate of these processes was crucial to obtaining single crystals of sufficient quality to be successfully characterised using SCD analysis. Another method included a vapour-diffusion technique, which entailed the preparation of a saturated solution housing the free ligand and a more volatile solvent would diffuse and interact with the solution resulting in a slow crystallisation process, provided the free ligand has poor solubility in the volatile solvent.

In the cases of the affiliated metal complexes, each of the free ligands **L1-L6** (20 mg) was reacted with the appropriate metal (II) acetate hydrate in an equimolar ratio (Eq. 2.1) in methanol or ethanol to ultimately yield a crude product which was washed with water and dried under vacuum. The products were then treated similarly to the method of single crystal growth of the free ligands mentioned earlier using polar solvents (mainly alcohols).

$$L + M(OAc)_2 \rightarrow M[L-2H] + 2AcOH \qquad \text{(Eq. 2.1)}$$

L = Free ligand

M = Cu, Ni, Co, Zn, Cd, Pb

In the experiments performed for this investigation, the acquisition of a single crystal of metal-ligand complexes proved challenging and only two of the copious attempts successfully yielded single crystals of a metal bound in the $[N_2O_2]^{2-}$ cavity. Each was analysed using FT-IR (ATR) spectroscopy and mass spectrometry to ensure that the picked single crystal was a good representation of the entire crystal sample.

2.2.2.5.2. Characterisation of free ligands L1 and L2

Single crystals of **L1** and **L2** were successfully prepared by a slow cooling technique in ethanol affording pale orange block-shaped crystals and yellow needle-shaped crystals for **L1** and **L2**, respectively. The crystallographic information pertaining to the data collection for these structures is illustrated in Table 2.5 and their elucidated solid-state structures are exemplified in Fig. 2.6 (**L1**) and Fig. 2.7 (**L2**). The selected bond lengths, bond angles and torsion angles for **L1** and **L2** are depicted in Table 2.6 and 2.7, respectively.

Both ligands possess a propyl chain linking the imine nitrogen atoms, however, the key structural difference is that for **L2**, a dimethyl group is present on the second carbon of this propyl chain. For this reason, a comparative analysis of their single crystal structures was viable. Moreover, these determined structures offer a framework to facilitate studies regarding the ensuing geometric changes which occur upon coordination to a metal ion.

TABLE 2.5 SCD data collection for **L1** and **L2**

Data Collection				
	L1		**L2**	
Chemical Formula	$C_{25}H_{34}N_2O_2$		$C_{27}H_{38}N_2O_2$	
F_w	394.56		422.61	
Melting Point (°C)	76.0-76.9		111-115	
Crystal Systems	Triclinic		Monoclinic	
Space Group	P î		P 2_1/n	
Unit Cell Dim. (Å, deg)	a = 6.093(4)	α = 96.867(9)	a = 16.9023(14)	α = 90.00
	b = 10.228(7)	β = 97.138(9)	b = 6.08866(5)	β = 107.7600(10)
	c = 17.960(13)	γ = 90.121(9)	c = 25.293(2)	γ = 90.00
Refinement method	Direct		Direct	
Temp (K)	100(2)		100(2)	
ρ (g/cm^{-3})	1.189		1.133	
F_{000}	428		920	
Z	2		4	
Vol (Å^3)	1102.5(14)		2478.0(4)	
Absorption coefficient (μ)	0.075		0.071	
Reflns collected	4793		5702	
Max sin[θ/λ] (Å^{-1}) with completeness ~ 99 %	0.970		0.998	
Independent reflns	2394 [R_{int} = 0.0964]		6350 [R_{int} = 0.0393]	
GOF on F^2	1.066		1.043	
θ range for data collection	2.19 to 28.29		1.69 to 28.56	
Restraints/Paramet.	0/273		0/290	
Final R indices [*I* > 2σ(*I*)]	R1 = 0.0964, wR2 = 0.3175		R1 = 0.0393, wR2 = 0.0957	
R indices (all data)	R1 = 0.1171, wR2 = 0.3313		R1 = 0.0476, wR2 = 0.1017	
Miller index ranges	-7 ≤ h ≤ 7, -13 ≤ k ≤ 12, -23 ≤ l ≤ 23		-21 ≤ h ≤ 22, -7 ≤ k ≤ 8, -30 ≤ l ≤ 32	
Largest diff. peak/hole (eA^{-1})	0.692/-0.530		0.293/-0.203	

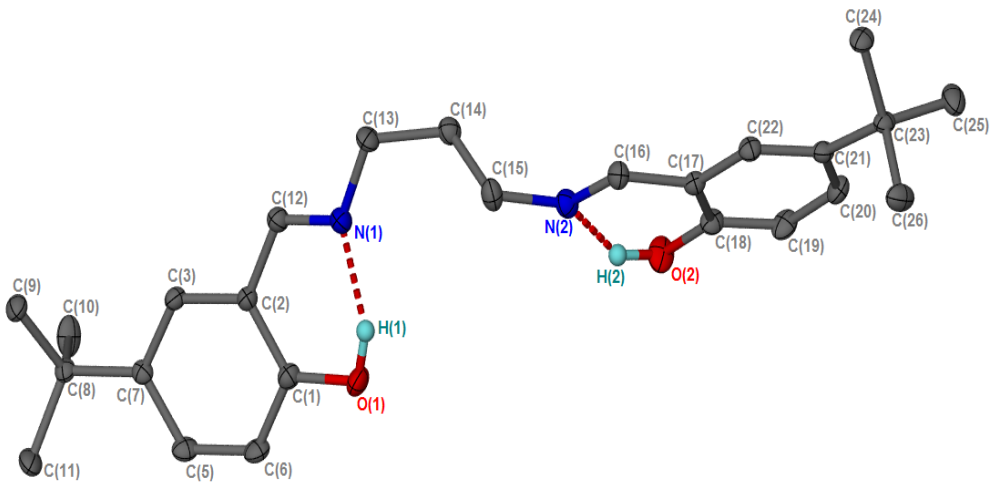

FIGURE 2.6 Solved structure of **L1** displaying the atomic labelling. Displacement ellipsoids are drawn at the 50 % probability level. Hydrogens not involved in intramolecular bonding are excluded for simplicity.

It was found that in both structures, intramolecular hydrogen bonding existed between the phenolate protons and imine nitrogen atoms on either side of the molecules. This is portrayed in the determined structures of **L1** (Fig. 2.6) and **L2** (Fig. 2.7). Confirmation of this interaction was achieved by measurement of the N··O distances which were shorter than 3.07 Å, the sum of the van der Waals radii for nitrogen and oxygen.[15] For **L1**, the N1··O1 and N2··O2 distances corresponded to 2.597 and 2.587 Å, respectively, whereas for **L2** these distances were 2.578 and 2.616 Å, respectively. The measured angles of O-H··N in both structures were in the range of 147 – 157°.

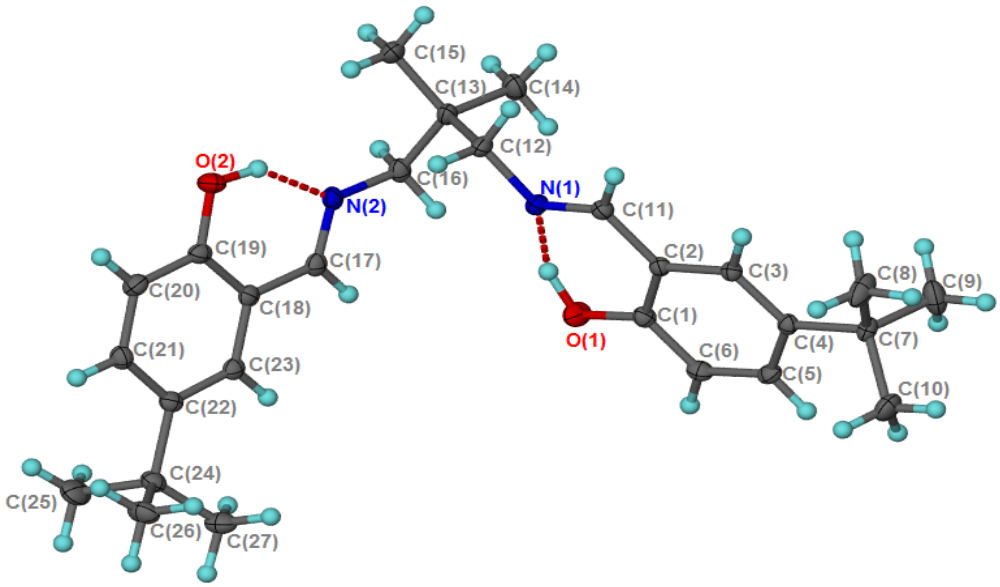

FIGURE 2.7 View of **L2** displaying the atomic numbering. Displacement ellipsoids are drawn at the 50 % probability level.

For both compounds, it is apparent that the enolimine tautomer is favoured over the ketamine tautomer. This is demonstrated by the C1-O1 and C18-O2 bond distances of **L1** which are 1.345(5) Å and 1.346(5) Å, respectively. These distances are compatible with typical C-O single bond lengths.[16] The same can be said for **L2**, having C1-O1 and C19-O2 bond distances of 1.3567(13) and 1.3515(13) Å, respectively. With respect to the imine groups, **L1** has C12-N1 and C15-N2 bond lengths of 1.275(5) and 1.461(5) Å, respectively. These distances correlate to typical C=N double bond lengths. Likewise, **L2** has C11-N1 and C17-N2 bond distances of 1.2792(13) and 1.2799(14) Å, respectively.

The solid-state structure of **L2** adopts an almost *cis* conformation with the two methyl groups positioned on the same side of the molecule. The phenyl rings are slightly twisted and do not lie in the same plane as a result of electron-electron repulsion of the oxygen lone electrons. An additional means of demonstrating these conformational differences is by assessing the O··O distances in each structure.[16] These distances were found to be 5.913 Å for **L1** and 6.890 Å for **L2**, indicating the phenolate oxygen atoms are further apart for **L2**. Finally, it can be postulated that with the current, determined geometries of **L1** and **L2**, coordination of a metal ion in the N_2O_2 cleft is unlikely due to these O··O distances being too far apart to effectively accommodate the metal ion.

TABLE 2.6 Selected bond lengths, bond angles and torsion angles of free ligand **L1**

Bond Lengths (Å)				**Bond Angles (°)**				**Torsion angle (°)**	
C_{18}-O_2	1.346(5)	C_1-O_1	1.345(5)	C_{16}-N_2-C_{15}	119.3(3)	C_{12}-N_1-C_{13}	118.3(3)	N_1-C_{13}-C_{14}-C_{15}	-74.3(4)
C_{16}-N_2	1.273(5)	C_{12}-N_1	1.275(5)	N_2-C_{15}-C_{14}	111.4(3)	N_1-C_{13}-C_{14}	109.7(3)	N_2-C_{15}-C_{14}-C_{13}	165.0(3)
N_2-C_{15}	1.461(5)	N_1-C_{13}	1.470(5)	C_{13}-C_{14}-C_{15}	111.6(3)	O_2-C_{18}-C_{17}	122.2(3)		
C_{17}-C_{16}	1.469(5)	C_2-C_{12}	1.468(5)	O_1-C_1-C_2	122.2(3)	N_2-C_{16}-C_{17}	121.1(4)		
C_{13}-C_{14}	1.527(5)	C_{14}-C_{15}	1.519(5)	N_1-C_{12}-C_2	121.2(4)	O_1-H_1··N_1	154		
				O_2-H_2··N_2	147				

TABLE 2.7 Selected bond lengths, bond angles and torsion angle of free ligand **L2**

Bond Lengths (Å)				**Bond Angles (°)**				**Torsion angle (°)**	
C_1-O_1	1.357(13)	C_{19}-O_2	1.352(13)	C_{11}-N_1-C_{12}	119.8(10)	C_{17}-N_2-C_{16}	119.0(10)	N_1-C_{12}-C_{13}-C_{16}	61.15(12)
C_{11}-N_1	1.279(13)	C_{17}-N_2	1.280(14)	N_1-C_{12}-C_{13}	111.5(9)	N_2-C_{16}-C_{13}	112.1(9)	N_2-C_{16}-C_{13}-C_{12}	60.51(12)
N_1-C_{12}	1.460(14)	N_2-C_{17}	1.537(15)	C_{16}-C_{13}-C_{12}	110.4(9)	O_1-C_1-C_2	121.6(10)		
C_2-C_{11}	1.462(14)	C_{18}-C_{17}	1.462(15)	O_2-C_{19}-C_{18}	122.6(10)	N_1-C_{11}-C_2	121.5(10)		
C_{16}-C_{13}	1.537(16)	C_{13}-C_{12}	1.537(15)	N_2-C_{17}-C_{18}	121.7(10)	O_2-H_1··N_2	149		
				O_1-H_2··N_1	157				

2.2.2.5.3. Characterisation of L3

Yellow, flat block-shaped single crystals of free ligand **L3** were successfully procured from a slow cooling method and analysed using SCD. Numerous attempts were made to acquire a single crystal of a complex of **L3**, unfortunately, all attempts recovered poor quality crystals which could not be studied using this characterisation technique. The crystallographic data relevant to **L3** can be found in Table 2.8.

TABLE 2.8 SCD data collection for **L3**

	L3
Chemical Formula	$C_{26}H_{36}N_2O_2$
F_w	408.58
Melting Point (°C)	120-122
Crystal Systems	Monoclinic
Space Group	P $2_1/n$
Unit Cell Dim. (Å, deg)	a = 5.916(3) α = 90.00 b = 19.157(10) β = 99.344(8) c = 10.354(5) γ = 90.00
Refinement method	Direct
Temp (K)	100(2)
ρ (g/cm^{-3})	1.166
F_{000}	440
Z	2
Vol (Å^3)	1157.8(10)
Absorption coefficient (μ)	0.073
Reflns collected	2684
Max sin[θ/λ] (Å^{-1}) with completeness ~ 99 %	0.966
Independent reflns	672 [R_{int} = 0.0667]
GOF on F^2	0.966
θ range for data collection	2.13 to 28.12
Restraints/Paramet.	0/152
Final R indices [*I* > 2*σ*(*I*)]	R1 = 0.0667, wR2 = 0.1623
R indices (all data)	R1 = 0.1416, wR2 = 0.2052
Miller index ranges	-7 ≤ h ≤ 6, -25 ≤ k ≤ 18, -13 ≤ l ≤ 13
Largest diff. peak/hole (eA^{-1})	0.275/-0.230

It was found that the asymmetric unit possessed half of the molecule and thus the fragment was grown using symmetry to afford the structure seen in Fig. 2.8. Important to note, is that the molecule appears to have two dimethyl moieties between the imine groups which is a result of it being generated by symmetry. Therefore, only geometric measurements could be made for the labelled atoms in Fig. 2.8.

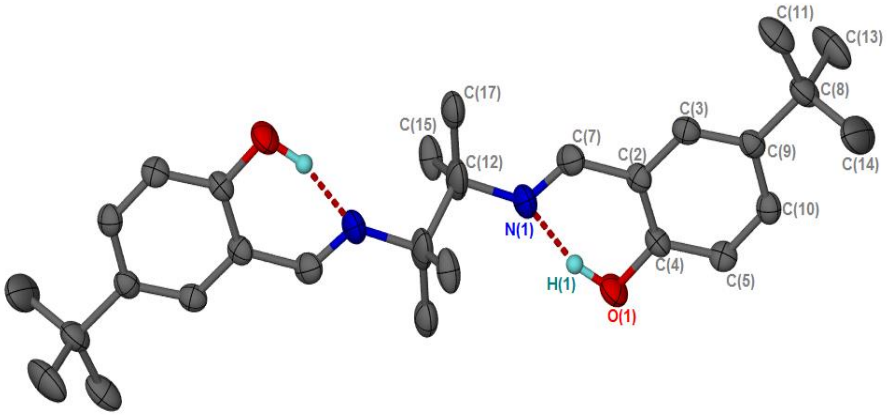

FIGURE 2.8 Solid-state structure of **L3** displaying the atomic numbering

Indication of intramolecular hydrogen bonding between the phenolate proton and imine nitrogen was found from geometric calculations using the program PLATON. This afforded the distance of 2.619 Å between N1··O1 and an angle of 155° for O1-H1··N1 which is consistent with intramolecular hydrogen bonding in such ligand systems. The enolimine tautomer is prevalent over its ketamine form with the C4-O1 bond length measured at 1.359(3) Å. Lastly, the C-N bond distance (C7-N1) was characteristic of a double bond having a length of 1.476(3) Å. The selected bond lengths, bond angles and torsion angles for the structure are reported in Table 2.9.

TABLE 2.9 Selected bond lengths, bond angles and torsion angle of free ligand **L3**

Bond Lengths (Å)				**Bond Angles (°)**				**Torsion angles (°)**	
C_4-O_1	1.359(3)	C_7-N_1	1.270(3)	C_7-N_1-C_{12}	119.3(3)	C_2-C_7-N_1	122.8(3)	C_4-C_2-C_7-N_1	1.3(4)
N_1-C_{12}	1.476(3)	C_2-C_7	1.454(3)	O_1-C_4-C_2	121.8(2)	O_2-H_2··N_1	165	O_1-C_4-C_2-C_7	0.0(4)
				O_1-H_1··N_1	155				

2.2.2.5.4. Characterisation of L4 and Ni[L4-2H]

Single crystals of **L4** were attained by slow evaporation of ethanol yielding pale orange block-shaped crystals and using the same method, a nickel complex of the same ligand (**Ni[L4-2H]**) yielded dark-red cuboidal single crystals. Each was subjected to SCD analysis where Table 2.10 provides the crystallographic data concerning the refinement of these structures, which are in turn, illustrated in Fig. 2.9 (**L4**) and Fig. 2.10 (**Ni[L4-2H]**).

TABLE 2.10 SCD data collection for **L4** and **Ni[L4-2H]**

Data Collection				
	L4		**Ni[L4-2H]**	
Chemical Formula	$C_{28}H_{32}N_2O_2$		$C_{28}H_{30}N_2O_2Ni$	
F_w	428.57		485.25	
Melting Point (°C)	176-178			
Crystal Systems	Monoclinic		Orthorhombic	
Space Group	P 2_1/c		P $2_12_12_1$	
Unit Cell Dim. (Å, deg)	a = 13.9552(16)	α = 90.00	a = 18.219(2)	α = 90
	b = 27.142(3)	β = 99.736(2)	b = 22.127(3)	β = 90
	c = 6.2454(7)	γ = 90.00	c = 33.507(4)	γ = 90
Refinement method	Direct		Direct	
Temp (K)	104(2)		100(2)	
ρ (g/cm^{-3})	1.221		1.0694	
F_{000}	920		4321.3662	
Z	4		4	
Vol (Å^3)	2331.5(5)		13507(3)	
Absorption coefficient (μ)	0.077		0.736	
Reflns collected	5562		15967	
Max sin[θ/λ] (Å^{-1}) with completeness ~ 99 %	0.998		0.9992	
Independent reflns	1656 [R_{int} = 0.0511]		9837 [R_{int} = 0.1511]	
GOF on F^2	1.002		3.561	
θ range for data collection	1.66 to 28.30		1. 10 to 21.73	
Restraints/Paramet.	0/297		0/628	
Final R indices [*I* > 2σ(*I*)]	R1 = 0.0511, wR2 = 0.1083		R1 = 0.1511, wR2 = 0.4167	
R indices (all data)	R1 = 0.0909, wR2 = 0.1257		R1 = 0.1585, wR2 = 0.4251	
Miller index ranges	-18 ≤ h ≤ 18, -35 ≤ k ≤ 33, -4 ≤ l ≤ 8		-18 ≤ h ≤ 18, -22 ≤ k ≤ 23, -34 ≤ l ≤ 34	
Largest diff. peak/hole (eA^{-1})	0.243/-0.274		4.3129/-0.9877	

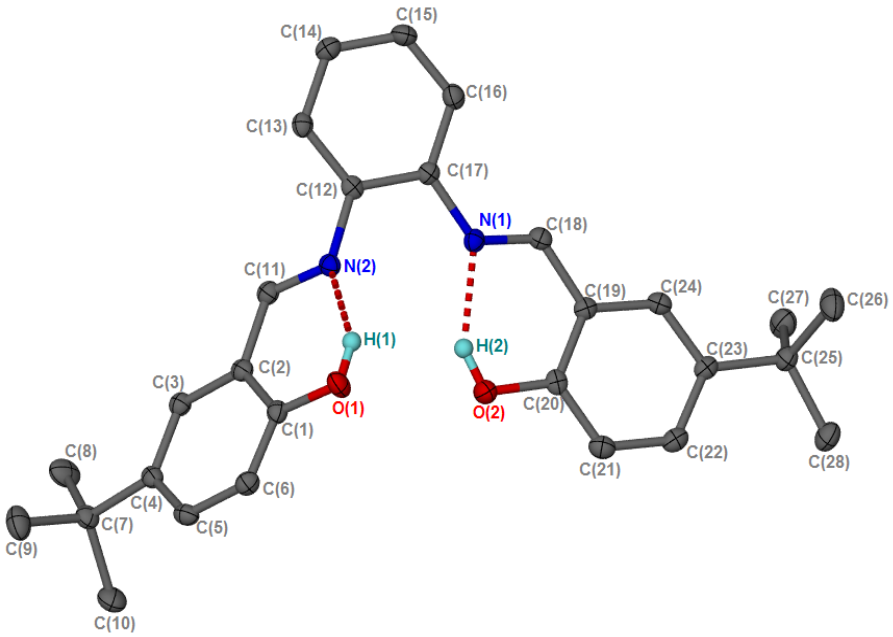

FIGURE 2.9 Visual representation of **L4** showing the atomic numbering. Displacement ellipsoids are drawn at the 50 % probability level. Hydrogen atoms not involved in intramolecular bonding are omitted for clarity.

The solid-state structure of **L4** illustrates intramolecular hydrogen bonding between the phenolate protons and the nitrogen which was identified using the program PLATON. The distance between the nitrogens and oxygens involved in the hydrogen bonding interaction are 2.595(3) Å (N2··O1) and 2.599(4) Å (N1··O2), which is less than their accumulative van der Waals radii.[15] The angles of O1-H1··N2 and O2-H2··N1 were 148° and 165°, respectively.

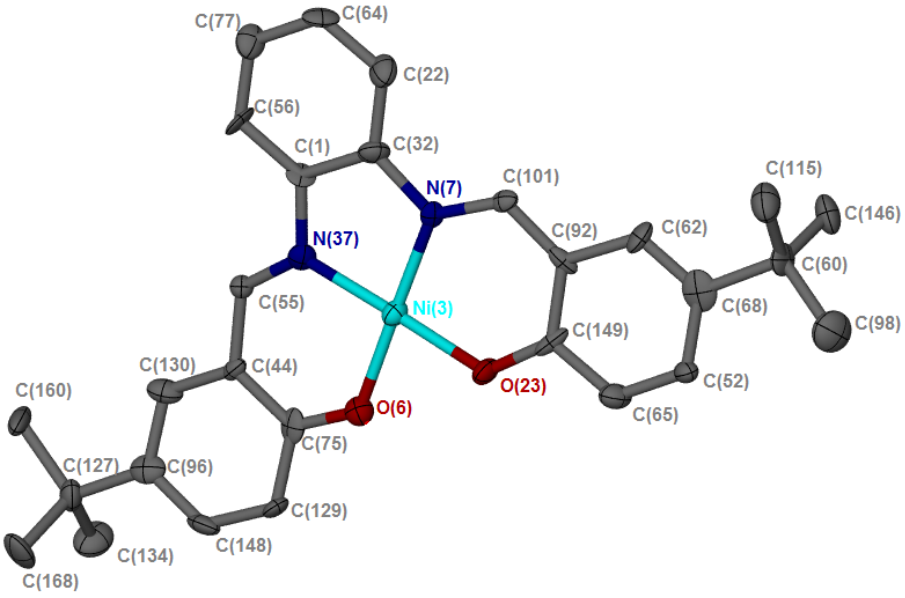

FIGURE 2.10 Visual representation of **Ni[L4-2H]** showing the atomic numbering. Displacement ellipsoids are drawn at the 50 % probability level. Hydrogen atoms and co-crystallised solvent molecules are omitted for clarity.

Looking at the solid-state structure of the Ni complex, there is a clear adjustment in the spatial orientation of the phenyl groups enabling **L4** to accommodate the nickel ion in the donor cavity. This was recognised by the change in distances between O··O in each of the structures which decreased from 3.368 Å (uncoordinated) to 2.498 Å (coordinated). The torsion angles N2-C12-C17-N1 (**L4**) and N37-C1-C32-N7 (**Ni[L4-2H]**) undergo a slight change from 6.08° to 1.71° and the N··O distances increase very slightly to provide room for the nickel ion in the inner coordination sphere.

The complex demonstrates a slightly-distorted square planar geometry around the central metal ion. The distortion from ideal square planar is shown by the angle of C75··O6··O23 (168.1°) which is less than the ideal value of 180°, indicating that the two phenolic mean planes are unable to completely achieve the flat conformation.[18] This is further signified by the O-Ni-O (84.6(5)°) and N-Ni-N (87.7(6)°) which are smaller than 90°. The Ni-N and Ni-O bond lengths range from 1.838(14) Å and 1.882(14) Å which are typical for high spin Ni(II) complexes[19, 20] and in agreement with the measurements disclosed by Byun and co-workers for a closely-related Ni-salen complex.[18]

TABLE 2.11 Selected bond lengths, bond angles and torsion angle of free ligand **L4**

Bond Lengths (Å)				**Bond Angles (°)**				**Torsion angle (°)**	
C_{20}-O_2	1.352(18)	C_1-O_1	1.353(18)	C_{18}-N_1-C_{17}	122.7(15)	C_{11}-N_2-C_{12}	121.4(14)	N_1-C_{17}-C_{12}-N_2	6.08
C_{18}-N_1	1.282(2)	C_{11}-N_2	1.287(2)	N_1-C_{17}-C_{12}	115.5(14)	N_2-C_{12}-C_{17}	118.3(14)		
N_1-C_{17}	1.416(2)	N_2-C_{12}	1.418(2)	O_2-C_{20}-C_{19}	122.4(15)	O_1-C_1-C_2	122.2(15)		
C_{19}-C_{18}	1.450(2)	C_2-C_{11}	1.453(2)	C_{19}-C_{18}-N_1	121.3(16)	C_2-C_{11}-N_2	120.3(15)		
C_{17}-C_{12}	1.402(2)			O_1-H_1··N_2	146	O_2-H_2··N_1	146		

TABLE 2.12 Selected bond lengths, bond angles and torsion angle of **Ni[L4-2H]**

Bond Lengths (Å)				**Bond Angles (°)**				**Torsion angle (°)**	
C_{149}-O_{23}	1.290(2)	C_{75}-O_6	1.330(2)	C_{101}-N_7-C_{32}	121.7(15)	C_{55}-N_{37}-C_1	116.5(15)	N_7-C_{32}-C_1-N_{37}	1.71
C_{101}-N_7	1.230(2)	C_{55}-N_{37}	1.330(2)	N_7-C_{32}-C_1	110.6(15)	N_{37}-C_1-C_{32}	116.5(15)		
N_7-C_{32}	1.530(2)	N_{37}-C_1	1.420(2)	O_{23}-C_{149}-C_{92}	120.6(16)	O_6-C_{75}-C_{44}	123.3(16)		
C_{92}-C_{101}	1.370(2)	C_{44}-C_{55}	1.510(3)	C_{92}-C_{101}-N_7	126.6(16)	C_{44}-C_{55}-N_{37}	119.5(16)		
C_{32}-C_1	1.400(3)	O_{23}-Ni_3	1.868(11)	N_7-Ni_3-O_6	174.4(6)	N_{37}-Ni_3-O_{23}	178.1(6)		
O_6-Ni_3	1.843(12)	N_7-Ni_3	1.882(14)	O_6-Ni_3-O_{23}	84.6(5)	N_{37}-Ni_3-N_7	87.7(6)		
N_{37}-Ni_3	1.838(14)			N_7-Ni_3-O_{23}	92.5(6)				

2.2.2.5.5. Characterisation of L6 and Cu[L6-2H]

Single crystals of **L6** and **Cu[L6-2H]** were obtained from ethanol via a slow evaporation process. This technique yielded bright yellow elongated bar/cuboidal-shaped crystals of **L6** whilst in the case of **Cu[L6-2H]**, they were isolated as dark grey needle-like crystals. **L6** and **Cu[L6-2H]** were analysed using SCD techniques, with the details concerning their crystallographic information provided in Table 2.13. Furthermore, their elucidated solid-state structures are seen in Fig. 2.11 and Fig. 2.12, respectively.

TABLE 2.13 SCD data collection for **L6** and **Cu[L6-2H]**

Data Collection				
	L6		**Cu[L6-2H]**	
Chemical Formula	$C_{28}H_{38}N_2O_2$		$C_{28}H_{36}CuN_2O_2$	
F_w	434.62		496.15	
Melting Point (°C)	165-170		Not determined	
Crystal Systems	Monoclinic		Monoclinic	
Space Group	C2/c		C2/c	
Unit Cell Dim. (Å, deg)	a = 29.919(14)	α = 90.00	a = 25.911(9)	α = 90.00
	b = 8.643(4)	β = 94.096(7)	b = 10.290(3)	β = 90.499(4)
	c = 19.521(9)	γ = 90.00	c = 11.300(4)	γ = 90.00
Refinement method	Direct		Patterson	
Temp (K)	173(2)		100(2)	
ρ (g/cm^{-3})	1.147		1.098	
F_{000}	1888		1060	
Z	8		4	
Vol (Å^3)	5035(4)		3012.9(17)	
Absorption coefficient (μ)	0.071		0.747	
Reflns collected	5814		8335	
Max sin[θ/λ] (Å^{-1}) with completeness ~ 99 %	0.998		0.996	
Independent reflns	3067 [R_{int} = 0.0973]		3116 [R_{int} = 0.0517]	
GOF on F^2	1.093		0.908	
θ range for data collection	2.09 to 28.26		1.57 to 26.52	
Restraints/Paramet.	0/329		0/183	
Final R indices [$I > 2\sigma(I)$]	R1 = 0.0973, wR2 = 0.2544		R1 = 0.0517, wR2 = 0.13	
R indices (all data)	R1 = 0.1358, wR2 = 0.2858		R1 = 0.072, wR2 = 0.1457	
Miller index ranges	-39 ≤ h ≤ 30, -11 ≤ k ≤ 11, -24 ≤ l ≤ 23		-32 ≤ h ≤ 22, -12 ≤ k ≤ 12, -13 ≤ l ≤ 14	
Largest diff. peak/hole (eA^{-1})	1.079/-0.913		0.697/-0.504	

In the case of **L6**, the tert-butyl groups were disordered over multiple positions in space and were refined over two positions. One of the tert-butyl groups shows a 60:40 % occupancy ratio with both occupancy sites being refined anisotropically. The second tert-butyl group showed disorder over the entire group and not merely the terminal carbons. The two positions of the tert-butyl group showed a 50:50 % occupancy ratio, with both sites refined anisotropically.

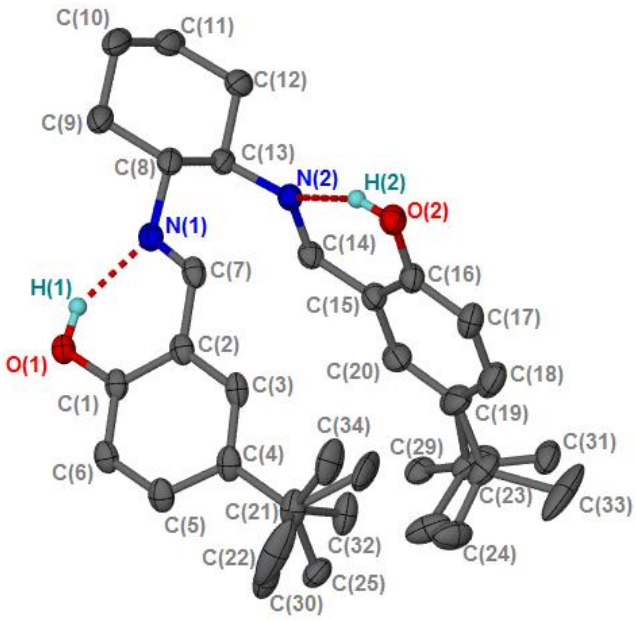

FIGURE 2.11 Visual representation of **L6** showing the atomic numbering. Displacement ellipsoids are drawn at the 50 % probability level. Hydrogens not involved in intramolecular bonding are omitted for clarity.

The solid-state structure of **L6** (Fig 2.11) demonstrates the presence of intramolecular hydrogen bonding with an average distance of 2.6 Å and angles for O-H··N (see Table 2.14) typical of such interactions.[15] This, along with the ligand's attempt at relieving lone pair-lone pair repulsion between the phenolate oxygens give the ligand its inherent trans-orientation. The inner coordination sphere then seems to possess a cavity suited to a metal preferring a tetrahedral geometry.

The two halves of the of the complex **Cu[L6-2H] (**Fig. 2.12**)** have the same geometry and are related by a twofold axis running through Cu and the mid-point of the bond C8-C8*. The geometry around the copper in **Cu[L6-2H]** is square planar slightly distorted toward tetrahedral. The Cu-N and Cu-O bond distances correlate well to those reported by Thomas *et al* for a closely-related salen Cu complex.[21] The angles O-Cu-O*, O-Cu-N, O*-Cu-N* and N-Cu-N* all differ only slightly from 90° and the O-Cu-N* and O*-Cu-N angles are close to 180° (See Table 2.15).

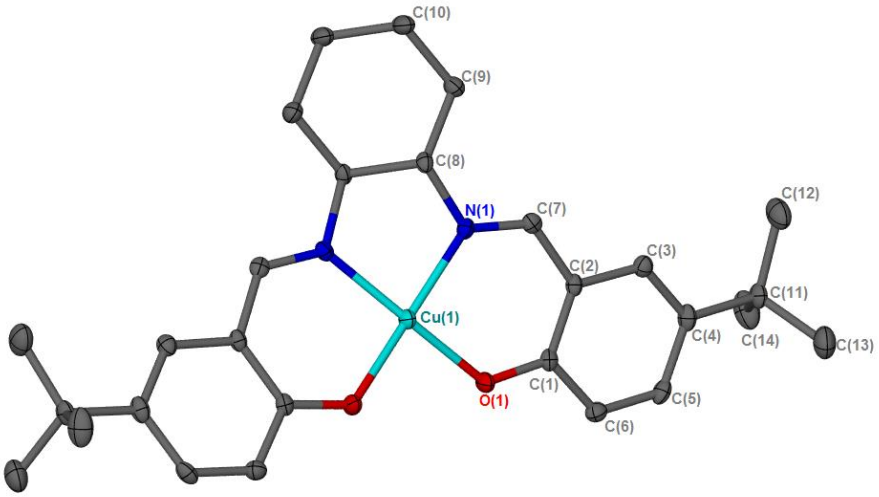

FIGURE 2.12 Visual representation of **Cu[L6-2H]** showing the atomic numbering. Displacement ellipsoids are drawn at the 50 % probability level. Hydrogen atoms and co-crystallised solvent molecules are omitted for clarity.

Comparing Fig. 2.11 and Fig. 2.12, it can be perceived that the ligand has undergone a conformational rearrangement to successfully coordinate to the metal which is marked by the adjustment of the O··O distances from 6.487 Å to 2.718 Å. What was also interesting to observe was the drastic decrease in the C14-N2-C13 bond angle of **L4** from 119.7° to 84.3° (C7-N1-C8) for the Cu complex. Additionally, the torsion angle N1-C8-C13-N2 for **L4** changes from -63.6° to 48.8° once coordination to the Cu(II) ion has occurred. These differences indicate the extent to which the inner coordination sphere adjusts to accommodate the metal ion. The selected bond lengths, bond angles and torsional angles for the solid-state structures of **L6** and **Cu[L6-2H]** can be found in Table 2.14 and Table 2.15, respectively.

TABLE 2.14 Selected bond lengths, bond angles and torsion angle of free **L6**

Bond Lengths (Å)				**Bond Angles (°)**				**Torsion angle (°)**	
C_{16}-O_2	1.351(4)	C_1-O_1	1.355(3)	C_{14}-N_2-C_{13}	119.5(2)	C_7-N_1-C_8	118.3(2)	N_2-C_{13}-C_8-N_1	-63.6(3)
C_{14}-N_2	1.278(4)	C_7-N_1	1.277(4)	N_2-C_{13}-C_8	108.2(2)	N_1-C_8-C_{13}	109.4(2)		
N_2-C_{13}	1.451(3)	N_1-C_8	1.465(4)	O_2-C_{16}-C_{15}	122.0(3)	O_1-C_1-C_2	121.2(3)		
C_{15}-C_{14}	1.452(4)	C_2-C_7	1.452(5)	C_{15}-C_{14}-N_2	121.9(3)	C_2-C_7-N_1	121.5(3)		
C_{13}-C_8	1.538(5)			O_1-H_1··N_1	148	O_2-H_2··N_2	165		

TABLE 2.15 Selected bond lengths, bond angles and torsion angle of **Cu[L6-2H]**

Bond Lengths (Å)				**Bond Angles (°)**				**Torsion angle (°)**	
C_1-O_1	1.326(3)	C_7-N_1	1.283(3)	C_7-N_1-C_8	121.4(2)	N_1-C_8-C_8^*	105.4(15)	N_1-C_8-C_8^*-N_1^*	48.8
N_1-C_8	1.478(3)	C_2-C_7	1.443(4)	C_2-C_1-O_1	124.3(2)	C_2-C_7-N_1	124.4(2)		
C_8-C_8^*	1.534(5)	O_1^*-Cu_1	1.914(18)	N_1^*-Cu_1-O_1	167.7(8)	N_1-Cu_1-N_1^*	84.24(12)		
O_1-Cu_1	1.914(18)	N_1^*-Cu_1	1.939(2)	N_1-Cu_1-O_1	93.86(8)	O_1-Cu_1-O_1	90.52(11)		
N_1-Cu_1	1.939(2)								

2.2.3. Additional characterisation of Ni[L4-2H] and Cu[L6-2H] by FT-IR (ATR) spectroscopy and mass spectrometry

The residual bulk crystalline samples from which the three respective single crystals originated were characterised using FT-IR (ATR) spectroscopy and ESI mass spectrometry to make certain that the chosen single crystal was an adequate representation of the entire sample. FT-IR (ATR) spectroscopy indicated a shift of the absorption band of the C=N bond associated with the imine, indicating that coordination via the imine to the metal ion had occurred. As a result of delocalisation of electron density from the imine functional group as a consequence of coordination and hence sharing of electron density of the nitrogen donor atom with the coordinated metal ion, a lower imine absorption frequency is registered. However, unexpectedly, this was not the case with **L4** upon coordination to Ni(II) possibly as a result of the aromatic withdrawing group having some sort of influence on the shift. Table 2.16 below depicts these observed shifts in the imine absorption band for the free ligands **L4** and **L6** in comparison to the metal complexes, **Ni[L4-2H]** and **Cu[L6-2H]**, respectively.

TABLE 2.16 Observed shifts of the imine absorption bands for the free ligands and corresponding metal complexes

Free Ligand	**$V_{C=N}$**	**Metal Complex**	**$V_{C=N}$**
L4	1611.88	**Ni[L4-2H]**	1619.31
L6	1628.00	**Cu[L6-2H]**	1620.75

Positive mode ESI-MS revealed the proton adducts, $[M+H]^+$, of **Ni[L4-2H]** and **Cu[L6-2H]** at 485.1739 *m/z* and 496.2159 *m/z*, respectively. These values correspond well to their predicted spectra with isotopic peaks suggesting the singly-charged adduct.

2.3. Methods and Materials

2.3.1. Solvents and reagents

All chemicals were used as received from various chemical-producing companies and used without further purification. The numerous chemicals used in the above experiments were purchased from the following companies; Fluka: 4-methyl-o-phenylenediamine; Scienceworld: NaOH pellets; Merck: methanol (MeOH), ethanol (EtOH), deuterated chloroform (*d*-$CHCl_3$), conc. H_2SO_4; Sigma-Aldrich: toluene, 4-tertbutylphenol, paraformaldehyde, 1,3-diaminopropane, 2,2-dimethyl-1,3-propanediamine, 1,2-diamino-2-methylpropane, o-phenylenediamine, 1,2-*trans*-diaminocyclohexane, copper (II) acetate monohydrate ($Cu(acetate)_2 \cdot H_2O$) , nickel (II) acetate tetrahydrate ($Ni(acetate)_2 \cdot 4H_2O$), cobalt (II) acetate hexahydrate ($Co(acetate)_2 \cdot 6H_2O$), zinc (II) acetate hexahydrate ($Zn(acetate)_2 \cdot 6H_2O$), cadmium (II) acetate tetrahydrate ($Cd(acetate)_2 \cdot 4H_2O$), lead (II) acetate ($Pb(acetate)_2$).

2.3.2. Instrumentation (applicable to Chapter 3)

All ^1H and ^{13}C nuclear magnetic resonance spectra were obtained using a 300 MHz Varian VNMRS, 400 MHz Varian Unity Inova or 600 MHz Varian Unity Inova NMR instrument using deuterated solvents. Chemical shifts (δ) were recorded using the residual solvent peak or external reference (TMS). All chemical shifts are reported in parts per million and all spectra were obtained at 25 °C. Data was processed using Mestrenova file version 10.0.2. Melting point determination was done using a Stuart Scientific melting point apparatus in open capillaries. Infrared spectra were readily obtained using a Nicolet Avatar 330 FT-IR instrument as neat samples (ATR), in some spectral collection cases, where necessary, the instrument was flushed with N_2 (g) to eliminate the manifestation of CO_2. Standard resolution mass spectrometry was performed by CAF (Central Analytical Facility) at Stellenbosch University using a Waters Synapt G2 spectrometer by direct injection of sample. In

the cases of SCD analysis, X-ray intensity data were collected on a Bruker-Nonius SMART Apex diffractometer equipped with a fine-focus sealed tube and a 0.5 mm Monocap collimator (monochromated Mo-Kα radiation, λ = 0.71073 Å).[22] Samples for EA analysis were done on a Perkin-Elmer 2400 Series II CHNS/O Elemental Analyser at the University of Kwa-Zulu Natal.

2.3.3. Synthesis of salicylaldehyde precursor & monotopic ligands (L1-L6)

2.3.3.1. Synthesis of 5-tert-butyl-2-hydroxybenzaldehyde

Magnesium pellets (11.0 g, 0.450 mol) were added to a two-neck round-bottom flask containing dry methanol (750 mL) over a period of two hours. The round-bottom flask was placed in an oil bath and on the addition of magnesium, the temperature was increased to below boiling point of the solvent to aid dissolution. The reaction was allowed to proceed under these conditions until no more hydrogen gas was released from the mixture. Thereafter, 4-tertbutylphenol (113 g, 0.453 mol) was added to the mixture which was refluxed for about 2 hours at 95 °C. The temperature was maintained at around 65 °C, and following the reflux step, distillation was done, and half of the methanol was distilled off at this temperature. Toluene (650 mL) was then added and distillation continued – the solution maintained a yellow-brown colour. The temperature began to rise towards 95 °C, and at this temperature, paraformaldehyde (69.6 g, 2.31 mol) in toluene (165 mL) was added to the solution in portions over an hour. The solution was left to stir at 95 °C for approximately two hours then cooled to room temperature resulting in a yellow solution. A 10 % H_2SO_4 solution (280 mL) was prepared in a beaker and the yellow solution was added to this. The beaker was placed on a magnetic stirrer and heated to between 30-40 °C for about two hours with stirring. The combined mixture produced two layers which were separated using a separation funnel and the aqueous layer was extracted with toluene (2 × 100 mL). The combined organic layers were washed with 10 % H_2SO_4 (50 mL) and distilled water (100 mL). The organic layer was then isolated and subjected to reduced pressure by using a rotary evaporator. This yielded a pale yellow oil which was subjected to fractional distillation in a fume hood affording the final yellow-colourless oil. Yield = 99.3 g, 73.9 %. **FT-IR** (neat): $\nu_{C=O}$ (1650.56 cm^{-1}); **^{1}H NMR** (600 MHz, $CDCl_3$) δ 9.89 (s, 1H, -C<u>H</u>O), 7.58 (dd, J = 8.7, 2.5 Hz, 1H, C^{Ar}-<u>H</u>), 7.52 (d, J = 2.5 Hz, 1H, C^{Ar}-<u>H</u>), 6.94 (d, J = 8.7 Hz, C^{Ar}-<u>H</u>), 1.33 (s, 9H, -

$C(C\underline{H}_3)_3$; **^{13}C NMR** (600 MHz, $CDCl_3$) δ 196.90 (-$\underline{C}$HO), 159.57 ($\underline{C}^{Ar}$-OH), 142.84 ($\underline{C}^{Ar}$-C$(CH_3)_3$), 134.78 ($\underline{C}^{Ar}$-CHO), 129.85 ($\underline{C}^{Ar}$-H), 126.44 ($\underline{C}^{Ar}$-H), 117.31 ($\underline{C}^{Ar}$- H), 34.18 (-$\underline{C}(CH_3)_3$), 31.34 (-C($\underline{C}H_3)_3$).

2.3.3.2. Synthesis of 2,2'-((1E,1'E)-(propane-1,3-diylbis(azanylylidene))bis(methanylylidene))bis(4-tert-butyl)phenol) (L1)

Roughly two equivalents of 5-tert-butyl-2-hydroxybenzaldehyde (6.46 g, 0.0362 mol, 2 eq.) were combined with 1,3-diaminopropane (1.35 g, 0.0182 mol, 1 eq.) in a two-necked round bottom flask and refluxed in absolute ethanol (90 mL) for approximately 18 hours. The solvent was removed under reduced pressure using a rotary evaporator. The flask containing the crude product was then connected to a high vacuum pump operating at reduced pressure to yield a yellow-like solid. The product was then purified by recrystallisation by re-dissolving in ethanol through heating and stirring for about an hour, followed by slow cooling to room temperature. Following this, the solution was placed in the fridge to allow for further cooling which resulted in the formation of yellow flake-like crystals. The solution remained in the fridge for a week to promote crystal formation. Thereafter, the crystals were isolated from the ethanol and possible starting aldehyde through filtration and washing with cold ethanol (50 mL). The crystals were then left to dry for approximately two days. Yield = 6.77 g, 94.3 %. *Anal.* Found: C, 76.05; H, 8.52; N, 7.12. $C_{25}H_{34}N_2O_2$ requires: C, 76.10; H, 8.69; N, 7.10.

2.3.3.3. Synthesis of 2,2'-((1E,1'E)-(2,2-dimethylpropane-1,3-diyl)bis(azanylylidene))bis(methanylylidene))bis(4-tert-butyl)phenol) (L2)

5-tert-butyl-2-hydroxybenzaldehyde (6.04 g, 0.0339 mol, 2 eq.) was reacted with 2,2-dimethyl-1,3-diaminopropane (1.73 g, 0.0169 mol, 1 eq.) in a two- neck round bottom flask and refluxed in absolute ethanol (90 mL) for roughly 18 hours. The solvent was removed under reduced pressure by using a rotary evaporator and further purified through the use of a high vacuum pump operating at reduced pressure to yield a yellow-white solid. The solid was then re-dissolved in ethanol through heating and stirring for about an hour and then left to cool to room temperature. Following this, the solution was placed in the fridge to further cool the solution yielding yellow-like crystals. The solution remained in the fridge for a few days to promote crystal formation. Thereafter, the crystals were isolated from the ethanol and possible starting aldehyde through filtration and

washed with cold ethanol (50 mL). The resulting crystals were then left to dry for approximately two days. Yield = 4.65 g, 65.1 %. *Anal.* Found: C, 76.56; H, 8.98; N, 6.56 %; $C_{27}H_{38}N_2O_2$ requires: C, 76.74; H, 9.06; N, 6.63 %.

2.3.3.4. Synthesis of 2,2'-((1E,1'E)-(1,1-dimethylethane-1,2-diyl)bis(azanylylidene))bis(methanylylidene))bis(4-tert-butyl)phenol) (L3)

Roughly two equivalents of 5-tert-butyl-2-hydroxybenzaldehyde (6.24 g, 0.0350 mol, 2 eq.) were reacted with 1,1-dimethyl-1,2-diaminoethane (1.54 g, 0.0175 mol, 1 eq.) in a two-necked round bottom flask and refluxed in absolute ethanol (90 mL) for about 15 hours. The solvent was removed *in vacuo* and the flask was then attached to a high vacuum pump operating at reduced pressure to further aid the removal of solvent and volatile impurities. This yielded a viscous orange-yellow oil which solidified over time as residual solvent was removed under reduced pressure. Yield = 6.33 g, 88.4 %. *Anal.* Found: C, 76.11; H, 8.33; N, 6.43 %; $C_{26}H_{36}N_2O_2$ requires: C, 76.43; H, 8.88; N, 6.86 %.

2.3.3.5. Synthesis of 2,2'-((1E,1'E)-(1,2-phenylenebis(azanylylidene))bis(methanylylidene))bis(4-tert-butyl)phenol) (L4)

5-tert-butyl-2-hydroxybenzaldehyde (5.95 g, 0.0334 mol, 2 eq.) was reacted with 1,2-diaminobenzene (1.80 g, 0.0167 mol, 1 eq.) and refluxed in absolute ethanol (90 mL) for approximately 18 hours. The solvent was removed under reduced pressure and subjected to high vacuum distillation to further aid the removal of solvent and volatile impurities to yield an orange-brown solid. The product was then purified by recrystallisation by re-dissolving in absolute ethanol through heating and stirring. Following this, the solution was allowed to cool to room temperature leading to the formation of orange crystals. The solution was left to stand for two days at room temperature to promote crystal formation. Thereafter, the crystals were isolated from the solvent and possible starting aldehyde by filtration using a sinter funnel operating under vacuum. The resulting solid was washed with cold ethanol (50 cm^3) and left to dry at room temperature for a few days. Yield = 6.80 g, 95.2 %. *Anal.* Found: C, 78.57; H, 7.00; N, 6.45 %. $C_{28}H_{32}N_2O_2$ requires: C, 78.47; H, 7.53; N, 6.54 %.

2.3.3.6. Synthesis of 2,2'-((1E,1'E)-(4-methyl-1,2-phenylenebis(azanylylidene))bis(methanylylidene))bis(4-tert-butyl)phenol) (L5)

5-tert-butyl-2-hydroxybenzaldehyde (5.76 g, 0.0323 mol, 2 eq.) was reacted with 1,2-diamino-5-methylbenzene (1.97 g, 0.0161 mol, 1 eq.) and refluxed in absolute ethanol (90 mL) for approximately 18 hours. The solvent was removed under reduced pressure and further purified by high vacuum distillation to yield a brown-orange solid. The solid was purified by recrystallisation by dissolving it in absolute ethanol through heating and stirring for about an hour. The solution was then cooled to room temperature, however, no crystals formed. The desired product was isolated from the ethanol through vacuum filtration and washing with cold ethanol (50 mL). The brown-orange solid which remained was dried by allowing it to stand for two days at room temperature. Yield = 7.02 g, 98.3 %. *Anal.* Found: C, 78.35; H, 7.64; N, 6.30 %. $C_{29}H_{34}N_2O_2$ requires: C, 78.70; H, 7.74; N, 6.33 %.

2.3.3.7. Synthesis of 2,2'-((1E,1'E)-((1S,2S)-cyclohexane-1,2-diylbis(azanylylidene)) bis(methanylylidene))bis(4-tert-butyl)phenol) (L6)

5-tert-butyl-2-hydroxybenzaldehyde (5.74 g, 0.0322 mol, 2 eq.) was added to a two-necked round bottom flask containing absolute ethanol (50 mL), with subsequent dropwise addition of 1,2-*trans*-diaminocyclohexane (1.84 g, 0.0161 mol, 1 eq.). This was allowed to reflux for 18 hours. The reaction was allowed to cool to ambient temperature which resulted in the formation of bright yellow crystals in the flask. The solution was then cooled further on an ice bath to encourage further crystallisation, where after the crystals were filtered off and washed with cold ethanol affording a bright yellow crystalline product. Yield = 6.30 g, 90.1 %. *Anal.* Found: C, 77.79; H, 8.63; N, 6.53 %. $C_{28}H_{38}N_2O_2$ requires: C, 77.38; H, 8.81; N, 6.49 %.

2.3.4. Synthesis of metal complexes suitable for SCD analysis

2.3.4.1. Single crystal synthesis of Ni[L4 – 2H]

L4 (20.0 mg, 0.0467 mmol, 1 eq.) was placed in a sample vial together with Ni(acetate)$_2$·4H$_2$O (8.25 mg, 0.0467 mmol, 1 eq.) and dissolved in approximately 3 mL of absolute ethanol producing a dark brown/black solution. The solution was stirred and heated on a magnetic stirrer hot plate until the solution appeared homogenous. Thereafter the solution was pipetted through cotton wool into a small vial and allowed to cool to room temperature. It was found that no crystals were yet produced and thus the vial was sealed using parafilm and placed in a refrigerator to aid crystal growth through a slow cooling strategy. After about ten days, dark brown/black needle-like crystals were procured which were analysed by SCD. **FT-IR (ATR)** neat: $\nu_{C=N}$ (1619.31 cm^{-1}); **ESI-MS**: $[M+H]^+$ 485.17 *m/z*.

2.3.4.2. Single crystal synthesis of Cu[L6 – 2H]

L6 (20.0 mg, 0.0489 mmol, 1 eq.) was combined with Cu(acetate)$_2$·H$_2$O (9.77 mg, 0.0489 mmol, 1 eq.) and added to a sample vial containing absolute ethanol (3 mL). A dark red solution resulted, which was stirred and heated using a magnetic stirrer hot plate for about two hours (until all components were thoroughly dissolved). Thereafter, the solution was pipetted through cotton wool into another sample vial and left to reach ambient temperature. Once the solution had been cooled to room temperature, a few small holes were poked into the lid of the sample vial. This was done to promote the slow evaporation of solvent, which was necessary for stimulating crystal growth. After about two weeks, dark red rod-shaped crystals were produced which were characterised using SCD. **FT-IR (ATR)** neat: $\nu_{C=N}$ (1620.75 cm^{-1}); **ESI-MS**: $[M+H]^+$ 496.22 *m/z*.

2.4. Concluding remarks

Chapter 2 presented and discussed the characterisation data of the monotopic ligand precursor, 5-tertbutyl-2-hydroxybenzaldehyde and monotopic ligands **L1**-**L6**. The precursor aldehyde was synthesised and through FT-IR (ATR) spectroscopy, ^{1}H and ^{13}C NMR spectroscopy, it was established that the product was of sufficient

purity to be used in the Schiff base reaction yielding **L1**-**L6**. These ligands were then fully characterised using FT-IR (ATR), ^{1}H and ^{13}C NMR spectroscopy, melting temperature determination, mass spectrometry, elemental analysis and in the instances of free ligands **L1**-**L4** and **L6** by SCD analysis. Single crystals of two metal-ligand complexes were successfully grown and were suitable for SCD analysis, these were **Ni[L4-2H]** and **Cu[L6-2H]**. It was further confirmed by way of FT-IR (ATR) spectroscopy and mass spectrometry that these chosen single crystals represented the entire crystal sample which was produced.

2.5. References

1. Atwood, D. A.; Harvey, M. J. *Chem. Rev.* **2001**, *101* (1), 37–52.
2. Cozzi, P. G. *Chem. Soc. Rev.* **2004**, *33* (7), 410–421.
3. El-sherif, A. *J. Coord. Chem.* **2013**, *66* (19), 3423–3468.
4. White, D. J.; Laing, N.; Miller, H.; Parsons, S.; Tasker, P. A. *Chem. Commun.* **1999**, 2077–2078.
5. Parkin, A. **2010**, 55–64.
6. Aldred, R.; Johnston, R.; Levin, D.; Neilan, J. *J. Chem. Soc. Perkin Trans. 1*. **1994**, 1823.
7. Ogata, Y.; Kawasaki, A.; Sugiura, F. *Tetrahedron* **1968**, *24* (14), 5001–5010.
8. Wynberg, H. *Chem. Rev.* **1960**, *60* (2), 169–184.
9. Reichardt, C. *J. für Prakt. Chemie.* **1999**, *341* (7), 609–615.
10. Sartori, G.; Casiraghi, G.; Bolzoni, L.; Casnati, G. *J . Org. Chem.* **1979**, *44* (5), 803–805.
11. Coletti, A.; Galloni, P.; Sartorel, A.; Conte, V.; Floris, B. *Catalysis Today*. **2012**, 192, 44-55.
12. Yao, X.; Qiu, M.; Lue, W.; Chen, H.; Zheng, Z. *Tetrahedron Assym*. **2001**, *12* (2), 197-204.
13. Achard, T.; Belokon, Y. N.; Fuentes, J. A.; North, M.; Parsons, T. *Tetrahedron*. **2004**, *60* (28), 5919-5930.
14. Stanjek, H. *Hyp. Interact.*, **2004**, 154, 107-119.
15. Bondi, A. *J. Phys. Chem.* **1964**, *68* (3), 441-451.

16. Corden, J. P.; Errington, W.; Moore, P.; Wallbridge, M. G. H. *Acta Crystallogr. Sect. C Cryst. Struct. Commun.* **1997**, *C53* (4), 486–488.

17. Lenoble, G.; Lacroix, P. G.; Daran, J. C.; Di Bella, S.; Nakatani, K. *Inorg. Chem.* **1998**, *37* (9), 2158-2165.

18. Byun, J. C.; Kim, K. J. *Inorg. Chem. Commun.* **2007**, *10* (4), 502-505.

19. Miller, H. A.; Laing, N.; Parsons, S.; Parkin, A.; Tasker, P. A.; White, D. J. *J. Chem. Soc. Dalt. Trans.* **2000**, No. 21, 3773-3782.

20. Benisvy, L.; Kannappan, R.; Song, Y. F.; Milikisyants, S.; Huber, M.; Mutikainen, I.; Turpeinen, U.; Gamez, P.; Bernasconi, L.; Baerends, E. J.; Hartl, F.; Reedijk, J. *Eur. J. Inorg. Chem.* **2007**, No. 5, 637-642.

21. Thomas, F.; Jarjayes, O.; Duboc, C.; Philouze, C.; Saint-aman, E.; Pierre, J. *J. Chem. Soc. Dalt. Trans.* **2004**, 2662-2669.

22. SMART Data Collection Software (version 5.629), Bruker AXS Inc. (Madison), WI, **2003**.

CHAPTER 3: SYNTHESIS & CHARACTERISATION OF LIGAND INTERMEDIATES & DITOPIC LIGANDS

3.1. Introduction

3.1.1. Synthetic anion-receptor chemistry

The preceding few decades have brought with them, a paradigm shift in our understanding of anion receptor chemistry. The trigger, which ultimately initiated research into synthetic anion receptor chemistry, was squeezed in 1968 by the work of Simmons and Park at DuPont Central Research in Delaware.[1] Their seminal work described the halide binding characteristics of several ammonium-based macrobicyclic receptors.[2] Serendipitously, the group came to the evident suggestion that the chloride anion may be bound within the central cavity of the positively-charged receptors exemplified in Fig. 3.1.

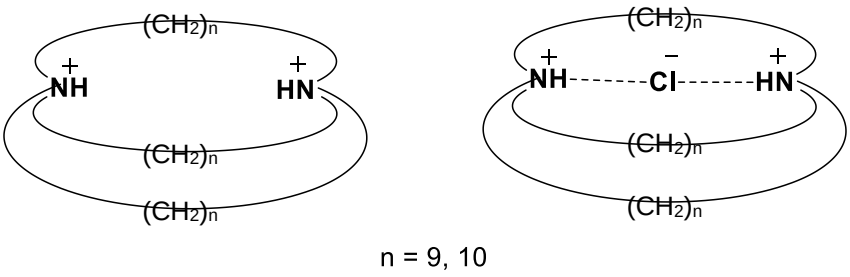

FIGURE 3.1 First isolated example of anion encapsulation by an organic ligand

These suggestions were later confirmed by the acquisition of a crystal structure of the same complex reported by Marsh and co-workers in 1975.[3] Further progress to the field was made in the mid-1970s by the work of Lehn and co-workers.[3, 4] The group, using similar anion receptor molecules produced by Simmons and Park, lucidly demonstrated how optimising the fit of an anion for a given charged cavity could lead to strong binding. In essence, these researchers were responsible for instigating the extensive exploration into this now booming field which has since, manifested and grown in various directions. Currently, chemists are mimicking the way nature uses many of the tools, such as hydrogen bonding, electrostatics, size/shape complementarity, metal-anion complex formation and hydrophobicity, in their efforts to achieve anion recognition.[3]

3.1.2. The design of ditopic ligands for metal salt extraction and transport

Since anions are inherently negatively charged, an instinctive way to achieve anion binding is through the use of positively charged species. Ammonium groups have been widely used for this purpose along with a range of other interesting anion recognition systems.[5] By implementing the knowledge which has been gathered from developments made to the field of anion receptor chemistry, numerous researchers have devised various organic ligands designed to bind a combination of a metal cation and its attendant anion, either by incorporating separate cation or anion binding sites into a single ligand or by arranging for the anion to interact directly with the metal centre *via* a vacant co-ordination site.[3]

Of particular interest to us are those molecules or mixtures of molecules capable of transporting metal ions and their attendant anions in liquid/liquid extractions or across membranes. Beer *et al*. have developed a new tripodal tris(amidobenzo-15-crown-5) heterotopic ligand which efficiently extracts and transports technetium as the [Na][TcO_4] ion pair.[6] Kavallieratos *et al*. found that the addition of benzene-1,3,5-tricarboxamide improved the extraction of $CsNO_3$ by tetrabenzo-24-crown-8 as a result of hydrogen bonding to the nitrate anion.[7] These and other researchers have also covalently linked anion and cation binding moieties into a single molecule capable of metal salt transport, a noteworthy example is the prevalent work executed by Tasker and his team at Edinburgh University in Scotland. A sizeable portion of the work conducted by Tasker's team has consisted of attaching dialkylamino methyl arms ortho- to the phenoxy oxygen atoms of salicylaldimine ligands permitting a zwitterionic form of the ligand. The zwitterionic nature of the ligand gives it the ability to extract and transport metal salts.

In the hopes of developing new types of chelating agents able to extract metal salts over mainstream cation and/or metallate anion extractants and further fueled by the desire to surmount the Hoffmeister bias, six H_2-salen-type ditopic ligands were designed with the intent of including anion binding sites of unique electronic and steric characteristics as well as varying diimine moieties. With this said, the current chapter deals with ligand design strategies selected for the purpose of a comparative study of chemical structure with respect to individual performance in competitive extraction and transport tests described in the next chapter. Furthermore, chapter 3 apprises the synthetic routes endeavored towards the final production of ditopic ligands **L7-L12 (**Fig. 3.2 and Fig 3.3). In effect, it centers on ligand intermediate synthesis and characterisation by FT-

IR (ATR) spectroscopy, ^{1}H and ^{13}C NMR spectroscopy. Using these techniques, enough information was gathered to ultimately advance through the convergent route towards the final synthesis of **L7-L10** whilst the production of **L11** and **L12** could not be completed due to a proposed steric issue in the final Schiff base reaction. Nonetheless, **L7-L10** were fully characterised by FT-IR (ATR) spectroscopy, ^{1}H and ^{13}C NMR spectroscopy, mass spectrometry and micro-elemental analysis.

3.1.3. Ligand design strategies

The chief objectives in formulating the ditopic ligands presented herein were three-fold. Firstly, a comparison could be made between the monotopic and ditopic ligands sharing the same diimine linker moiety in terms of metal extraction and transport efficiency ie: **L2** and **L7**; **L3** and **L8**; **L6**, **L9** and **L10**. Secondly, the anion extraction and transport efficiency of ditopic ligands **L7-L9** could be compared as they shared the same pendant piperidinyl moiety with varying diimine linkers. In other words, an insight could be gained in terms of the role of the diimine moiety in anion coordination. Lastly, for ditopic ligands **L9** and **L10**, keeping the diimine moiety the same and varying the structure of the pendant alkylamino methyl groups would assist in revealing the effect of these different groups on anion binding.

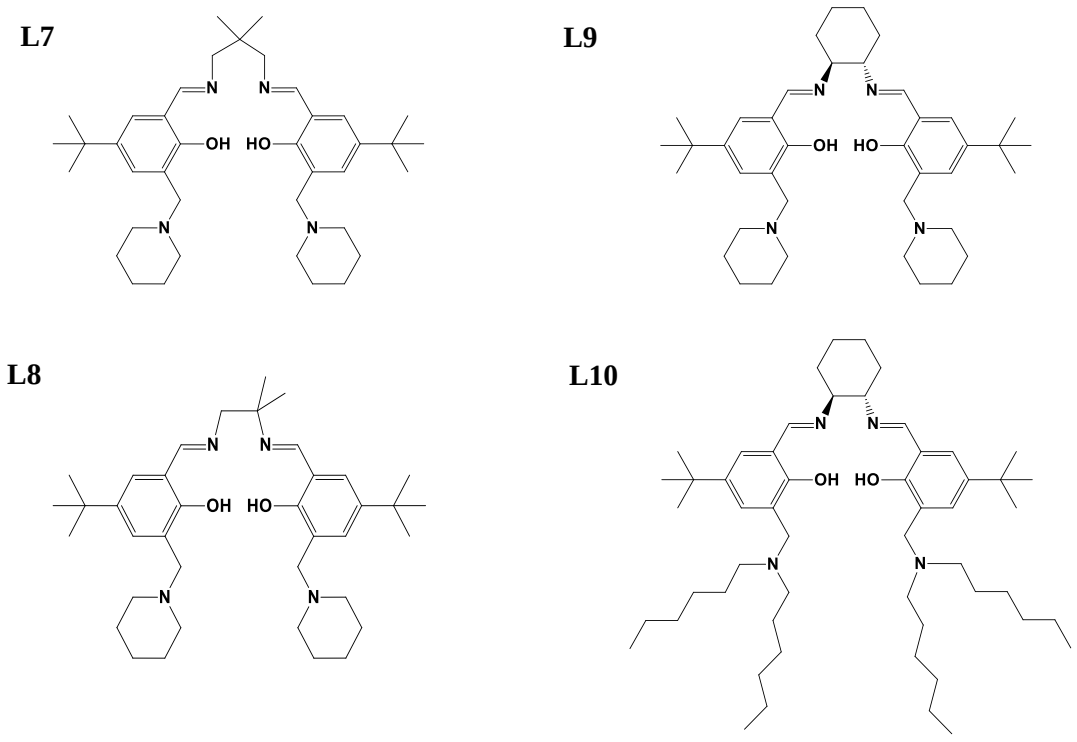

FIGURE 3.2 Structural illustration of ditopic ligands **L7-L10**

Worth noting, is that during the course of this investigation, some other ligand designs were considered. Unfortunately, due to a combination of factors such as time constraints, purification obstacles and the quantity of each ligand required for the testing procedures presented herein, these were abandoned to focus on the ligands **L7-L10**. The additional ditopic ligands which were considered in addition to their syntheses up to the last intermediate is described in this dissertation. Unfortunately, due to a postulated steric issue **L11** could not be produced in high enough quantities to be subjected to any analysis. In the construction of **L12**, too little pure product was isolated to fully characterise and sequentially use in the solvent extraction tests described in Chapter 4.

L11

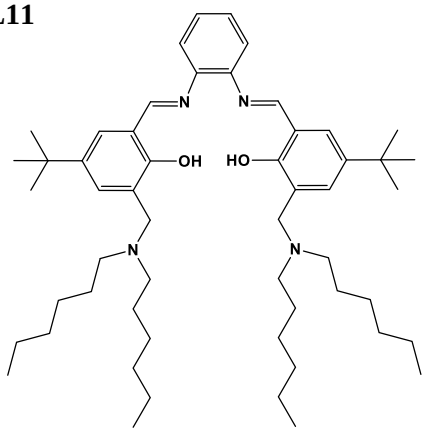

L12

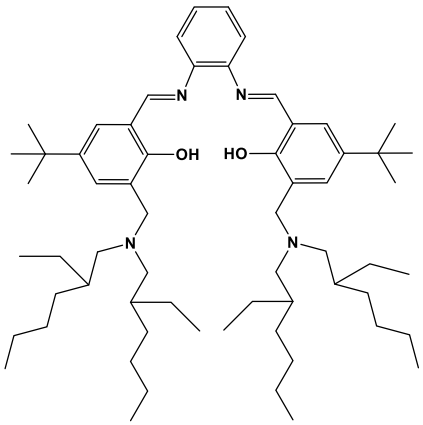

FIGURE 3.3 Structural illustration of proposed ditopic ligands **L11** and **L12**

3.1.4. General synthetic pathway towards ditopic ligands L7-L12

At the close of the millennium, White and co-workers[8] illustrated an innovative way to prepare salen-type dicationic and dianionic ligands. Their devised synthetic route entails a four-step convergent synthesis (Scheme 3.1) which commences by way of a base-catalysed mannich-type reaction. This step is responsible for transmuting the secondary amine to serve as the anion binding motif to its corresponding aminol ether species (step i – Scheme 3.1). Following this, is an electrophilic aromatic substitution reaction with 5-tertbutyl salicylaldehyde and the aminol ether generated in the first step (step ii – Scheme 3.1). This reaction affords the

alkylamino methyl functionalised salicylaldehyde species which is then further submitted to a final Schiff base reaction. The Schiff base reaction requires 2 mol equivalents of the functionalised aldehyde species and 1 mol equivalent of the diamine of choice (step iii – Scheme 3.1) to engender **L7**-**L10**. In this dissertation, the same synthetic route was adopted to manufacture the ligands presented in this chapter with a few adaptations of alternative work-up procedures proposed in the literature.

It is critical to note that there are two unique classes of intermediate molecules which needed to be produced and purified before each final ditopic ligand could be fully synthesised. These are the intermediates after step i and ii, respectively. Since three unique anion-binding sites were to be incorporated into the final ligand structures, three intermediates needed to be generated after step i and these species have been denoted as **A1**-**A3**, where **A1** has the required piperidinyl moiety as a potential anion binding site for the production of **L7, L8** and **L9**. **A2** is a ligand precursor towards the production of **L10** and **L11** (both sharing the dihexylamino methyl moieties as pendant arms). Finally, **A3** is the intermediate headed for the production of **L13** which contains the required bis(2-ethylhexyl)amino methyl group. Similarly, the ligand precursors (functionalised aldehydes) after step ii are denoted **B1**-**B3**, respectively and are generated after the reaction of **A1**-**A3** and 5-tertbutyl-2-hydroxybenzaldehyde. Thus, **B1**-**B3** each have analogous NR_2 groups to their **A1**-**A3** reagents. These annotations will be made clearer in the schemes to follow.

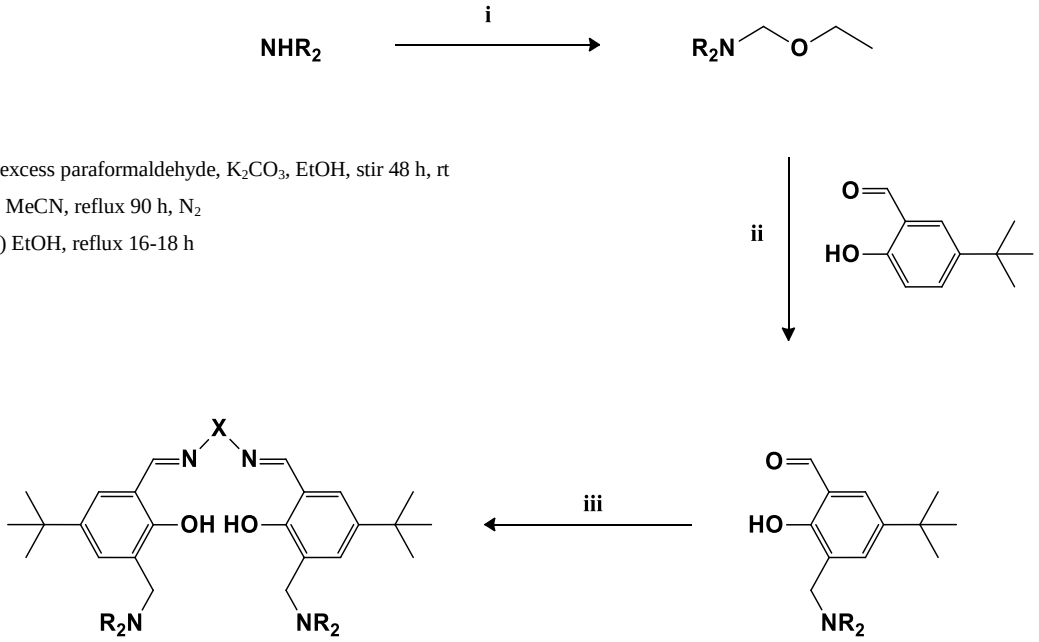

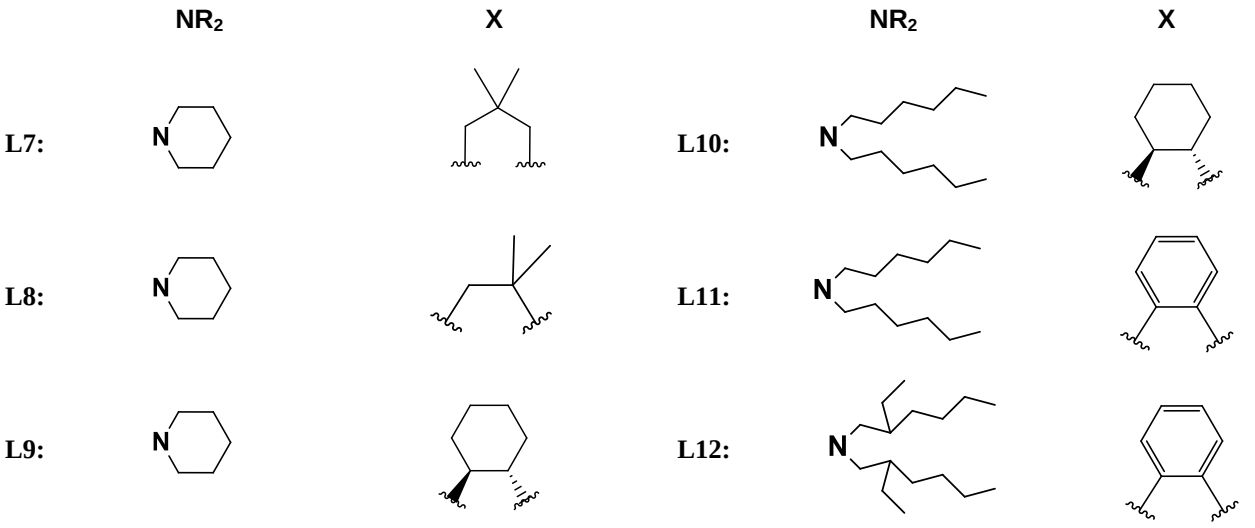

SCHEME 3.1 Four step convergent synthesis towards the preparation of ditopic ligands **L7-L12**

3.2. Results and Discussion

3.2.1. Synthesis & characterisation of ditopic ligand precursors (A1-A3)

Aminol ether intermediates, **A1-A3**, were procured from their corresponding secondary amines in yields between 60 and 70 %. The procedure followed for this reaction shadowed the method proposed by Adams *et al.*[9] Using morpholine as their prevalent example, they instituted a base-catalysed mannich-type reaction converting morpholine to N-ethoxymethylmorpholine using K_2CO_3 as their base, paraformaldehyde and ethanol. In this reaction ethanol must act as the nucleophile to introduce the ethoxy moiety into the final product and thus must be deprotonated to its ethoxy anionic form before attacking the iminium salt intermediate produced from the reaction of formaldehyde and the secondary amine. It was therefore necessary to execute vigorous stirring in this reaction to promote potassium carbonate interacting with ethanol to render it more nucleophilic.

In the case of the aminol ether intermediates presented herein, all were attained as colourless oils by fractional distillation. As expected, of the intermediates, **A1** proved to have the lowest boiling point in comparison to **A2** and **A3** due to fewer London dispersive forces between these molecules.

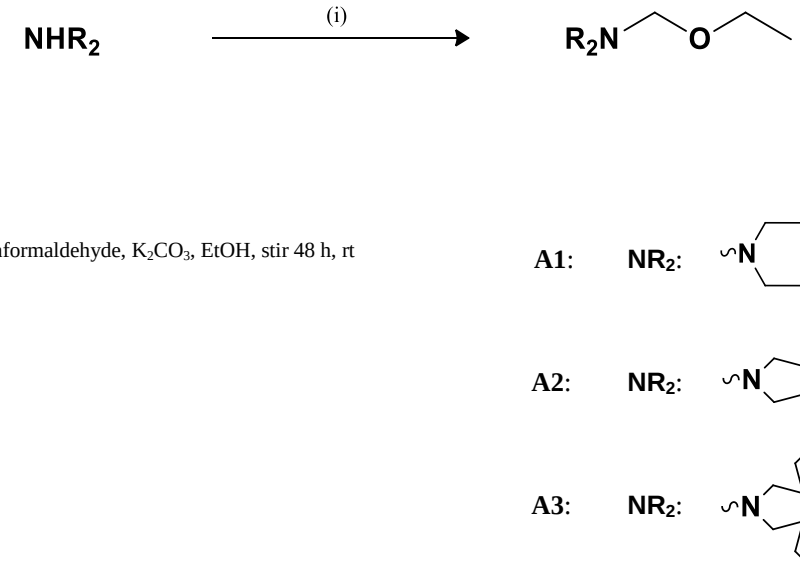

SCHEME 3.2 Mannich-type reaction affording aminol ether intermediates **A1**-**A3** (step i)

Intermediates **A1**-**A3** were characterised by FT-IR (ATR) spectroscopy, ^{1}H and ^{13}C NMR spectroscopy. In the FT-IR spectra, attention was focused on absorption bands arising for the C-O stretching frequency and the disappearance of the band corresponding to the N-H stretching frequency. Characterisation by means of ^{1}H NMR spectroscopy monitored the change in chemical shifts in the aliphatic region and disappearance of the proton signal associated with the amine group. In the ^{1}H NMR spectra, three discrete resonances were relevant and were indicative of the successful formation of the desired aminol ether. These chemical environments are denoted **1**-**3** in the numbering scheme (Fig 3.4) used to construct the proton and carbon NMR data presented in Table 3.1.

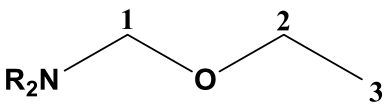

FIGURE 3.4 Numbering scheme for relevant ^{1}H and ^{13}C NMR chemical shifts for compounds **A1**-**A3**

It was found that the newly-formed products showed slightly shifted aliphatic chemical shifts in comparison to their analogous amines as a result of the slight change in their chemical environments once functionalisation

had occurred. Furthermore, the methylene protons exemplified by **1** in the numbering scheme existed as an expected singlet which resided most downfield in comparison to all other proton resonances due to de-shielding as a result of existing between two electronegative heteroatoms. The anticipated quartet and triplet signals resonating from proton environments **2** and **3**, respectively, were also observed and further confirmed that molecules **A1**-**A3** were of adequate purity for use as reagents in the subsequent reaction.

TABLE 3.1 Important ^{1}H and ^{13}C NMR shifts for **A1**-**A3**

	A1	**A2**	**A3**
H_1	4.11 (s, 2H)	4.13 (s, 2H)	4.08 (s, 2H)
H_2	3.43 - 3.50 (q, ^{3}J(H2-H3) 7.0 Hz, 2H)	3.39 - 3.45 (q, ^{3}J(H3-H2) 7.0 Hz, 2H)	3.39 - 3.46 (q, ^{3}J(H3-H2) 7.0 Hz, 2H)
H_3	1.17 (t, ^{3}J(H3-H2) 7.0 Hz, 3H)	1.16 (t, ^{3}J(H3-H2) 7.0 Hz,3H)	1.17 (t, ^{3}J(H3-H2), 7.0 Hz, 3H)
C_1	82.89	86.26	86.27
C_2	64.32	63.37	63.39
C_3	15.43	15.45	15.46

3.2.2. Synthesis & characterisation of ditopic ligand precursors B1-B3

Ligand precursor molecules **B1**-**B3** were crafted by way of an electrophilic aromatic substitution reaction with the prepared aminol ethers **A1**-**A3**, respectively, and 5-tert-butyl-2-hydroxybenzaldehyde. These intermediates were formed in modest yields ranging between 70 % and 80 % and found to be soluble in polar organic solvents. Compound **B1** was attained as an ‘off-white’ crystalline material whereas compounds **B2** and **B3** were isolated as light-orange oils at room temperature.

The synthetic method was appropriated from Miller *et al.*[10], where they make use of 4-ethoxymethylmorpholine and 5-tert-butyl-2-hydroxybenzaldehyde in acetonitrile under inert N_2 conditions to achieve functionalisation of the salicylaldehyde. Although there are several other strategies one could have

adopted to generate compounds **B1**-**B3,** the method followed was, to our knowledge, the most straight-forward and did not involve stringent conditions.

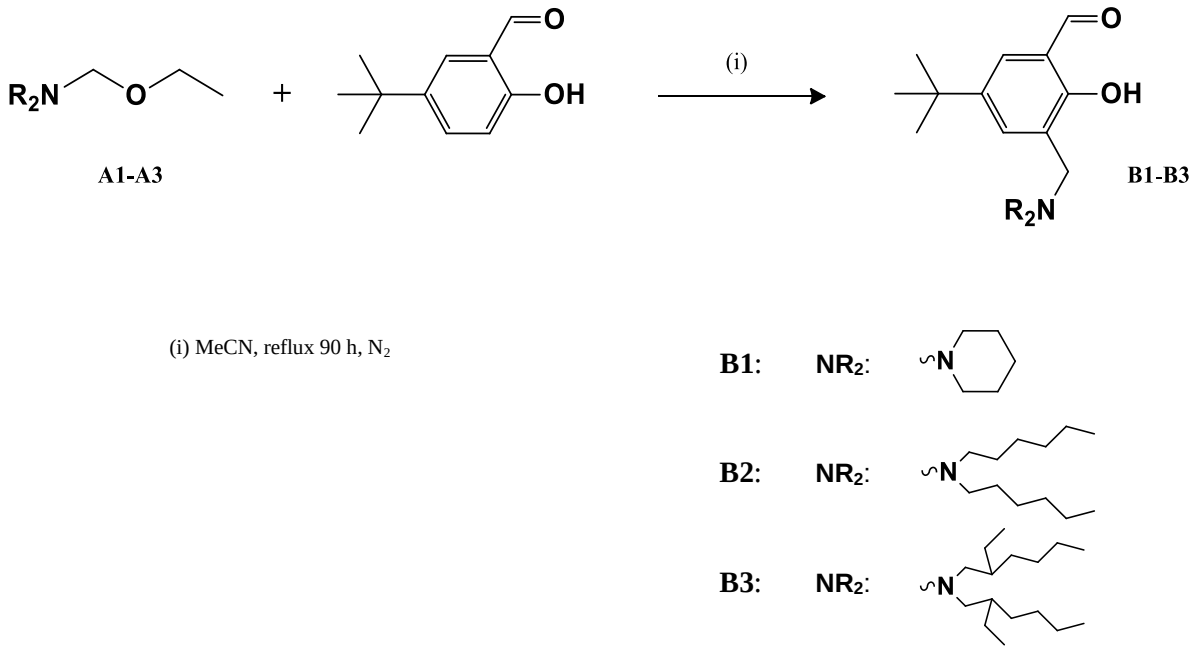

SCHEME 3.3 Electrophilic aromatic substitution reaction producing compounds **B1**-**B3** (step ii)

Before compounds **B1**-**B3** could undergo their final Schiff base reaction with the diamine of choice, it was crucial that the product mixture was pure and consisted of no starting 5-tertbutyl-2-hydroxybenzaldehyde. The reason for this being that if 5-tertbutyl-2-hydroxybenzaldehyde were indeed present, it could lead to asymmetric products at the completion of the Schiff base reaction. This would result in a greater final purification obstacle as the final ditopic ligand and its associated asymmetric counterpart would share an almost indistinguishable polarity. This would render it more difficult to isolate the ditopic ligands in high purity.

Various purification strategies were undertaken for **B1**-**B3**, most of which, were found in the literature. Adams *et al*.[9] proposed an acid base extraction in which they successfully isolated the hydroxy-3-(morpholin-4-ylmethyl)benzaldehyde. In their procedure, the crude product is dissolved in DCM and extracted with a 0.1 M HCl aqueous solution. The pendant nitrogen incorporated on the molecule is protonatable and it is thus expected to become soluble in the acidic aqueous media once protonated. The resulting aqueous phase is then neutralised and the desired compound is re-extracted into the organic phase.

The proposed acid base extraction was not effective in purifying **B1**-**B3**. It seemed that none of the desired product was sequestered into the acidic aqueous phase and if so, not quantitatively. This was justified by the fact that no product was recovered even when the aqueous solution was basified to high pH values. A possible explanation for the failure of this strategy was that in literature, the compounds already exhibit higher polarity than the compounds presented herein. Thus with this advantage, the compounds would be preferentially soluble in the aqueous phase once protonated as they are more polar in comparison to **B1**-**B3**.

Nevertheless, a strategy was devised and effectively afforded **B1**-**B3** in high purity. The strategy entailed a solvent extraction procedure in which DCM housing the crude product is mixed with an immiscible ethanol solution (30 %). It was envisaged that the 5-tertbutyl-2-hydroxybenzaldehyde was more polar than the desired product and would be more soluble in the ethanol solution, ultimately removing unwanted 5-tertbutyl-2-hydroxybenzaldehyde from the organic layer and affording the desired compounds **B1**-**B3**, in the DCM layer.

Compounds **B1**-**B3** were characterised using FT-IR (ATR), ^{1}H and ^{13}C NMR spectroscopy. Main characterisation signals assuring high purity, was the complete disappearance of peaks corresponding to 5-tertbutyl-2-hydroxybenzaldehyde in the aromatic chemical shift range in the ^{1}H and ^{13}C NMR spectra. Furthermore, the absence of the C=O stretching band in the FT-IR spectra corresponding to the carbonyl moiety of 5-tertbutyl-2-hydroxybenzaldehyde, as well as a shifted aldehyde signal in both the ^{1}H and ^{13}C NMR spectra. Fig. 3.5 below denotes the chemical environments unique to **B1**-**B3** which aided the characterisation process. The characterisation data connected to these environments is reported in Table 3.2.

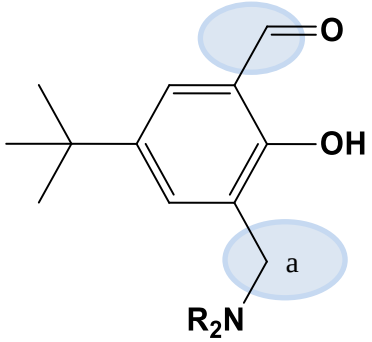

FIGURE 3.5 Numbering scheme for relevant ^{1}H and ^{13}C NMR chemical shifts for compounds **B1**-**B3**

TABLE 3.2 Important characteristic data for **B1**-**B3**

	B1	**B2**	**B3**
$\upsilon_{C=O}$ (cm^{-1})	1670.48	1679.77	1681.59
O=C-H	10.40 (s, 1H)	10.41 (s, 1H)	10.29 (s, 1H)
H_a	3.69 (s, 2H)	3.78 (s, 2H)	3.65 (s, 2H)
O=C-H	191.15	191.24	192.68
C_a	61.49	57.52	59.92

3.2.3. Synthesis & characterisation of final ditopic ligands L7-L10

The final ligands, **L7-L10**, were prepared by a Schiff base condensation of two equivalents of **B1**-**B3** with various electronically unique diamines (Scheme 3.4). **L7** and **L9** existed as solids where **L7** was attained as a yellow crystalline solid and **L10** as a yellow-orange amorphous solid. **L8** and **L10** were recovered as viscous oils after the work-up procedures, where **L8** was isolated as an orange oil and **L10** was found to be an orange-red oil at room temperature. **L7-L10** exhibited solubility in polar organic solvents. Molecules **L7** and **L8** are novel while the synthesis of **L9** and **L10** has been previously reported. [11, 12]

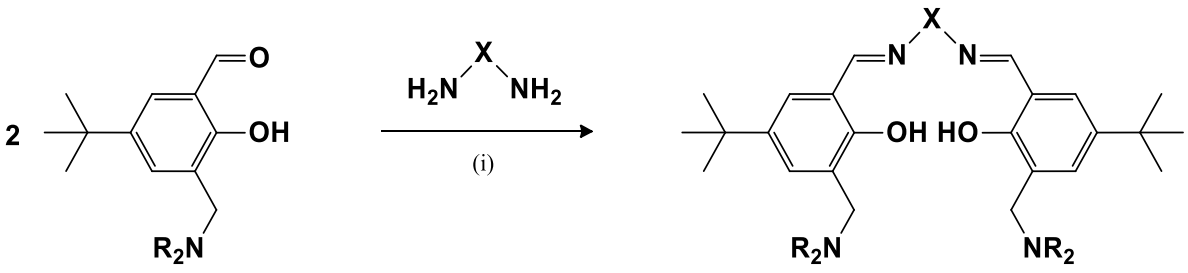

(i) EtOH reflux 18-24 h

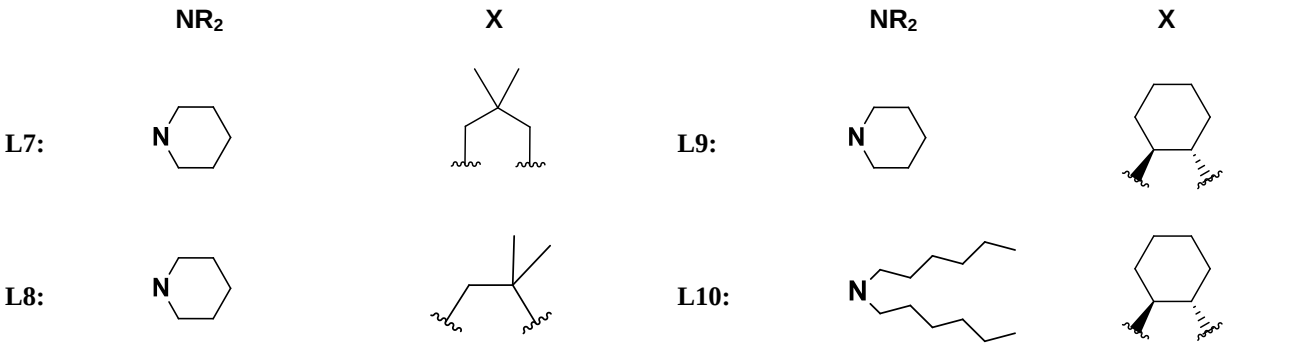

SCHEME 3.4 Schiff base reaction producing final ditopic ligands **L7-L10**

Several characterisation techniques were used to ensure these chemical species were of high purity to be thoroughly assessed as chelating agents in the coordination tests described in the next chapter. These techniques, which will be discussed in the following order, include melting point determination (for the case of **L7** and **L9**), ESI-MS, FT-IR (ATR) spectroscopy, ^{1}H and ^{13}C NMR spectroscopy and micro-elemental analysis.

3.2.3.1. Characterisation by melting point, mass spectrometry & FT-IR (ATR) spectroscopy

Table 3.3 below bares some conclusive characteristic data relating to the synthesis of **L7-L10**. This comprises the FT-IR absorption frequency for the imine C=N stretch, the *m/z* value of the proton adduct in the acquired mass spectra and in the cases of **L7** and **L9**, the determined melting temperatures.

TABLE 3.3 Characteristic data applicable to the synthesis of **L7-L10**

Ligand	FT-IR[a] ($\upsilon_{C=N}$, cm^{-1})	ESI-MS[b] (*m/z*)	Melting Point[c] (°C)
L7	1629.91	617.48 (616.93)	125-130
L8	1628.15	603.46 (602.90)	-
L9	1625.50	629.48 (628.94)	85.8 - 90.2
L10	1629.24	829.90 (829.35)	-

[a] Recorded as neat spectra on a ZnSe crystal, using an ATR accessory. [b]Reported ion corresponds to the proton adduct of the molecular ion, [M + H]+, [c] Melting points recorded are uncorrected.

The FT-IR spectra of the Schiff base products were scrutinised for the disappearance of the carbonyl absorption band of reactants **B1** and **B2** and the appearance of an intense peak in the range of 1600-1650 cm^{-1} indicative of the newly-formed imine functionality. Individually, all ditopic ligands delivered sharp peaks in the imine wavenumber region. Further characterisation was carried out using high resolution ESI-MS. The molecular ion for each of the ligands corresponds to the proton adduct $[M+H]^+$ which was observed at an *m/z* value reported in Table 3.3 and the molar mass of each ligand is depicted in parenthesis. These values correlate well to the calculated molecular masses of each ligand indicating that the ligands were in fact made in high yield. In the mass spectra, a doubly-charged molecular ion $[M+2H]^{2+}$ was observed for each ligand, inferring that two protons are incorporated into the neutral organic molecule through protonation of the two phenolate groups. This doubly-charged pseudo molecular ion represented the base peak. The doubly-charged proton adduct had a *m/z* value which equated to $(M_r + 2)/2$ indicating the presence of the $[M+2H]^{2+}$ species. Further evidence of a doubly-charged pseudo molecular ion was deduced by its associated isotopic peaks which differ by 0.5 mass units.

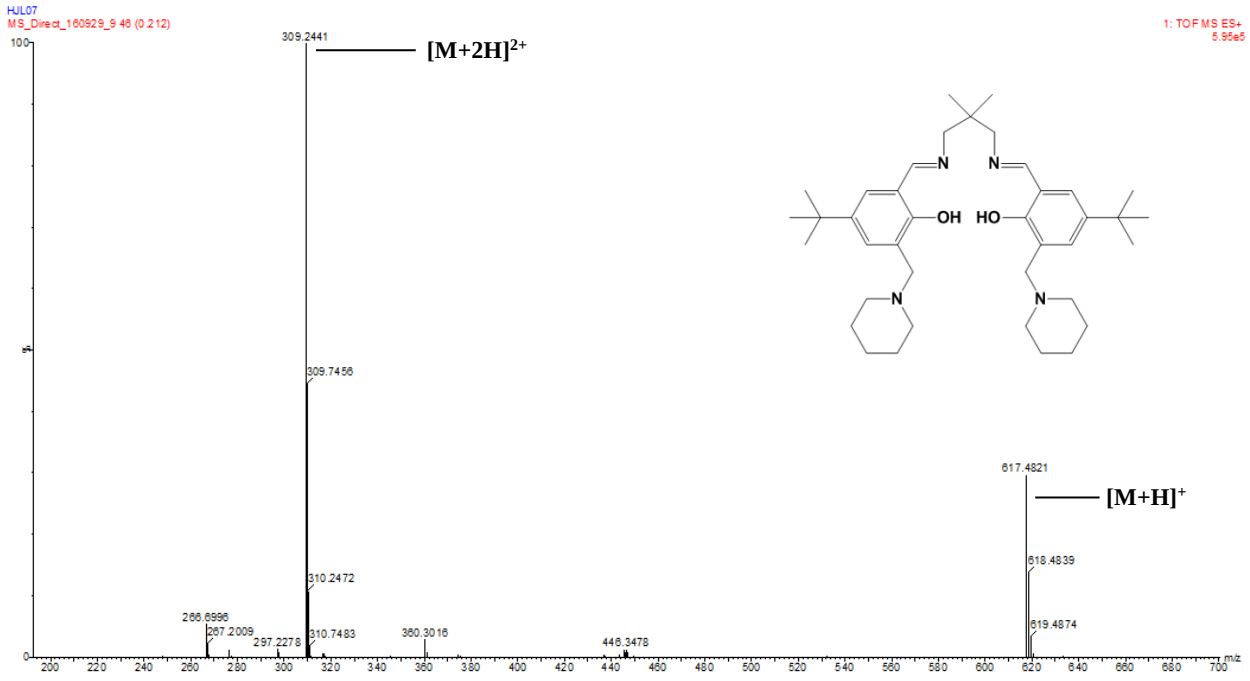

FIGURE 3.6 ESI-MS (positive mode) spectrum of **L7** with major fragments annotated.

The melting temperature for **L9** corresponds well to that acquired by Fennie and co-workers for the same compound.[11]

3.2.3.2. Characterisation by ^{1}H NMR spectroscopy

The numbering of protons and carbons for ditopic ligands **L7-L10**, and used for constructing Tables 3.4 and 3.5, is exemplified in Fig. 3.7. The phenoxy groups and linked imines on either side of the diimine moiety are labelled (i) and (ii), respectively. This is to denote the symmetrical relationship of these groups in the numbering system. Furthermore, the proton and carbon environments present on the incorporated alkylaminomethyl pendant groups are assigned by the letters **a-g** seen below.

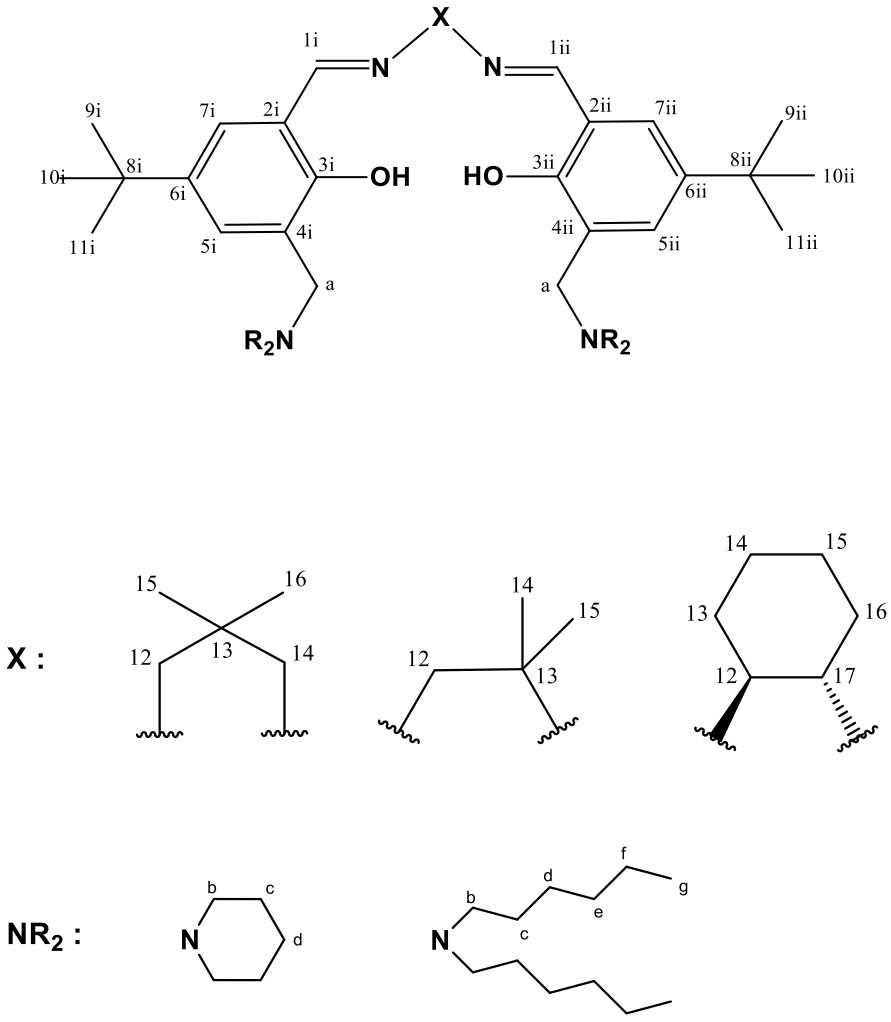

FIGURE 3.7 Numbering scheme for **L7-L10** used in the annotations of the ^{1}H and ^{13}C NMR spectra and respective tables.

Characterisation by means of ^{1}H NMR spectroscopy provided ample confirmation of the successful formation of ditopic ligands **L7-L10**. Critical signals pointing towards the successful production of the respective Schiff base products were recognised by the disappearance of the resonance associated with the aldehyde proton of **B1** and **B2** and the appearance of a distinct resonance in the region of roughly 8.20–8.60 ppm, indicative of the proton associated with the imine functionality. **L7-L10** displayed imine resonances in the range 8.28-8.39 ppm. It was observed that **L3** produced two chemically inequivalent imine proton resonances which was due to the lower symmetry introduced by 1, 2-diamino-1, 1-dimethylethane.

In closing, all proton resonances were accounted for with integral values corresponding well to the number of protons present in the desired products. For simplistic purposes, the fully annotated ^{1}H NMR spectrum of the novel ligand **L7** (Fig 3.8) is shown as a representative of similar spectra obtained for the other ditopic ligands **L8**-**L10**.

3.2.3.3. Characterisation by ^{13}C NMR spectroscopy

The success of the Schiff base reaction generating **L7-L10** in high purity was further confirmed using ^{13}C NMR spectroscopy and all peaks are accounted for as expressed in the numbering system exemplified in Fig. 3.7. All ligands have imine carbon resonance peaks in the range of 162-167 ppm and due to the reduced symmetry of **L8**, there are two resonance peaks corresponding to each of the imine carbons of **L8**.

Ultimately, all four ditopic ligands delivered carbon-13 resonances in the appropriate chemical shift regions of which, all were accounted for as exemplified in Table 3.5. For simplicity, the fully annotated ^{13}C NMR spectrum of **L7** is provided in Fig. 3.9 and serves as representation of similar spectra obtained for **L8**-**L10**.

Table 3.4 ^{1}H NMR spectral data of **L7**-**L10**[a]

Compound	***CH*=*N***	**Aromatic region**	**Aliphatic region**		
			-CH-	***-CH_2-***	***-CH_3***
L7	8.37 (s, 2H, H^1)	7.19 (d, *J* = 2.5 Hz, 2H, H^7), 7.45 (dd, *J* = 8.7, 2.6 Hz, 2H, H^5)	–	1.44 (m, 8H, H^c), 1.61 (m, 4H, H^d), 2.48 (t, *J* = 6.6 Hz, 8H, H^b), 3.48 (s, 4H, $H^{12,14}$), 3.61 (s, 4H, H^a)	1.07 (s, 6H, $H^{15,16}$), 1.32 (s, 18H, H^{9-11})
L8	8.36 (s, 1H, H^1), 8.39 (s, 1H, H^1)	7.14 – 7.24 (m, 2H, H^5), 7.39 – 7.44 (m, 2H, H^7)	–	1.41-1.47 (m, 8H, H^c), 1.58-1.62 (m, 4H, H^d), 2.40-2.52 (m, 8H, H^b), 3.57 (d, *J* = 4.2 Hz, 2H, H^{12}), 3.69 (s, 4H, H^a)	1.31 (s, 6H, $H^{14,15}$), 1.29 (s, 18H, H^{9-11})
L9	8.28 (s, 2H, H^1)	7.06 (d, *J* = 2.5 Hz, 2H, H^7), 7.33 (d, *J* = 2.5 Hz, 2H, H^5)	4.77 (m, 2H, $H^{12,17}$)	1.40-1.46 (m, 8H, H^c), 1.54-1.64 (m, 8H, $H^{d,14,15}$), 1.87 (m, 4H, $H^{13,16}$), 2.43 (m, 4H, H^b), 3.65 (s, 4H, H^a)	1.24 (s, 18H, H^{9-11})
L10	8.29 (s, 2H, H^1)	7.04 (d, *J* = 2.5 Hz, 2H, H^7), 7.48 (d, *J* = 2.5 Hz, 2H, H^5)	4.68-4.80 (m, 2H, $H^{12,17}$)	1.20-1.31 (m, 32H, H^{c-f}), 1.56-2.66 (m, 16H, $H^{b,13-16}$), 2.40-2.47 (m, 8H, H^b), 3.52-3.62 (m, 4H, H^a)	0.84 (t, *J* = 6.7 Hz, 12H, H^g), 1.24 (s, 18H, H^{9-11})

[a] Spectra run in $CDCl_3$ at 25 °C. Chemical shifts reported as δ ppm values, referenced relative to the residual solvent peak. Superscripts denote protons as per numbering scheme (Fig. 3.7)

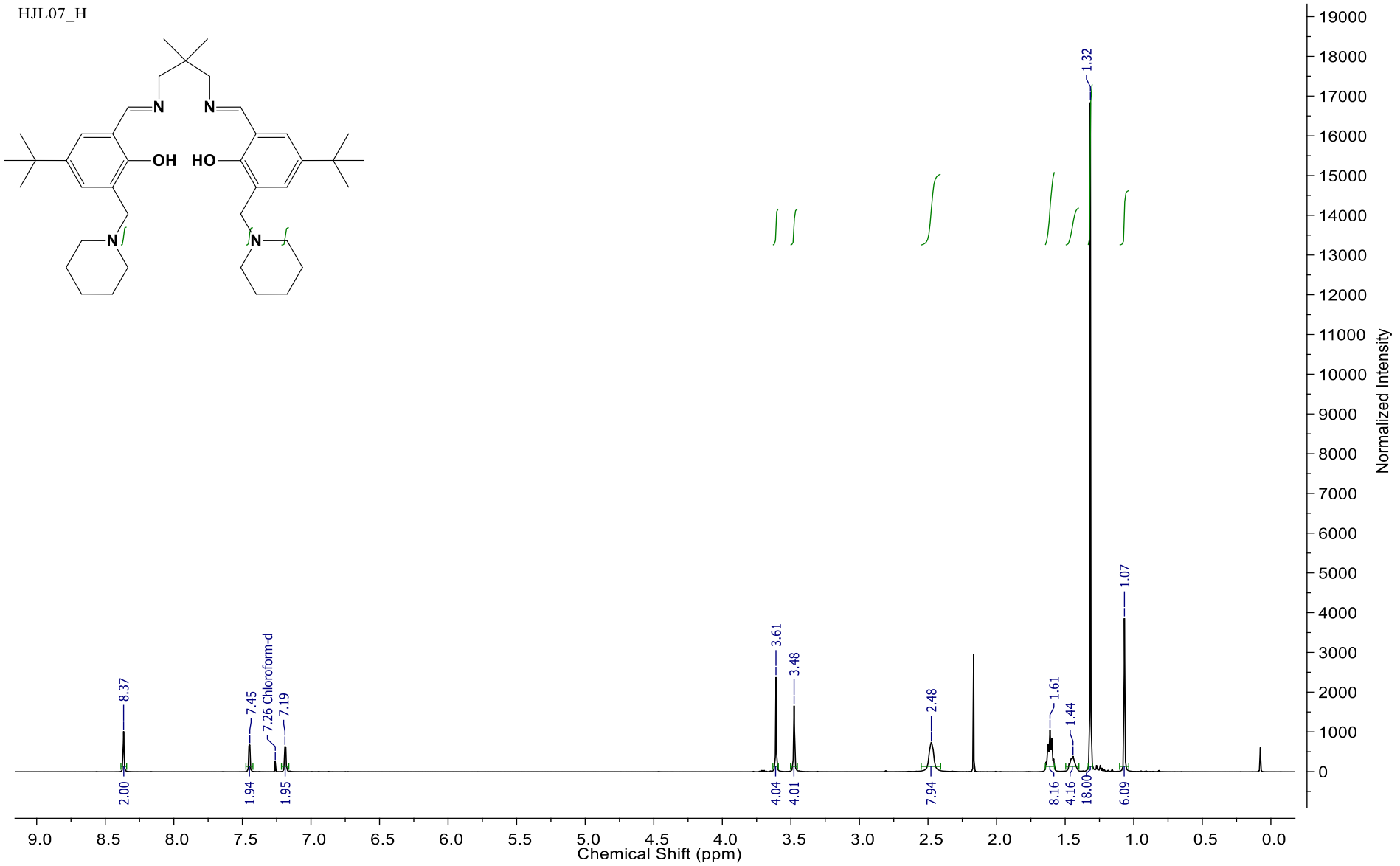

FIGURE 3.8 ^{1}H NMR spectrum of **L7** recorded in $CDCl_3$ at 25 °C

Table 3.5 ^{13}C NMR spectral data of **L7-L10**[a]

Compound	**C**H=N	Aromatic region	Aliphatic region			
			-**C**-	-**C**H-	-**C**H$_2$-	-**C**H$_3$
L7	165.84$^{(1)}$	117.97$^{(4)}$, 125.21$^{(2)}$, 126.29$^{(7)}$, 130.77$^{(5)}$, 140.68$^{(6)}$, 157.46$^{(3)}$	34.08$^{(8)}$, 36.48$^{(13)}$	–	24.54$^{(d)}$, 24.59$^{(c)}$, 54.64$^{(b)}$ 57.04$^{(a)}$, 68.57$^{(12,14)}$	26.17$^{(15-16)}$, 31.60$^{(9-11)}$
L8	[165.85, 166.33]$^{(1i-ii)}$	[117.95, 118.09]$^{(4i-ii)}$, [124.98, 125.10] $^{(2i-ii)}$, [126.19, 126.34]$^{(7i-ii)}$, [130.82, 130.87]$^{(5i-ii)}$, [140.44, 140.73]$^{(6i-ii)}$, [157.31, 157.79]$^{(3i-ii)}$	[34.04, 34.08]$^{(8i-ii)}$, 60.27$^{(13)}$	–	[24.49, 24.53]$^{(d)(i-ii)}$, 26.11$^{(c)}$, [54.57, 54.67]$^{(b)(i-ii)}$, [57.09, 57.22]$^{(a)(i-ii)}$ 70.83$^{(12)}$	28.86$^{(14,15)}$, [31.57, 31.60]$^{(9-11)(1i-ii)}$
L9	164.93$^{(1)}$	118.00$^{(4)}$, 124.70$^{(2)}$, 126.65$^{(7)}$, 130.97$^{(5)}$, 140.57$^{(6)}$, 157.37$^{(3)}$	34.00$^{(8)}$	72.82$^{(12,17)}$	24.39$^{(d)}$, 24.48$^{(14, 15)}$, 26.01$^{(c)}$, 33.41(^{13,16}), 54.63$^{(b)}$, 57.22$^{(a)}$	31.52$^{(9-11)}$
L10	164.89$^{(1)}$	117.67$^{(4)}$, 125.93$^{(2)}$, 126.82$^{(7)}$, 129.92$^{(5)}$, 140.54$^{(6)}$, 157.01$^{(3)}$	33.99$^{(8)}$	72.81$^{(12,17)}$	22.75$^{(f)}$, 24.32$^{(14,15)}$, 27.16$^{(d)}$ 27.39$^{(c)}$, 31.95$^{(e)}$, 33.37$^{(13,16)}$, 54.42$^{(b)}$, 58.02$^{(a)}$	14.12$^{(g)}$, 31.48$^{(9-11)}$

[a] Spectra run in $CDCl_3$ at 25 °C. Chemical shifts reported as δ ppm values, referenced relative to the residual solvent peak. Superscripts denote carbons as per numbering scheme (Fig. 3.7)

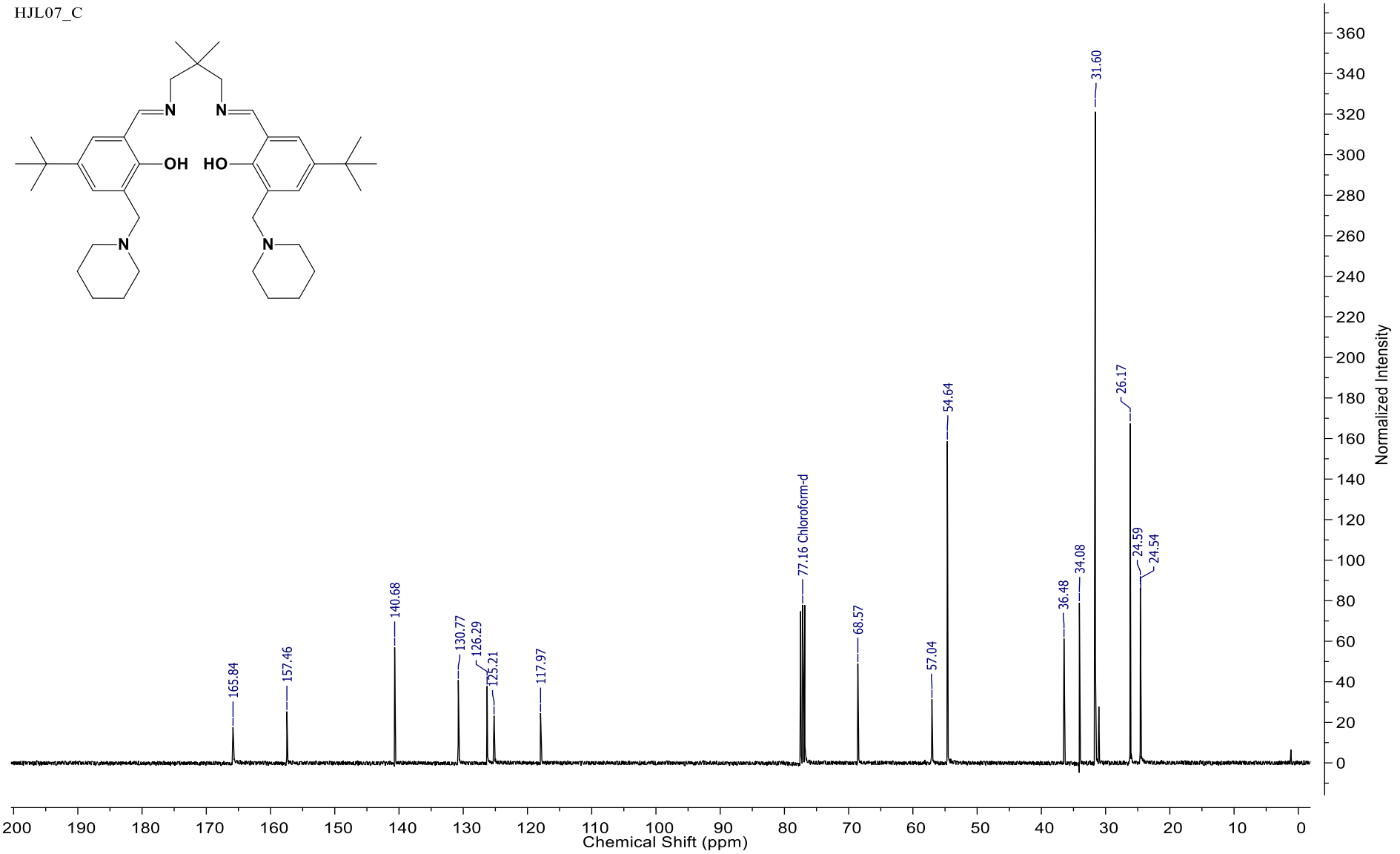

FIGURE 3.9 ^{13}C NMR spectrum of **L7** recorded in $CDCl_3$ at 25 °C

3.2.3.4. Characterisation by Elemental Analysis

Characterisation by EA confirmed the high purity of the ditopic ligands. The experimentally determined percentage carbon, hydrogen and nitrogen correlated well with the calculated percentages with less than 0.5 % deviations. The only exception was **L10**, which showed a deviation of 1.85 % for carbon. Due to the dihexylaminomethyl groups present on **L10**, in addition to it existing as an oil at room temperature, it is likely to entrap some solvent molecules. It was highly probable that some water had been encapsulated by the ligand after the work-up procedure, explaining the percentage difference. Table 3.6 below provides the data acquired from EA where the found value is an average of the results obtained from a duplicate testing of each ligand.

Table 3.6 Elemental analysis data of **L7-L10**

Ligand	Elemental Analysis: Found (Calculated)		
	% C	**% H**	**% N**
L7	75.73 (75.93)	9.80 (9.80)	8.63 (9.08)
L8	75.35 (75.70)	9.83 (9.70)	9.10 (9.29)
L9	76.37 (76.39)	9.26 (9.62)	8.43 (8.91)
L10[a]	77.56 (78.20)	10.93 (11.18)	6.63 (6.76)

[a] Inclusion of one molecule of water.

3.2.4. Synthesis & characterisation of "copper-only" complexes of L7-L10

Prior to the anion extraction tests, "copper-only" complexes of the ditopic ligands **L7-L10** were prepared using the same method reported by Plieger and co-workers[13]. This was done to ensure only free anions could compete for the protonated nitrogen moiety present on the dialkylaminomethyl pendant arms of the ditopic ligands.

The "copper-only" complexes were characterised by FT-IR (ATR) spectroscopy with special attention paid to the shift of the absorption band arising from the imine functional group. It was anticipated that the absorption band would undergo a hypsochromic shift to lower wavenumbers as a result of delocalisation of electron

density from the C=N bond as a result of coordination. This was indeed the case, with the FT-IR data depicted in Table 3.7.

TABLE 3.7 Observed shifts of the imine absorption bands for the free ligands and corresponding "copper-only" species

Free Ligand		**Copper-only Complex**	
	$\nu_{C=N}$		**$\nu_{C=N}$**
L7	1629.91	**Cu[L7-2H]**	1619.19
L8	1628.15	**Cu[L8-2H]**	1619.15
L9	1625.50	**Cu[L9-2H]**	1622.41
L10	1629.24	**Cu[L10-2H]**	1617.49

3.2.5. Attempted synthesis of L11 and L12

Using intermediates **B2** and **B3**, a Schiff base reaction was performed using a phenyldiamine linker (1,2 – diaminobenzene) to produce **L11** and **L12**, respectively. This particular reaction posed a few issues and suggested that the Schiff base products were forming in low yields. Characterisation of the products suggested that a mixture of components existed. The FT-IR spectra indicated two different C=N stretches and the ^{1}H and ^{13}C NMR spectra exhibited an extensive range of peaks in the aromatic chemical shift region. The Schiff base reaction was attempted a number of times with varying conditions but with little success. It was eventually abandoned due to purification obstacles and time constraints.

It was postulated that a probable steric issue exists for the phenyldiamine linker. Since the linker possesses an aromatic withdrawing group, electron density is localised in the aromatic ring and away from the nitrogens of the amine groups. This renders the amine groups less nucleophilic in comparison to the diamine used for **L9** and **L10**. It was envisaged that a large portion of the components present in the product mixture were

asymmetric products. In other words, it was likely that only one of the amines of the diamine had undergone a successful Schiff base reaction. In addition, it was predicted that the second unreacted amine group should be even less nucleophilic than when it was simply present on 1,2-diaminobenzene. The additional steric hindrance imposed by the alkyl and aromatic groups (incorporated on the newly-formed imine) as well as the rigidity of the phenyl group, further reduce the likelihood of the second Schiff base reaction occurring.

The proposed steric effect is illustrated in Scheme 3.5 which compares the accessibility of the unreacted amine for the two different diamine linkers.

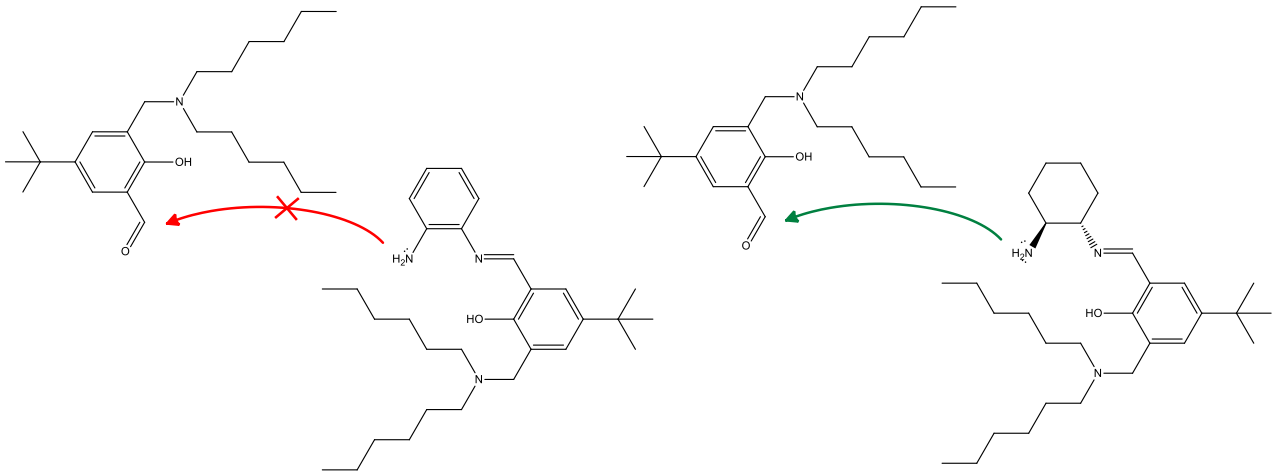

SCHEME 3.5 Schematic depicting the suggested steric issue of the final Schiff base reaction using 1,2-diaminobenzene compared to 1,2-*trans*-diaminocyclohexane

3.3. General conclusions

To summarise, all intermediates headed for the final formation of the ditopic ligands were successfully produced and characterised using FT-IR (ATR) spectroscopy, ^{1}H and ^{13}C NMR spectroscopy. The final ditopic ligands **L7-L10** were generated in adequate yields and were fully characterised using FT-IR (ATR) spectroscopy, ^{1}H and ^{13}C NMR spectroscopy, ESI-MS and micro-elemental analysis. They were thus applicable to be thoroughly assessed as extractants in the solvent extraction tests presented in the next chapter.

In addition, the "copper-only" complexes of **L7**-**L10** were successfully prepared and characterised using FT-IR (ATR) spectroscopy. Lastly, the proposed ligands **L11** and **L12** were not effectively isolated and were not assessed in the tests described in the next chapter.

3.4. Materials and Methods

3.4.1. Solvents and reagents

All chemicals were used as received from various chemical-producing companies. The assortment of chemicals used in the above experiments were purchased from the following companies; Scienceworld: NaOH pellets; Merck: methanol (MeOH), ethanol (EtOH), deuterated chloroform ($CDCl_3$), chloroform ($CHCl_3$), diethyl ether, dichloromethane (DCM), conc. H_2SO_4, anhydrous $MgSO_4$, $NaHCO_3$, HCl; Sigma-Aldrich: acetonitrile (CH_3CN), anhydrous K_2CO_3, paraformaldehyde, piperidine, dihexylamine, bis(2-ethylhexyl)amine, 2,2-dimethyl-1,3-propanediamine, o-phenylenediamine, 1,2-*trans*-diaminocyclohexane.

3.4.2. Instrumentation

All ^{1}H and ^{13}C nuclear magnetic resonance spectra were obtained using a 300 MHz Varian VNMRS, 400 MHz Varian Unity Inova or 600 MHz Varian Unity Inova NMR instrument using deuterated solvents. Chemical shifts (δ) were recorded using the residual solvent peak or external reference (TMS). All chemical shifts are reported in parts per million and all spectra were obtained at 25 °C. Data was processed using Mestrenova file version 10.0.2. Melting point determination was done using a Stuart Scientific melting point apparatus in open capillaries. Infrared spectra were readily obtained using a Nicolet Avatar 330 FT-IR instrument as neat samples (ATR), in some spectral collection cases, where necessary, the instrument was flushed with N_2 (g) to eliminate the manifestation of CO_2. Standard resolution mass spectrometry was performed by CAF (Central Analytical Facility) at Stellenbosch University using a Waters Synapt G2 spectrometer by direct injection of sample. Samples for EA analysis were done on a Perkin-Elmer 2400 Series II CHNS/O Elemental Analyser at the University of Kwa-Zulu Natal.

3.4.3. Experimental procedures

3.4.3.1. Synthesis of 1-(ethoxymethyl)piperidine (A1)

Piperidine (18.1 g, 0.212 mol, 1 eq.) was added dropwise to a suspension of paraformaldehyde (7.96 g, 0.265 mol, 1.25 eq.) and anhydrous potassium carbonate (58.6 g, 0.424 mol, 2 eq.) in absolute EtOH (200 mL) with external cooling in an ice bath. The mixture was then stirred vigorously for 48 h using a magnetic stirrer allowing the temperature to reach ambient gradually. The solid was then filtered off and washed with dried diethyl ether (2 × 50 mL). The resulting filtrate was concentrated *in vacuo* to yield a grey-colourless oil which was fractionally distilled through a Kugelrohr vacuum distillation apparatus operating at 80 °C at 3.5 mbar affording the product as a colourless oil (18.9 g, 62.2 %). **^{1}H NMR** (300 MHz, $CDCl_3$) δ 3.95 (s, 2H, O-C$\underline{H_2}$-N), 3.39 (q, J = 7.0 Hz, 2H, O-C$\underline{H_2}$-CH_3), 2.54 (m, 4H, -N-C$\underline{H_2}$-CH_2-CH_2-), 1.30-1.51 (m, 6H, -N-CH_2-C$\underline{H_2}$-C$\underline{H_2}$-), 1.09 (t, J = 7.0 Hz, 3H, O-CH_2-C$\underline{H_3}$); **^{13}C NMR** (300 MHz, $CDCl_3$) δ 82.89 (O-C$\underline{H_2}$-N), 64.32 (-O-C$\underline{H_2}$-CH_3), 53.20 (-N-C$\underline{H_2}$-CH_2-CH_2-), 26.07 (-N-CH_2-C$\underline{H_2}$-CH_2-), 25.04 (-N-CH_2-CH_2-C$\underline{H_2}$-), 15.43 (-O-CH_2-C$\underline{H_3}$).

3.4.3.2. Synthesis of N-(ethoxymethyl)-N-hexylhexan-1-amine (A2)

Dihexylamine (18.5 g, 0.100 mol, 1 eq.) and anhydrous potassium carbonate (27.6 g, 0.200 mol, 2 eq.) were stirred together in absolute EtOH (100 mL) for approximately 1.5 h at room temperature. Paraformaldehyde (3.75 g, 0.125 mol, 1.125 eq.) was then added to the mixture which was stirred vigorously for 48 h using a magnetic stirrer. Ensuing this, the reaction mixture was filtered using a Buchner filter and washed with diethyl ether (2 × 50 mL). The resulting filtrate was concentrated *in vacuo* affording a clear-light yellow liquid. The product was then subjected to fractional distillation using a Kugelrhor apparatus operating at 130 °C and approximately 3.5 mbar affording a pale yellow to colourless oil in moderate yield (14.4 g, 59.0 %). **^{1}H NMR** (600 MHz, $CDCl_3$) δ 4.13 (s, 2H, -O-C$\underline{H_2}$-N-), 3.42 (q, J = 7.0 Hz, 2H, -O-C$\underline{H_2}$-CH_3), 2.59 (m, 4H, -N-C$\underline{H_2}$-C$\underline{H_2}$-CH_2-CH_2-CH_2-CH_3), 1.45 (m, 2H, -N-CH_2-C$\underline{H_2}$-CH_2-CH_2-CH_2-CH_3) 1.24 – 1.33 (m, 12H, -N-CH_2-CH_2-C$\underline{H_2}$-C$\underline{H_2}$-C$\underline{H_2}$-CH_3), 1.16 (t, J = 7.0 Hz, 3H, -O-CH_2-C$\underline{H_3}$), 0.86 (t, J = 7.0 Hz, 6H, -CH_2-CH_2-C$\underline{H_3}$); **^{13}C NMR** (600 MHz, $CDCl_3$) δ 86.26 (O-C$\underline{H_2}$-N), 63.37 (O-C$\underline{H_2}$-CH_3), 52.12 (-N-C$\underline{H_2}$-CH_2-), 32.07 (-N-CH_2-CH_2-CH_2-

$\underline{C}H_2$-), 28.25 (-N-CH_2-$\underline{C}H_2$-CH_2-), 27.44 (-N-CH_2-CH_2-$\underline{C}H_2$-), 22.83 (-N-CH_2-CH_2-CH_2-CH_2-$\underline{C}H_2$-), 15.45 (O-CH_2-$\underline{C}H_3$), 14.16 (-CH_2-CH_2-$\underline{C}H_3$).

3.4.3.3. Synthesis of N-(ethoxymethyl)-2-ethyl-N-(2-ethylhexyl)hexan-1-amine (A3)

Bis(2-ethylhexyl)amine (24.1 g, 0.100 mol, 1 eq.) was added dropwise to a suspension of paraformaldehyde (3.75 g, 0.125 mol, 1.125 eq.) and anhydrous potassium carbonate (27.6 g, 0.200 mol, 2 eq.) in absolute EtOH (150 mL) with external cooling in an ice bath. The mixture was then stirred vigorously for 48 h permitting the temperature to steadily reach ambient. After the reaction, the solid was filtered off and the resulting filtrate was washed with dried diethyl ether (2 × 50 mL). The filtrate was then concentrated *in vacuo* to give a viscous orange-red oil which was fractionally distilled through a Kugelrohr vacuum distillation apparatus operating at 150°C at 3.5 mbar yielding the product as a light yellow-orange oil (14.5 g, 48.5 %). **^{1}H NMR** (600 MHz, $CDCl_3$) δ 4.07 (s, 2H, O-C$\underline{H}_2$-N), 3.43 (q, J = 7.0 Hz, 2H, O-C$\underline{H}_2$-CH_3), 2.42 (m, 2H, -N-C$\underline{H}_2$-CH-) 2.19 (m, 2H, -N-C$\underline{H}_2$-CH(C_2H_5)CH_2-), 1.71 (m, 2H, -C$\underline{H}$(CH_2-CH_3)CH_2-), 1.20-1.42 (m, 4H, -CH(C$\underline{H}_2$-CH_3)CH_2-), 1.20 – 1.42 (m, 12H, -N-CH_2-C$\underline{H}$(C$\underline{H}_2$$CH_3$)C$\underline{H}_2$-C$\underline{H}_2$-C$\underline{H}_2$-$CH_3$), 1.16 (t, J = 7.0 Hz, 3H, -O-CH_2-C$\underline{H}_3$), 0.80-0.90 (t, J = 7.0 Hz, 6H, -CH(CH_2-C$\underline{H}_3$)CH_2-), 0.80-0.90 (t, J = 7.0 Hz, 6H, -N-CH_2-CH(C_2H_5)CH_2-CH_2-CH_2-C$\underline{H}_3$); **^{13}C NMR** (400 MHz, $CDCl_3$) δ 86.27 (O-$\underline{C}H_2$-N), 63.39 (O-$\underline{C}H_2$-CH_3), 56.90 (-N-$\underline{C}H_2$-CH-), 37.78 (-$\underline{C}$H(CH_2-CH_3)CH_2-), 31.19 (-N-CH_2-CH(C_2H_5)$\underline{C}H_2$-), 28.99 (-N-CH_2-CH(C_2H_5)-CH_2-$\underline{C}H_2$-), 24.44 (-CH($\underline{C}H_2$-CH_3)CH_2-), 23.38 (-CH(C_2H_5)CH_2-CH_2-$\underline{C}H_2$-CH_3), 15.46 (-O-CH_2-$\underline{C}H_3$), 14.29 (-CH(C_2H_5)CH_2-CH_2-CH_2-$\underline{C}H_3$), 10.86 (-CH(CH_2-$\underline{C}H_3$)CH_2-).

3.4.3.4. Synthesis of 5-(tert-butyl)-2-hydroxy-3-(piperidin-1-ylmethyl)benzaldehyde (B1)

5-(tert-butyl)-2-hydroxybenzaldehyde (7.60 g, 0.0427 mol, 1 eq.) and **A1** (6.11 g, 0.0427 mol, 1 eq.) were dissolved in acetonitrile (100 mL) and refluxed under a nitrogen atmosphere for approximately 90 h. The resultant solution was cooled to room temperature and the solvent removed *in vacuo* to yield an orange-red oil. The crude product was then re-dissolved in absolute EtOH so as to achieve a saturated solution and placed in an ice bath. After fewer than two days, it was found that white-transparent crystals had formed which were

then filtered and washed with cold EtOH and dried under reduced pressure yielding the product as an off-white crystalline material (7.65 g, 65.1 %). **FT-IR** (neat): $\nu_{C=O}$ (1670.48 cm^{-1}); **^{1}H NMR** (400 MHz, $CDCl_3$) δ 10.40 (s, 1H, -CHO), 7.63 (d, J = 4.0 Hz, C^{Ar}-H), 7.23 (d, J = 4.0 Hz, C^{Ar}-H), 3.69 (s, 2H, C^{Ar}-CH_2-N), 2.52 (m, 4H, -N-CH_2-CH_2-CH_2-), 1.63 (m, 4H, -N-CH_2-CH_2-CH_2-), 1.49 (m, 2H, -N-CH_2-CH_2-CH_2-), 1.26 (s, 9H, -C(CH_3)$_3$); **^{13}C NMR** (600 MHz, $CDCl_3$) δ 191.15 (-CHO), 160.07 (C^{Ar}-OH), 141.51 (C^{Ar}-C(CH_3)$_3$), 132.37 (C^{Ar}-H), 123.82 (C^{Ar}-CHO), 122.90 (C^{Ar}-H), 122.45 (C^{Ar}-CH_2-N-), 61.49 (Ar-CH_2-N), 53.97 (-N-CH_2-CH_2-CH_2-), 34.13 (-C(CH_3)$_3$), 31.40 (-C(CH_3)$_3$), 25.80 (-N-CH_2-CH_2-CH_2-), 23.92 (-N-CH_2-CH_2-CH_2-).

3.4.3.5. Synthesis of 5-(tert-butyl)-3-((dihexylamino)methyl)-2-hydroxybenzaldehyde (B2)

5-(tert-butyl)-2-hydroxybenzaldehyde (3.76 g, 15.5 mmol, 1 eq.) and **A2** (3.78 g, 15.5 mmol, 1 eq.) were dissolved in acetonitrile (100 mL) and refluxed under a nitrogen atmosphere for approximately 90 h. The resulting solution was cooled to room temperature and the solvent removed under reduced pressure to yield a brown-red oil. This crude product was dissolved in DCM and extracted with distilled water (3 × 30 mL) using a separating funnel. The organic layer was isolated and dried using $MgSO_4$ which was then filtered off. The filtrate was then isolated and the solvent removed using a rotary evaporator affording a light-orange oil (4.24 g, 72.8 %). **FT-IR** (neat): $\nu_{C=O}$ (1679.77 cm^{-1}); **^{1}H NMR** (600 MHz, $CDCl_3$) δ 10.41 (s, 1H, -CHO), 7.64 (d, J = 2.5 Hz, 1H, C^{Ar}-H), 7.25 (d, J = 2.5 Hz, 1H, C^{Ar}-H), 3.78 (s, 2H, C^{Ar}-CH_2-N), 2.52 (m, 4H, -N-CH_2-CH_2-CH_2-), 1.25 – 1.30 (m, 16H, -N-CH_2-CH_2-CH_2-CH_2-CH_2-CH_3), 1.32 (s, 9H, -C(CH_3)$_3$), 0.87 (m, 6H, -CH_2-CH_2-CH_3); **^{13}C NMR** (600 MHz, $CDCl_3$) δ 191.24 (-CHO), 160.25 (C^{Ar}-OH), 141.48 (C^{Ar}-C(CH_3)$_3$), 132.25 (C^{Ar}-H), 123.76 (C^{Ar}-CHO), 123.63 (C^{Ar}-H), 122.47 (C^{Ar}-CH_2-N-), 57.52 (C^{Ar}-CH_2-N), 53.62 (-N-CH_2-CH_2-), 34.18 (-C(CH_3)$_3$), 31.73 (-CH_2-CH_2-CH_3), 31.43 (-C(CH_3)$_3$), 27.10 (-N-CH_2-CH_2-CH_2-), 26.32 (-N-CH_2-CH_2-CH_2-), 22.64 (-CH_2-CH_2-CH_3), 14.11 (-CH_2-CH_2-CH_3).

3.4.3.6. Synthesis of 3-((bis(2-ethylhexyl)amino)methyl)-5-(tert-butyl)-2-hydroxybenzaldehyde (B3)

5-(tert-butyl)-2-hydroxybenzaldehyde (1.20 g, 6.75 mmol, 1 eq.) and **A3** (2.02 g, 6.75 mmol, 1 eq.) were dissolved in acetonitrile (100 mL) and refluxed under nitrogen atmosphere for approximately 90 hours. The resulting solution was cooled to room temperature and the solvent removed under reduced pressure to yield a viscous brown-red oil. The oil was then dissolved in DCM and extracted with a 30 % ethanol solution (3 × 30 mL). Immediately, a colour change was observed in the aqueous phase (clear to bright yellow). The DCM layer was then isolated and dried using $MgSO_4$ which then was filtered. The solvent was removed from the filtrate yielding a light-orange-red oil (2.07 g, 70.9 %). **FT-IR** (neat): $\nu_{C=O}$ (1681.59 cm^{-1}); **^{1}H NMR** (600 MHz, $CDCl_3$) δ 10.29 (s, 1H, -C<u>H</u>O), 7.58 (d, J = 2.5 Hz, C^{Ar}-<u>H</u>), 7.42 (d, J = 4.0 Hz, C^{Ar}-<u>H</u>), 3.65 (s, 2H, C^{Ar}-C<u>H_2</u>-N), 2.47 (d, J = 6.3 Hz, 2H, -N-C<u>H_2</u>-CH-), 2.26 (d, 2H, J = 6.7 Hz, -N-C<u>H_2</u>-CH), 1.15 - 1.65 (m, 27H, -C<u>H</u>($C\underline{H_2}$-CH_3)$C\underline{H_2}$-$C\underline{H_2}$-$C\underline{H_2}$-CH_3) 1.29 (s, 9H, -C($C\underline{H_3}$)$_3$), 0.77 - 0.92 (m, 12H, -CH(CH_2-$C\underline{H_3}$)CH_2-CH_2-CH_2-$C\underline{H_3}$); **^{13}C NMR** (600 MHz, $CDCl_3$) δ 192.68 (-<u>C</u>HO), 159.22 ($\underline{C}^{Ar}$-OH), 141.86 ($\underline{C}^{Ar}$-C(CH_3)$_3$), 133.34 ($\underline{C}^{Ar}$-CHO), 125.46 ($\underline{C}^{Ar}$-H), 124.60 ($\underline{C}^{Ar}$-H), 121.80 ($\underline{C}^{Ar}$-CH_2-N-), 59.88 (-N-<u>CH_2</u>-CH-), 57.50 (C^{Ar}-<u>CH_2</u>-N), 37.10 (-<u>C</u>H(CH_2-CH_3)CH_2-), 34.20 (-<u>C</u>(CH_3)$_3$), 31.50 (-N-CH_2-CH(C_2H_5)<u>CH_2</u>-), 31.42 (-C(<u>CH_3</u>)$_3$), 28.80 (-CH(C_2H_5)-CH_2-<u>CH_2</u>-), 24.68 (-CH(<u>CH_2</u>-CH_3)CH_2-), 23.22 (-CH(C_2H_5)CH_2-CH_2-<u>CH_2</u>-CH_3), 14.21 (-CH_2-CH_2-<u>CH_3</u>), 10.74 (-CH(CH_2-<u>CH_3</u>)CH_2-).

3.4.3.7. Synthesis of 6,6'–((1E,1'E)-((2,2-dimethylpropane-1,3-diyl)bis(azanylylidene)) bis(methanylylidene))bis(4-(tert-butyl)-2-(piperidin-1-ylmethyl)phenol) (L7)

Compound **B1** (2.57 g, 9.34 mmol, 2 eq.) was dissolved in $CHCl_3$ (40 mL) and transferred to a two-neck round bottom flask (200 mL). The solution was heated and stirred using a magnetic stirrer hot plate while 2,2-dimethylpropane-1,3-diamine (0.478 g, 4.68 mmol, 1 eq.) in EtOH (60 mL) was added dropwise. A colour change was observed from a bright yellow to a light yellow/off-green colour. The resulting solution was then refluxed for approximately 20 h. Thereafter, the solvent was removed *in vacuo* affording a light yellow oil which was re-crystallised from absolute EtOH. The crystals were washed with cold EtOH (3 × 25 mL) and

dried under vacuum yielding pale yellow crystals (2.43 g, 84.2 %). *Anal.* Found: C, 75.73; H, 9.80; N, 8.63 %. $C_{39}H_{60}N_4O_2$ requires: C, 75.93; H, 9.80; N, 9.08 %.

3.4.3.8. Synthesis of 6,6'–((1E,1'E)-((1,1-dimethylethane-1,3-diyl)bis(azanylylidene)) bis(methanylylidene))bis(4-(tert-butyl)-2-(piperidin-1-ylmethyl)phenol) (L8)

Compound **B1** (1.91 g, 6.93 mmol, 2 eq.) was dissolved in $CHCl_3$ (40 mL) and stirred and heated in a two-neck round bottom flask (200 mL) while one equivalent (slight molar excess) of 1,1-dimethyl-1,2-diaminoethane (0.348 g, 3.47 mmol, 1 eq.) in EtOH (30 mL) was added drop-wise to the solution which transitioned from a bright yellow to a yellow-orange colour. The solution was allowed to reflux for approximately 18 hours. Thereafter, the solvent was removed *in vacuo* affording an orange oil. Re-crystallisation from EtOH was not effective and so the oil was dissolved in DCM (50 mL) and washed with distilled water (3 × 25 mL) using a separating funnel. Subsequently, the DCM solution was isolated and the solvent removed *in vacuo* affording a yellow-orange oil which was further dried under vacuum (1.90 g, 91.0 %). *Anal.* Found: C, 75.73; H, 9.83; N, 9.10 %. $C_{38}H_{58}N_4O_2$ requires: C, 75.70; H, 9.70; N, 9.29 %.

3.4.3.9. Synthesis of 6,6'–((1E,1'E)-((1S,2S)-cyclohexane-1,2-diylbis(azanylylidene)) bis(methanylylidene))bis(4-(tert-butyl)-2-(piperidin-1-ylmethyl)phenol) (L9)

Compound **B1** (1.71 g, 6.21 mmol, 2 eq.) was dissolved in $CHCl_3$ (40 mL) and stirred and heated in a 200 mL two-neck round bottom flask while one equivalent (slight molar excess) of 1,2-*trans*-diaminocyclohexane (0.355 g, 3.11 mmol, 1 eq.) in EtOH (30 mL) was added drop-wise to the solution which went from a bright yellow to a light orange colour. The solution was then refluxed for about 24 h. Thereafter, the solvent was removed *in vacuo* affording a yellow/orange oil which was dissolved in absolute EtOH. The product was precipitated from the EtOH solution at low temperatures using an ice bath. The product was then filtered and washed with cold EtOH (3 × 25 mL) and dried on a high vacuum line yielding a yellow/orange powder (1.73 g, 88.4 %). *Anal.* Found: C, 76.37; H, 9.26; N, 8.43 %. $C_{40}H_{54}N_4O_2$ requires C, 76.39; H, 9.62; N, 8.91 %.

3.4.3.10. Synthesis of 6,6'-((1E,1'E) –((1S,2S)-cyclohexane-1,2-diylbis(azanylylidene)) bis(methanylylidene))bis(4-(tert-butyl)-2-((dihexylamino)methyl)phenol) (L10)

Compound **B2** (7.20 g, 0.0192 mol, 2 eq.) in slight molar excess in $CHCl_3$ (90 mL) was treated drop-wise with slight excess of 1,2-*trans*-diaminocyclohexane (1.17 g, 0.0103 mol, 1 eq.) in EtOH (50 mL). This was then allowed to stir at room temperature for 24 hours. The solvent was removed *in vacuo* to yield an orange oil. This oil was then dissolved in 50 mL DCM and extracted with 3 × 30 mL distilled water. The organic layer was dried over anhydrous magnesium sulfate, after which, it was filtered and the solvent once again removed to yield a viscous orange oily substance. Attempted further purification by way of chromatography (100 % EtOAc) showed insignificant improvement in purity. The final product was obtained in moderate yield (3.85 g, 48.4 %). *Anal.* Found: C, 76.45; H, 10.93; N, 6.63 %. $C_{52}H_{92}N_4O_2$ requires C, 78.20; H, 11.18; N, 6.76 %.

3.4.3.11. General synthesis of "copper-only" complexes of L7-L10

Solutions of the appropriate ligand **L7-L10** (1.22 mmol, 1 eq.) in $CHCl_3$ (30 mL) and $Cu(CH_3COO)_2 \cdot H_2O$ (0.244 g, 1.22 mmol, 1 eq.) in MeOH (50 mL) were mixed together and stirred for 24 h. The solvent was removed *in vacuo* to yield a black amorphous solid (this was the case in all instances), which was re-dissolved in $CHCl_3$ (60 mL) and washed with a pH 9 NH_3 solution (2 × 30 mL). The resulting organic phase was dried with anhydrous $MgSO_4$, filtered and then concentrated *in vacuo* to yield the metal complex which was used without further purification.

3.4.3.12. Attempted synthesis of 6,6'-((1E,1'E) –(1,2-phenylenebis(azanylylidene)) bis(methanylylidene))bis(4-(tert-butyl)-2-((dihexylamino)methyl)phenol) (L11)

Compound **B2** (7.198 g, 0.01916 mol, 2 eq.) in slight molar excess in $CHCl_3$ (90 mL) was treated drop-wise with 1,2-diaminobenzene (1.172 g, 0.01026 mol, 1.07 eq.) in EtOH (50 mL). The solution was then refluxed for approximately 20 h, after which, the solvent was removed *in vacuo* to afford an orange-brown oil. The oil was then dissolved in 50 mL DCM and extracted with distilled water (3 × 30 mL). The organic layer was dried

over anhydrous magnesium sulfate, after which, it was filtered and the solvent once again removed to yield a viscous brown-orange oily substance which was found to be highly impure. Attempted purification was unsuccessful. A re-attempt of the synthesis with an even slower dropwise addition of the linker over a period of 2 h did not improve the yield.

3.4.3.13. Attempted synthesis of 6,6'-((1E,1'E)–(1,2-phenylenebis(azanylylidene)) bis(methanylylidene))bis(2-((bis(2-ethylhexyl)amino)methyl)-4-(tert-butyl)phenol) (L12)

Two equivalents of **B3** (1.998 g, 0.4628 mmol, 2 eq.) in slight molar excess in $CHCl_3$ (60 mL) was transferred to a two-neck round bottom flask (200 mL) and allowed to stir vigorously while 1,2-diaminobenzene (1.172 g, 0.2314 mmol, 1 eq.) in EtOH (40 mL) was added dropwise over a period of 1 h. The solution was then refluxed for approximately 24 h. Thereafter, the solvent was removed *in vacuo* affording a dark red-brown viscous oil. This crude product was dissolved in 50 mL DCM and extracted with distilled water (3 × 30 mL). The organic layer was dried over anhydrous magnesium sulfate, which was filtered off and washed with DCM (2 × 20 mL). The filtrate solvent was removed *in vacuo* producing a similar substance to the crude product. Characterisation showed a mixture of components and ultimately further purification was ineffective. The reaction could not be re-attempted due to the depleted supply of **B3**.

3.5. References

1. Gale, P. A. *Chem. Commun.* **2011**, *47* (1), 82–86.
2. Simmons. *Jacs.* **1968**, *90*, 2428–2429.
3. Sessler, J. L.; Gale, P. A.; Cho, W.-S. *Anion Receptor Chemistry*; Royal Society of Chemistry, 2006.
4. Sundius, T. **1988**, *175*, 319–322.
5. Gale, P. A; Busschaert, N.; Haynes, C. J. E.; Karagiannidis, L. E.; Kirby, I. L. *Chem. Soc. Rev.* **2014**, *43* (1), 205–241.
6. D. Beer, P.; K. Hopkins, P.; D. McKinney, J. *Chem. Commun.* **1999**, No. 13, 1253–1254.

7. Kavallieratos, K.; Sachleben, R. A; Van Berkel, G. J.; Moyer, B. A. *Chem. Commun.* **2000**, No. 3, 187–188.

8. White, D. J.; Laing, N.; Miller, H.; Parsons, S.; Tasker, P. A. *Chem. Commun.* **1999**, 2077–2078.

9. Adams, H.; Bailey, N. A.; Fenton, D. E.; Papageorgiou, G. **1995**, No. 1, 1883–1886.

10. Miller, H. A.; Laing, N.; Parsons, S.; Parkin, A.; Tasker, P. A.; White, D. J. *J. Chem. Soc. Dalt. Trans.* **2000**, No. 21, 3773–3782.

11. Fennie, M. W.; DiMauro, E. F.; O'Brien, E. M.; Annamalai, V.; Kozlowski, M. C. *Tetrahedron.* **2005**, *61* (26), 6249–6265.

12. Tasker, P. A.; Tong, C. C.; Westra, A. N. *Coord. Chem. Rev.* **2007**, *251* (13–14 SPEC. ISS.), 1868–1877.

13. Plieger, P. G.; Tasker, P. A.; Galbraith, S. G. *Dalt. Trans.* **2004**, No. 2, 313–318.

CHAPTER 4: EXTRACTION & BULK LIQUID MEMBRANE TRANSPORT STUDIES PERFORMED ON MONOTOPIC & DITOPIC LIGANDS

4.1. Introduction

Solvent extraction of metals is an eminent technology in hydrometallurgical industry, analytical separations and liquid waste treatment.[1] Metal ions, cations and anions are extracted from an aqueous phase into an organic phase through reversible chemical reactions. The extractant usually exhibits a very low solubility in the aqueous phase, however is able to interact with metal ions present in the aqueous phase at the liquid-liquid interface and isolate them into an organic phase via the generation of an organic-soluble neutral complex. So, extraction is described by a heterogeneous chemical reaction on either side of the aqueous-organic interface to the final equilibrium concentrations of the reaction products.[2]

Competitive metal ion extraction is a solvent extraction procedure in which more than one type of metal capable of binding to the extractant is dissolved in the aqueous solution. The extractive nature of a chelating agent can be assessed by simulating industrial techniques for the separation and concentration unit operations in a hydrometallurgical flowsheet. Competitive metal extraction deals with a collection of metals in an aqueous feed solution which compete with one another to coordinate to the donor sites of the ligand present in the organic solvent. Similarly, metal salt preferences of combinations of metal cations and the anions tested in these experiments can be determined for ditopic ligands **L7**-**L10**. Competitive anion extraction deals with different anionic species competing for the positively-charged nitrogen present on the pendant alkylamino methyl group of these ditopic ligands as they exist in their zwitterionic forms.

With this said, chapter 4 deals with understanding the coordination characteristics of monotopic ligands (**L1**-**L6**) and ditopic ligands (**L7**-**L10**) through interpreting results obtained from extraction and transport experiments conducted using Cu(II), Ni(II), Zn(II), Co(II), Cd(II) and Pb(II) for the case of all ligands and the anions; Cl^-, NO_3^- and SO_4^{2-} for ditopic ligands. In the metal extraction and transport studies comparisons are drawn from the results to assess the differences between the monotopic ligands and ditopic ligands in these tests. The chapter is divided into three sections, where the first section deals with all competitive metal

extraction studies performed on **L1**-**L10** as well as a short discussion on non-competitive metal extraction tests attempted at varying pH values. The second section concerns the competitive bulk liquid membrane transport experiments tested for metal cations employing all ligands **L1**-**L10.** Lastly, the final section discusses the results of competitive anion extraction and transport experiments conducted with the "copper-only" complexes of the ditopic ligands **L7**-**L10**.

4.2. Results and Discussion

4.2.1. Competitive extraction of metal cations

In view of competitive metal extraction, the tests performed in this chapter examine the partitioning of metal cations between an aqueous phase and an organic phase which is promoted by a chelating agent (**L1**-**L10**). The aqueous solution is made up of NaOAc/AcOH buffer with a pH of 5.05, containing equimolar concentrations (0.01 M) of the six metal ions. The organic phase is made up of a saturated chloroform solution accommodating either **L1**-**L10** (0.01 M) in a 1:1 molar ratio to each metal ion. The two layers are shaken for 24 h at 220 rpm using an oscillating labcon-shaker. Using ICP-OES analysis the amount of metal ions present in the aqueous phase can be monitored. Provided there is minimal leaking during the 24 h shaking, ICP-OES analysis of the aqueous solution before and after the experiment allows for the determination of the percentage of metal which is extracted into the organic solution by the respective ligand.

4.2.1.1. Monotopic ligands (L1-L6)

Monotopic ligands **L1**-**L6** dissolved in the organic phase interact with the doubly charged metal cation dissolved in the aqueous phase at the liquid-liquid interface during the course of shaking. In the cases of **L1**-**L6**, for every metal ion extracted into the organic phase, two protons are transferred to the aqueous phase which further reduces its pH. This extraction process is shown by Eq. 4.1 below.[3]

$$LH_{2(org)} + M^{2+}_{(aq)} \rightleftharpoons M[L\text{-}2H]_{(org)} + 2H^{+}_{(aq)} \qquad \text{(Eq. 4.1)}$$

The results for the competitive extraction experiments, performed in quadruplicate using **L1-L6,** are depicted graphically in Fig 4.1 below. The metal ions which are not seen in the graph are within experimental error and are not reported.

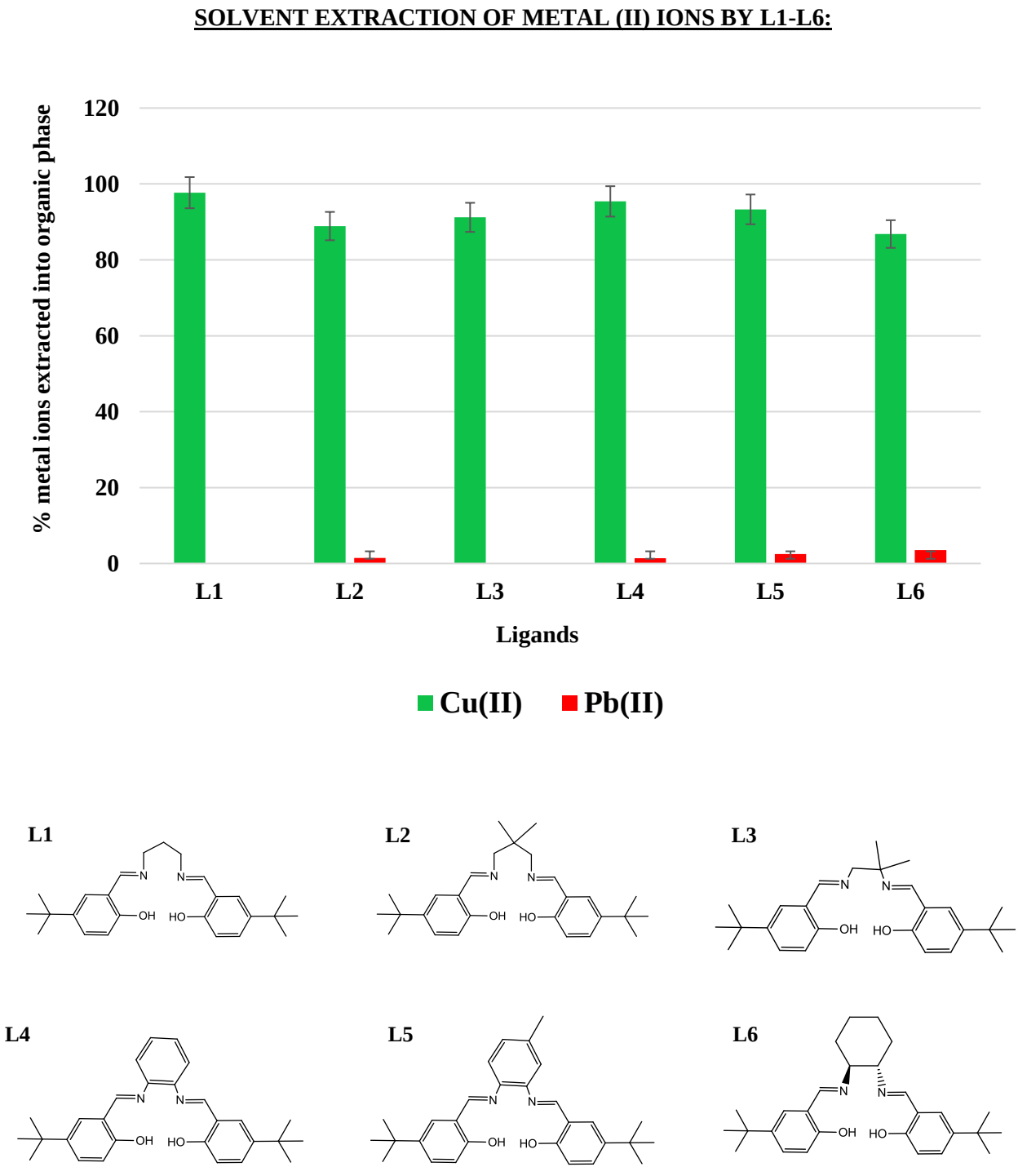

FIGURE 4.1 Above: Percentage metal ion extraction for **L1-L6** obtained from competitive extraction tests performed in quadruplicate (Error bars denote the standard deviation between experimentally measured values Below: Chemical structures of **L1-L6.** Prior to experiment: [M] = 0.01 M in aqueous source phase (pH = 5.05). [L] = 0.01 M in organic membrane phase.

It is clear from Fig. 4.1 that all six salen-type monotopic ligands show an exceptional selectivity towards the copper ion over the other five metal ions present within the aqueous phase. This preference may be rationalised by the Irving-Williams series in combination with the HSAB principle. In this experiment, copper is present among five other metal cations and this study is thus referred to as competitive extraction. In other words, metal ions must out-compete other metal ions to bind to the $[N_2O_2]^{2-}$ donor set at the liquid-liquid interface in order to be selectively extracted from the aqueous phase into the organic phase. From these results, Cu(II) is the preferred metal ion to be complexed within the ligand cavity. The differences in percentage uptake of Cu(II) for the six monotopic ligands, is in effect due to the varying electronic and structural nature of the diimine linker moiety incorporated in the salen-type ligands. It is observed that an enhanced electron-donating ability of the linker moiety affects the electronic nature of the $[N_2O_2]^{2-}$ donor cavity and through increasing electron density on the nitrogen and oxygen donor atoms, leads to a lower selectivity towards copper. The reason for this stems from the HSAB principle, in that an increase in electron density on these donor atoms makes them more "soft" in nature and leads to a broader selectivity for larger and more polarisable metal ions such as Pb(II). Furthermore, an important parameter to be acknowledged in justifying the selectivity of these metal ions under investigation is the formation of a pseudo-macrocyclic metal complex upon complexation of a metal to the monotopic ligand. The size of the cavity formed during this binding process is thus crucial to the stability of the metal complex which is generated. It can be identified that **L3**-**L6** would produce the same size chelate rings upon metal complexation, whereas for **L1** and **L2**, the chelate ring formed between the two nitrogen donor atoms will be one carbon more and thus bigger than those formed for ligands **L3**-**L6**.

4.2.1.2. Ditopic ligands (L7-L10)

Ditopic ligands **L7**-**L10** dissolved in $CHCl_3$ (organic phase) interact with the doubly-charged metal cation dissolved in the aqueous phase at the liquid-liquid interface during shaking according to Eq. 4.2 below.[3]

$$LH_{2(org)} + M^{2+}{}_{(aq)} \rightleftharpoons M[LH_2]X_{2\,(org)} \qquad \text{(Eq. 4.2)}$$

X = Cl_2, (NO_3) or SO_4. If X = SO_4, then $M[LH_2]X_{(org)}$

Ditopic ligands **L7**-**L10** were similarly exposed to competitive metal ion extraction tests with the same metal ions as those used for the monotopic ligands. The results of these tests are presented in Fig. 4.2.

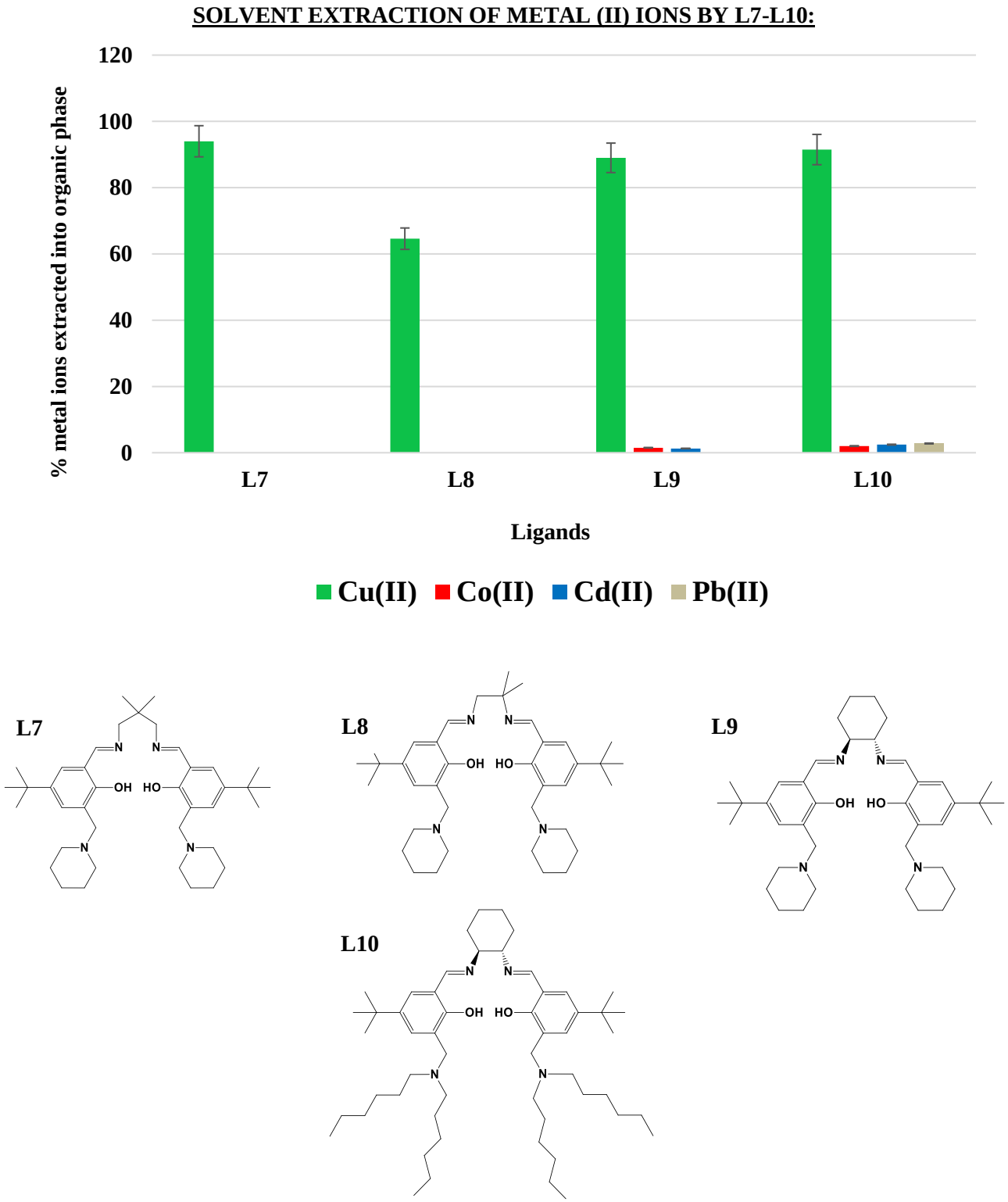

FIGURE 4.2 Above: Percentage metal extraction for **L7**-**L10** obtained from competitive extraction tests performed in quadruplicate (metal ions not included are within experimental error, error bars denote standard deviations) Below: Chemical structures of **L7**-**L10.** Prior to experiment: [M] = 0.01 M in aqueous source phase (pH = 5.05). [L] = 0.01 M in organic membrane phase.

It is evident that **L7**-**L10** show a remarkable selectivity towards Cu(II) over the other five metal ions. **L9** displays a slightly lower uptake of Cu(II) into the organic phase in comparison to **L10**. Additionally, **L10** displays greater uptake of Co(II), Cd(II) and Pb(II) in comparison to **L9**. Since these ligands share the same diimine linker moiety, it is highly likely that the varying anion-binding motif is the property responsible for this difference. A probable explanation for this being that the more polar piperidinyl aminomethyl groups on **L9** make it slightly more susceptible to "bleeding" into the aqueous phase in relation to **L10** which possesses the more non-polar dihexylaminomethyl groups. This allows it to be retained in the organic phase more effectively in relation to **L9** and thus leading to a higher extraction of metal ions. On his note, **L7** showed a similar trend with respect to **L2** (analogous monotopic ligand) where **L7** extracts more Cu(II). This is likely because **L2** is more inclined to "bleed" into the aqueous phase. It was unexpected to see that **L8** extracted less Cu(II) in comparison to the analogous **L3** despite having the additional non-polar piperidinyl moieties. The study was performed in triplicate and it is evident in the picture below that after the 24 h shaking procedure the aqueous phase remains somewhat blue indicating a higher amount of Cu(II) remaining in the aqueous phase after extraction in comparison to **L7**.

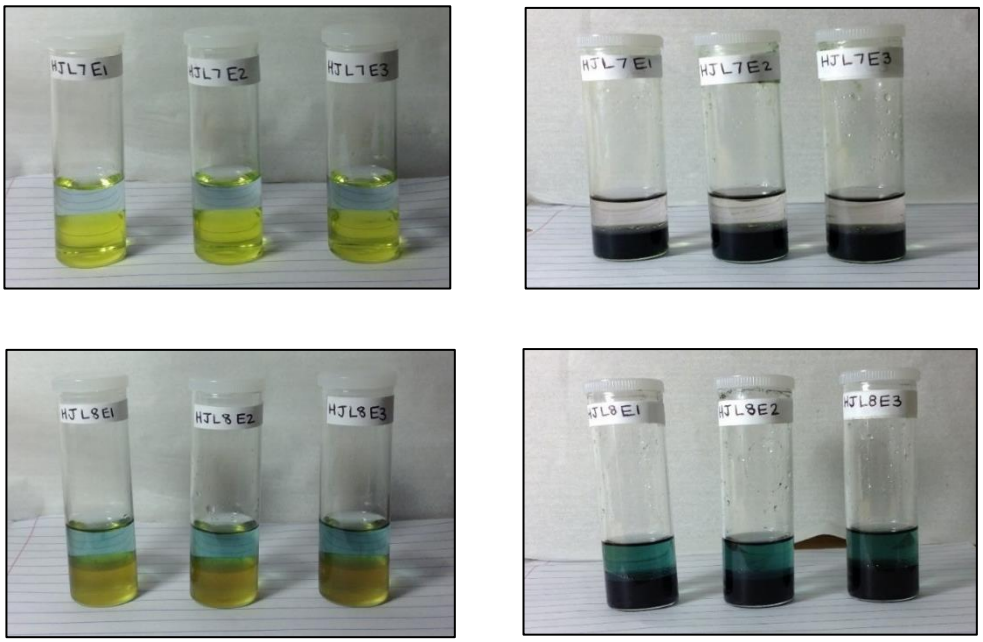

FIGURE 4.3 Competitive metal extraction experiments using ditopic ligands **L7** (top) and **L8** (bottom). *Left:* Before shaking; top layer contains an aqueous buffer solution with a pH of 5.05 comprising Cu(II), Ni(II), Co(II), Zn(II), Cd(II) and Pb(II) each with a concentration of 0.01 M, bottom layer contains an organic solution of 0.01 M concentration of the respective ligand. *Right:* After shaking for 24 h.

From the above sets of results, it is clear that all these ligands prefer coordination to copper over the other metal ions. The expected differences between the monotopic and ditopic ligands is that as a result of incorporating additional dialkylaminomethyl pendant arms to generate ditopic ligands **L7**-**L10**, a greater organic solubility will be imparted to these ditopic ligands and as a result, the extent to which the ligand is leached into the aqueous phase, is lowered.

4.2.2. Competitive bulk liquid membrane transport studies involving metal cations

4.2.2.1. Introduction

The transport experiments utilised a 'concentric cell'[4] in which three phases are effectively separated from one another. The aqueous source phase (10 cm^3) is separated from the aqueous receiving phase (30 cm^3) by the organic membrane phase (50 cm^3). The details of the transport apparatus used in these experiments is illustrated by the 2-D schematic diagram in Fig. 4.4. For the metal transport tests described in this chapter, the organic membrane phase consisted of a saturated chloroform solution containing the respective ligand **L1**-**L10** (0.01 M). The aqueous source phase contained the six metal (II) ions under investigation in an equimolar ratio to the ligand within a sodium acetate/acetic acid buffer solution with a measured pH of 5.05. The aqueous receiving phase consisted of a 0.1 M HNO_3 solution with a measured pH of 1.00.

For each experiment both aqueous phases and the chloroform phase were stirred separately at 10 rpm using stirring paddles (for the receiving phase) and propellers (for the source and organic phase) connected to a single mechanical stirrer. The concentric cell was enveloped by a water jacket controlled at 25 °C. All transport runs were terminated after 24 h and ICP-OES was used to quantify the amount of each metal ion transported over this period.

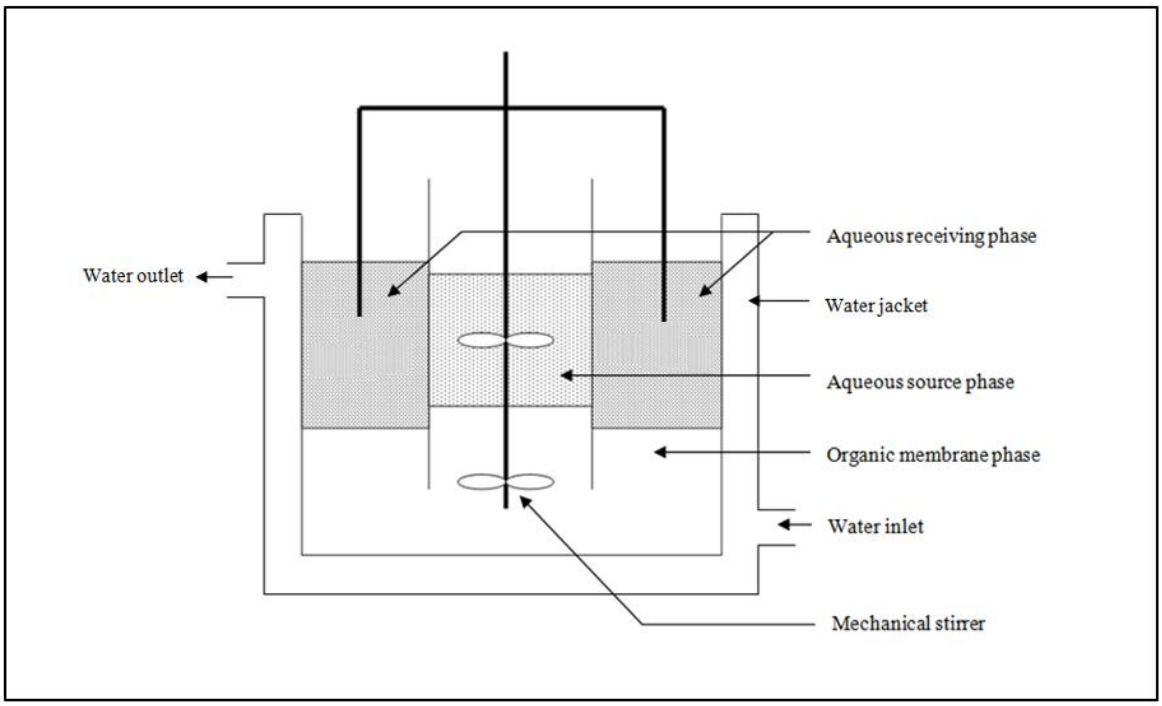

FIGURE 4.4 Schematic diagram of the 'concentric cell' employed in the transport experiments

The principle behind this technique is that the slow stirring of the phases promotes the diffusion of the analytes to the liquid-liquid interfaces. The extractant preferentially coordinates to specific metal ions producing organic-metal complexes which may diffuse within the organic membrane phase against a proton gradient meeting at the liquid-liquid interface of the organic membrane phase and the aqueous receiving phase. At this point, if the pH of the aqueous receiving phase is low enough, the metal ion can be effectively stripped into the aqueous receiving phase. The stripping of the metal ion from the ligand is dependent on the formation constant of the metal ion with the ligand. Provided the ligand has not been hydrolysed by the low pH of the aqueous receiving phase, it is recycled and may transport more metal ions from the source phase to the receiving phase.

The transport efficiency under the experimental conditions employed can be judged by calculating the cation flux rate (J) for each metal ion present in the receiving phase after the 24 h experiment.[4] The cation flux rate can be elucidated using Eq. 4.3 below.

$$J = \frac{C_{(receiving)} \times V_{(receiving)}}{t} \qquad \text{(Eq. 4.3)}$$

J = Cation flux rate (mol/h)
$V_{(receiving)}$ = Volume of aqueous receiving phase (0.03 L)
$C_{(receiving)}$ = Concentration of metal ion in aqueous receiving phase after 24 h (mol/L)

The cation flux rate (mol h^{-1}) is dependent on the quantity of the metal ion transported into the aqueous receiving phase. It denotes the number of moles of the metal ion found in the receiving phase after the 24 h experiment. The moles of the metal ion present in the receiving phase can be determined by its concentration in the receiving phase as well as the volume of the receiving phase. The concentration of the metal ion in the receiving phase is provided by results from ICP-OES and the volume of the aqueous receiving phase is known (30 mL) and t is the duration of the experiment which ran for 24 h. This makes it possible to calculate the cation flux rate for any metal ion found in the aqueous receiving phase after the experiment is terminated.

The transport results are presented as the average of duplicate runs carried out in parallel using unique cells (within experimental error). The values which are reported for these parallel runs did not differ by more than 5 percent. J values less than 2.2 x 10^{-8} were considered to be within experimental error and thus ignored in the reporting of the results.

4.2.2.2. Monotopic ligands (L1-L6)

L1-**L6** were subjected to transport studies in an attempt to understand and further learn their coordination characteristics. Table 4.1 illustrates the experimental values obtained from the competitive transport experiments performed in duplicate using monotopic ligands **L1**-**L6**. An average value is reported in the table and it was found that the experimental values did not differ by more than 5 %.

TABLE 4.1 Experimental data for six-metal ions participating in competitive transport across a bulk chloroform membrane employing **L1**-**L6** at 25 °C. pH of aqueous source phase = 5.05. pH of aqueous receiving phase = 1.00.

Ligand	Cu(II)	Ni(II)	Co(II)	Zn(II)	Cd(II)	Pb(II)
L1						
% (Receiving)[a]	6.0	–	–	–	–	–
% (Membrane)[b]	8.4	–	–	–	–	–
J (mol per h)[c]	74.8	–	–	–	–	–
L2						
% (Receiving)[a]	–	–	–	–	–	–
% (Membrane)[b]	5.4	–	–	–	–	–
J (mol per h)[c]	–	–	–	–	–	–
L3						
% (Receiving)[a]	–	–	–	–	–	–
% (Membrane)[b]	11.4	–	–	–	–	18.9
J (mol per h)[c]	–	–	–	–	–	–
L4						
% (Receiving)[a]	–	–	–	–	–	–
% (Membrane)[b]	82.8	–	–	–	–	5.6
J (mol per h)[c]	–	–	–	–	–	–
L5						
% (Receiving)[a]	–	–	–	–	–	–
% (Membrane)[b]	74.1	–	–	–	–	13.8
J (mol per h)[c]	–	–	–	–	–	–
L6						
% (Receiving)[a]	–	–	–	–	–	–
% (Membrane)[b]	14.7	–	–	–	–	–
J (mol per h)[c]	–	–	–	–	–	–

[a] Percent of total metal cations in the receiving phase after 24 h.
[b] Percent of total metal cations in the membrane phase after 24 h.
[c] All values are × 10^{-8}.

It can be seen that the monotopic ligands show a consistent preference for Cu(II) ions. The key difference between these tests and the competitive extraction trials, in terms of uptake into the organic phase, is that the three-phase setup was only stirred at 10 rpm compared to a shaking speed of 220 rpm for the competitive extraction tests. It is therefore expected that more metal (Cu(II) in these cases) will be sequestered into the organic phase if the solutions are stirred faster and mixed more thoroughly. This prediction is based on the fundamental collision theory, in which molecules with higher kinetic energies will interact more at the liquid-liquid interface than molecules with lower kinetic energies.

An important coordination characteristic pertaining to these monotopic ligands could be deduced through these competitive transport experiments, namely, relative formation constants. The only metal ion found to be

present in the receiving phase was Cu(II) for **L1**. The ligand was found to extract 8.4 % of Cu(II) of the possible 100 % available in the aqueous source phase. Since for **L1**, a relatively large portion of the metals taken into the organic phase were released into the aqueous receiving phase, this indicated that **L1** is stripped more easily in comparison to the other ligands.

L4 and **L5** transport the most Cu(II) ions into the organic membrane phase in comparison to **L1**-**L3** which is consistent with what was observed in the competitive extraction and non-competitive extraction trials. From the results, it can be postulated that **L4** has the highest formation constant with Cu(II) in comparison to the other monotopic ligands. This is noted by a 82.8 % transport of Cu(II) from the aqueous source phase which is notably greater than the other monotopic ligands. Furthermore, no Cu(II) was transported to the receiving phase indicating that the organic metal complex, **Cu[L4-2H]**, is highly stable in comparison to the other copper complexes formed. Comparatively, **L5** is likely to have the second highest formation constant having transported about 74.1 % of the Cu(II) into the membrane phase and releasing none into the aqueous receiving phase. These observations suggest that the electron-withdrawing groups incorporated on their diimine linkers result in a higher formation constant with Cu(II) under the experimental conditions employed. This is likely due to the delocalisation of electron density from the donor atoms rendering them more ‘hard’ and therefore coordinating more strongly to the relatively hard Cu(II) ions.

Remarkably, **L3**-**L5** were the only ligands in these tests which showed selectivity towards another metal ion other than Cu(II). **L3** showed more interest in Pb(II) than Cu(II) with its uptake of Pb(II) being about 18.9 % compared to Cu(II) at 11.4 %. With this said, the ligands which were less symmetrical showed more selectivity towards Pb(II).

4.2.2.3. Ditopic ligands (L7-L10)

L7-**L10** were tested in transport studies using the same experimental conditions as those described for the monotopic ligands. Table 4.2 presents the experimental values collected from the competitive transport experiments conducted in duplicate using ditopic ligands **L7**-**L10**. The reported values are an average of the duplicate measurements which differed by less than 5 % from one another.

TABLE 4.2 Experimental data for six-metal ions involved in competitive transport across a bulk chloroform membrane employing **L7**-**L10** at 25 °C. pH of aqueous source phase = 5.05. pH of aqueous receiving phase = 1.00.

Ligand	Cu(II)	Ni(II)	Co(II)	Zn(II)	Cd(II)	Pb(II)
L7						
% (Receiving)[a]	2.3	–	–	15.9	–	–
% (Membrane)[b]	45.0	–	–	18.4	–	–
J (mol per h)[c]	29.0	–	–	199	–	–
L8						
% (Receiving)[a]	3.8	8.8	–	16.7	–	–
% (Membrane)[b]	68.3	19.1	–	17.2	–	–
J (mol per h)[c]	47.6	110	–	209	–	–
L9						
% (Receiving)[a]	15.3	–	–	9.8	–	–
% (Membrane)[b]	61.8	–	–	16.0	–	–
J (mol per h)[c]	191	–	–	123	–	–
L10						
% (Receiving)[a]	4.8	–	–	9.3	–	–
% (Membrane)[b]	70.3	–	–	12.5	–	–
J (mol per h)[c]	59.9	–	–	116	–	–

[a] Percent of total metal cations in the receiving phase after 24 h.
[b] Percent of total metal cations in the membrane phase after 24 h.
[c] All values are × 10^{-8}.

The competitive transport experiments performed using ditopic ligands **L7**-**L10** delivered some unexpected results. Surprisingly, Zn(II) was found to be the most abundant metal ion present in the aqueous receiving phase in all instances. These observations illustrate the potential of these extractants to transport Zn(II), where **L8** has the highest *J* value for Zn(II) of 209 × 10^{-8} mol h^{-1} . **L7** on the other hand, has the second highest *J* value for Zn(II). In addition, **L7** extracts the least Cu(II) into the organic membrane phase and has lowest cation flux rate for Cu(II) of 29.0 × 10^{-8} mol h^{-1} in comparison to the other ditopic ligands. The electron-donating groups positioned on the diimine linker of **L7** and **L8** may assist in further 'softening' their donor atoms by electronic induction. As a result, the cavity size should increase due to electron-electron repulsion between donor atoms and possibly provide an arrangement toward the tetrahedral geometry favoured by Zn(II).[5] It is also possible that the pendant groups present on the ditopic ligands are somehow facilitating the transport of Zn(II) across the membrane.

The stoichiometry of these ligands is expected to be 1:1 (ligand:metal), although it is possible that these ligands may possess varying stoichiometries and may be able to adopt other arrangements around metal ions giving

rise to other geometries. Although this is speculation, it would certainly be insightful to acquire a single crystal of a Zn(II) complex of these ligands to determine the absolute geometry and stoichiometry adopted by these species.

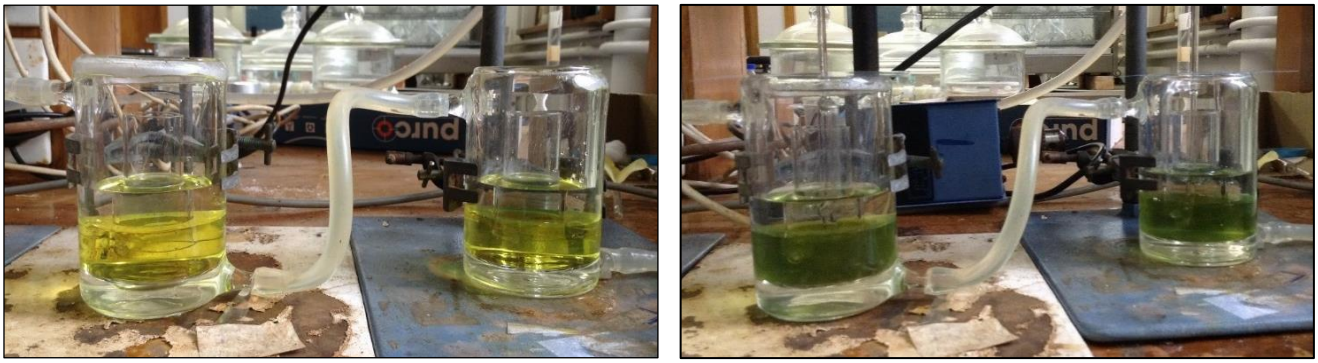

FIGURE 4.5 Competitive metal ion transport experiment using **L7** performed in duplicate. *Left*: Before 24 h of stirring at 10 rpm. *Right*: After 24 h of stirring at 10 rpm.

Prior to acquiring the results for these transport experiments, it was envisaged that Cu(II) would be removed from the aqueous source phase based on the results attained from the competitive extraction tests. In all cases, this was established experimentally and the results of the transport experiments therefore complemented the competitive extraction findings. Ditopic ligands **L9** and **L10** shared the same diimine moiety making it possible to compare the effect of the attached dialkylaminomethyl groups. **L9** transported less Cu(II) into the membrane phase in comparison to the comparable **L10**. This was ascribed to the greater solubility of **L10** in the organic phase due to having the more non-polar dihexylaminomethyl arms compared to the piperidinylmethyl arms present on **L9**.

For both the monotopic and ditopic ligands under scrutiny, very little Cu(II) which was sequestered into the organic membrane phase was subsequently delivered to the aqueous receiving phase. This implies a high formation constant of Cu(II) for these ligands and may be attributed to the general salen-scaffold employed and the trend of the Irving-Williams series. Lastly, the ditopic ligands transported more copper in comparison to their analogous monotopic ligands explicated by the higher cation flux rates. This is likely a result of the increased solubility of the ditopic ligands in the organic membrane phase which leads to a higher transport of Cu(II) into the organic phase and affording an increased probability of these ions to be stripped into the aqueous receiving phase.

4.2.3. Competitive extraction of anions by ditopic ligands (L7-L10)

The "copper-only" complexes, **Cu[L-2H]**, of **L7-L10** underwent a solvent extraction test to determine the quantities of NO_3^-, Cl^- and SO_4^{2-} which were sequestered into the organic phase using these complexes. The idea behind this trial is that all three anions exist at an equimolar concentration in relation to one another and are dissolved in an aqueous solution exhibiting a pH of approximately 2.09. An immiscible organic phase comprised of an equimolar concentration of the "copper-only" complex in saturated chloroform is contacted with the aqueous phase. The system undergoes shaking at 220 rpm using an industrial laboratory shaker. Upon interaction at the liquid-liquid interface, the alkylaminomethyl pendant arms are protonated by the acidic source phase generating a dicationic site which serves as the anion-binding site. The anions coordinate to these positively-charged motifs and are taken into the organic phase by the metal salt extractant. Before and afterwards, the aqueous phase is analysed using ion chromatography to determine the percentage of each anionic species which has been withdrawn from it by each ligand complex. These results are graphically depicted in Figure 4.6 below where the percentage of each ion taken into the organic phase by the respective ditopic ligand system used, the copper complexes of **L7-L10**.

SOLVENT EXTRACTION OF ANIONS BY 'COPPER-ONLY' COMPLEXES OF L7-L10:

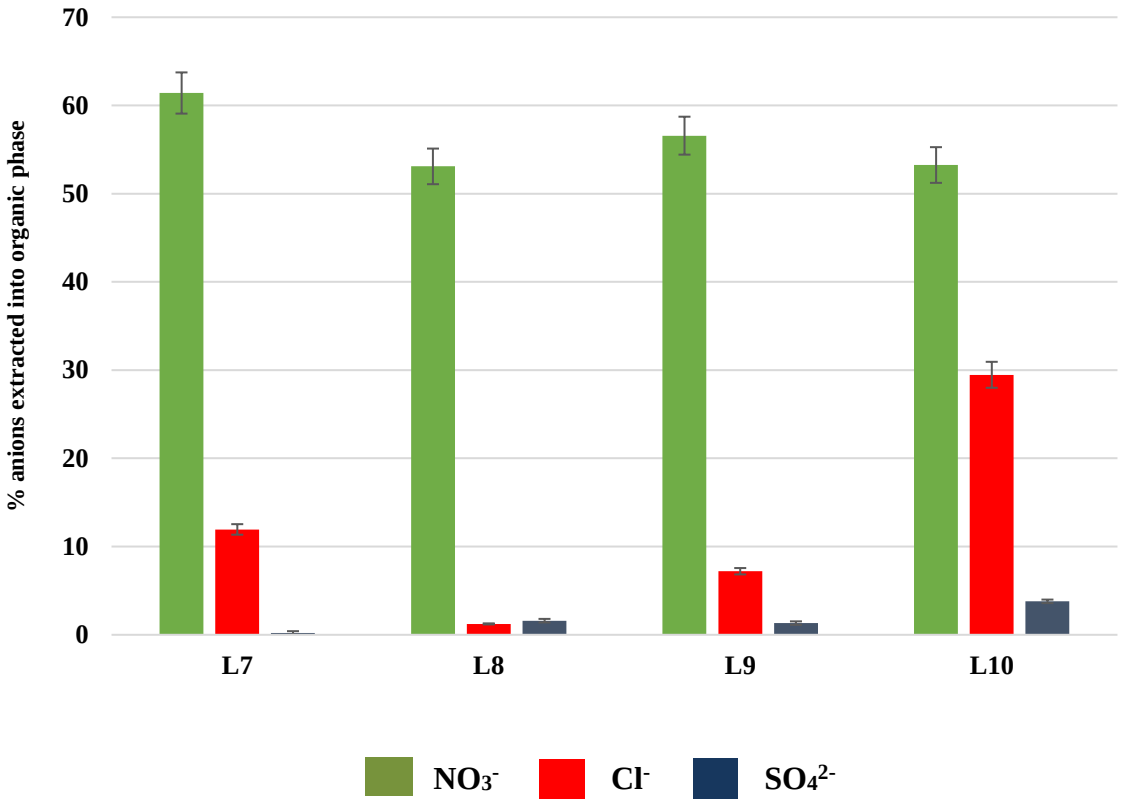

FIGURE 4.6 Percentage anion extracted from the aqueous phase into the organic phase by **L7**-**L10** in the competitive anion extraction tests performed in triplicate. $[NO_3^-] = [Cl^-] = [SO_4^{2-}] = 0.01$ M in aqueous source phase (pH = 2.09). 'Copper-only' complex = 0.01 M in organic phase.

It is observed that NO_3^- is the most extracted anion whereas SO_4^{2-} is the least extracted anion. The low extraction of the sulfate dianion is an expected result as it is in accordance with the Hoffmeister bias. Additionally, the uptake of the univalent NO_3^- and Cl^- ions would be prevalent over the bivalent SO_4^{2-} ion as each ditopic ligand is able to coordinate two univalent anions while only one sulfate dianion can be extracted for each ditopic ligand. The difference in the anion preferences for **L7**-**L9** is a consequence of the varying diimine moiety incorporated into these ligands. Conversely, the difference between the anion preference of **L9** and **L10** is predicated solely on the differing anion-binding motif since they share the same diimine moiety. Therefore, it was found that the use of the dihexylaminomethyl pendant arms resulted in a slight increase in the extraction of Cl^- and SO_4^{2-} anions with a small decrease in the extraction of the NO_3^-. Below is a picture

of the competitive anion extraction experiment using the "copper-only" complex of **L7** (Fig. 4.7) which is shown as a representation of the other "copper-only" complexes.

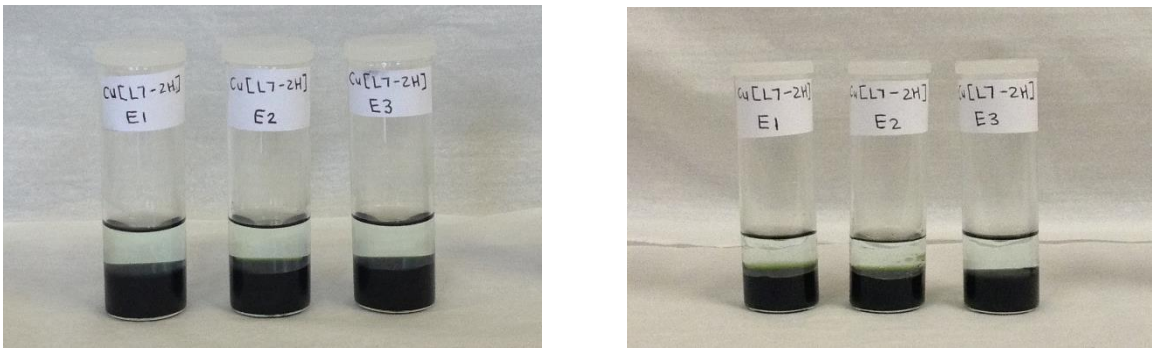

FIGURE 4.7 Competitive anion extraction using the "copper-only" complex of ditopic ligand **L7**. Left: Before shaking; top layer contains aqueous solution of Cl^-, NO_3^- and SO_4^{2-} in 0.01 M concentration with their respective copper salts; bottom layer contains organic solution of 0.01 M concentration of **L7**. Right: After shaking for 24 h.

Galbraith *et al.*[6] investigated the anion extraction capability of salen derivatives possessing additional protonatable sites and hydrogen-bond donors for anion binding. The copper complexes of these ligands were shown to extract HCl and H_2SO_4 into chloroform solutions with a marked selectivity for Cl^- over SO_4^{2-} extraction. The group also performed potentiometric titrations in 95:5 methanol:water which revealed that the copper complexes could bind sulfate more potently than chloride. They finally arrived at the assumption that the extraction selectivity of these compounds tended to be highly dependent on the hydrophobicity of the anions rather than the strength of anion binding. The relative hydrophobicities of a collection of anions is reflected by the Hoffmeister bias (Fig. 4.8).[7]

Strongly hydrated ⟷ Weakly hydrated

$$SO_4^{2-} \sim HPO_4^{2-} > AcO^- > Cl^- > NO_3^- > ClO_4^-$$

FIGURE 4.8 The Hoffmeister bias[7]

The results for the competitive extraction of the anions using the copper complexes described herein, evidently shadows the trend of the Hoffmeister bias with an order of decreasing uptake into the organic phase given by

the series NO_3^- > Cl^- > SO_4^{2-}. These results correlate to similar observations based on the work executed by Forgan and co-workers[8] using similar zwitterionic extractants.

4.2.4. Competitive bulk liquid membrane transport studies involving anions by ditopic ligands (L7-L10)

The competitive transport of anions across a bulk liquid membrane was studied using the "copper-only" complexes of the ditopic ligands. The experimental set-up resembled that used for the transport of metal ions except for the phase compositions. In these experiments the aqueous receiving phase was made up of a KH_2PO_4 buffer solution having a measured pH of 6.50. The source phase consisted of the anions; Cl^-, NO_3^- and SO_4^{2-} each having a concentration of 0.005 M. The organic membrane phase was comprised of a saturated chloroform solution containing the "copper-only" complex (0.005 M).

In each experiment, the temperature was maintained at 25 °C and all three phases were stirred separately at 10 rpm using stirrers coupled to a single mechanical gear. All transport runs were terminated after 24 h and ion chromatography was used to quantify each anion transported over this 24 h period. Table 4.3 provides the experimental measurements which were obtained from the competitive transport experiments which were conducted in duplicate for each of the "copper-only" complexes.

TABLE 4.3 Experimental data for the three anions tested in competitive transport across a bulk chloroform membrane employing copper-only complexes of **L7-L10** at 25 °C. [NO_3^-] = [Cl^-] = [SO_4^{2-}] = 0.005 M in aqueous source phase (pH = 2.09). 'Copper-only' complex = 0.005 M in organic phase. pH of aqueous receiving phase = 6.50.

Compound	Cl^-	NO_3^-	SO_4^{2-}
Cu[L7-2H]			
% (Receiving)[a]	8.4	4.6	3.4
% (Membrane)[b]	21.0	46.5	7.4
Cu[L8-2H]			
% (Receiving)[a]	6.2	3.5	2.7[c]
% (Membrane)[b]	18.5	45.2	8.5
Cu[L9-2H]			
% (Receiving)[a]	5.5	2.7[c]	3.0
% (Membrane)[b]	19.7	44.2	11.6

Cu[L10-2H]			
% (Receiving)[a]	5.6	2.6[c]	3.9
%(Membrane)[b]	20.0	35.6	9.3

[a] Percent of total anions in the receiving phase after 24 h.
[b] Percent of total anions in the membrane phase after 24 h.
[c] Values are possibly within experimental error.

The results show that once again NO_3^- is favourably transported into the organic membrane phase over the other anions, whereas SO_4^{2-} is poorly transported from the aqueous source phase. This trend adheres to the Hoffmeister bias and further complements the competitive anion extraction results. There is no distinct differences in percentage transport between these ditopic ligands. This suggests that using these salen-type ditopic systems to surmount the Hoffmeister bias is unlikely.

Tasker *et al.*[9] investigated the bulk liquid membrane transport using salen ditopic ligands, similar to the ones which were employed in these tests. The group tested the transport of Cl^-, Br^-, NO_3^-, PO_4^{3-} and SO_4^{2-} and noted that the observed transport selectivity obeyed the Hoffmeister bias. Their findings revealed that the halide anions and nitrate were transported most efficiently whereas no transport was observed for sulfate or phosphate.

The employment of traditional lipophilic cationic sites, such as phosphonium, imidazolium, or ammonium centers (protonated or quaternary) rely entirely on a solvation-based selectivity. This inhibits the anion exchange of hydrophilic anions and is controlled by the Hoffmeister bias. For this reason, a novel ligand system, or systems, needs to be constructed which does not rely on this mechanism of anion exchange. Exciting advances have already been demonstrated by Fowler and co-workers[10] offering a simple way to achieve non-Hoffmeister selectivity in liquid-liquid anion exchange by combining a synthetic H-bond-donating (HBD) anion receptor with a standard quaternary ammonium type extractant.

4.2.5. Attempted non-competitive metal extraction studies

Another type of investigation was carried out using monotopic ligands **L1**-**L6**; an extraction study which was not competitive in nature. It entailed contacting an aqueous phase housing a single metal with an organic phase accommodating the ligand of interest. Both the metal ion and ligand in their separate phases were in a 1:1 molar ratio with one another, each having a concentration of 0.01 M. The experiment was executed in such a way so as to ensure that the extraction was performed at about six different pH measurements recorded for the aqueous phase. The purpose of the experiment was to generate S curves (pH isotherms) for each ligand with metal ions it showed some sort of selectivity towards in the competitive extraction tests. The ligands were hence tested with Cu(II) and Pb(II) to generate S curves for these metal ions.

These experiments brought with them a number of issues. Firstly, the pH of the aqueous phase was adjusted by the addition of small drops of concentrated NaOH solution or HNO_3. This was problematic since the volume of the aqueous phase is slightly changed by altering the pH of the aqueous phase to achieve a pH range of one-unit increments. On this note, results from ICP-OES and the colour changes seen to the organic phase were not consistent with the expected pH incremental adjustments. Therefore it was speculated that either the pH reading was incorrect or some drops of NaOH or HNO_3 had adhered to the walls of the cylindrical sample vial and was thus not considered to produce an accurate final pH value. These experiments were ultimately abandoned due to time constraints, however they did assist in verifying certain coordination aspects specifically relating to the extraction of Cu(II) by **L4** and **L5**.

The notion that **L4** and **L5** had higher formation constants with Cu(II) was visualised in these tests by the pronounced colour change of the organic phase over all pH measurements. These colour changes are indicative of the formation of the neutral organic copper complex. With respect to all the ligands tested, the formation of the copper complex with **L4** and **L5** was more favoured even at the lowest pH values recorded. The other ligands showed minor colour changes to the organic phase but tended to get slightly darker with increasing pH. Fig 4.9 depicts these distinct colour changes for **L4** and **L5** in comparison to **L2** which acts as a representation for the other ligands tested.

Before shaking **After shaking**

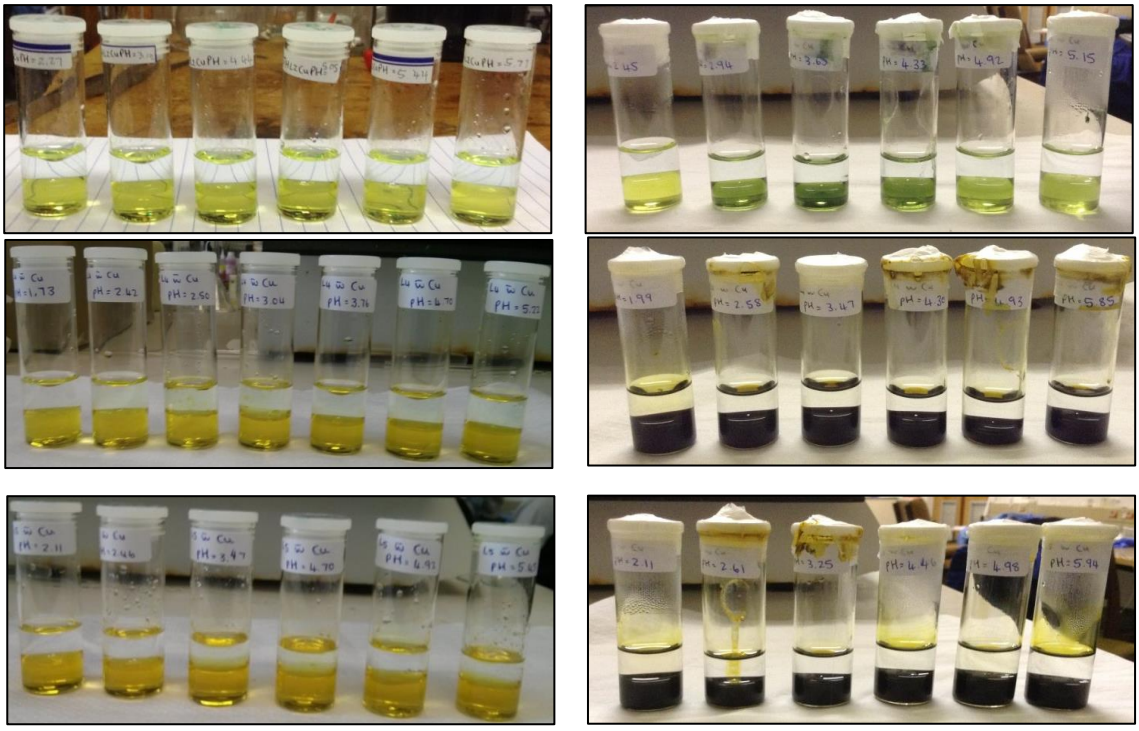

FIGURE 4.9 Top: **L2** pH isotherm experiments with Cu(II) at pH values (left to right) 2.27, 3.13, 4.04, 5.05, 5.44, 5.72. Middle: **L4** pH isotherm experiments with Cu(II) at pH values (left to right) 1.73, 2.42, 2.50, 3.04, 3.74, 4.70. Bottom: **L5** pH isotherm experiments with Cu(II) at pH values (left to right) 2.11, 2.44, 3.47, 4.70, 4.92, 5.45.

4.3. General conclusions

The competitive metal extraction experiments showed that **L1**-**L10** exclusively selected Cu(II) over the other five metal ions which were tested. This was justified by the Irving Williams series, in combination with the Hard-Soft Acid Base principle. For monotopic ligands, **L1**-**L6**, the percentage differences in Cu(II) selection under the experimental conditions employed was a consequence of the unique electronic and structural properties of the diamine linker used to produce these ligands. It was found that the electron-withdrawing diamines producing **L4** and **L5**, respectively resulted in a much higher preference for Cu(II). This observation was further complemented by the preliminary non-competitive metal extraction tests as well as the bulk membrane transport studies performed using these ligands. The metal extraction results for the ditopic ligands showed that as a result of the incorporation of the pendant alkylaminomethyl groups, an increase in the solubility of these extractants results, which in turn, leads to less leaching of these ligands into the aqueous

phase during the extraction procedure. The anion selectivities of the "copper-only" complexes of ditopic ligands **L7-L10** followed the Hoffmeister bias showing selectivity in the order; $SO_4^{2-} < Cl^- < NO_3^-$.

4.4. Methods and Materials

4.4.1. Solvents & reagents

All chemicals were used as received from various chemical-producing companies and used without further purification. The numerous chemicals used in the above experiments were purchased from the following chemical-producing companies; *Scienceworld:* NaOH pellets; *Merck*: methanol, ethanol, conc. H_2SO_4, anhydrous sodium acetate, standard buffer solutions for pH meter calibration (pH = 7.00 and pH = 4.00), molecular sieves (0.400 nm), glacial acetic acid (CH_3COOH), cobalt (II) nitrate hexahydrate, lead (II) nitrate; *Sigma-Aldrich*: copper (II) acetate monohydrate, nickel (II) acetate tetrahydrate, cobalt (II) acetate hexahydrate ($Co(acetate)_2 \cdot 6H_2O$), zinc (II) acetate hexahydrate, cadmium (II) acetate tetrahydrate, lead (II) acetate, copper (II) nitrate trihydrate, nickel (II) nitrate hexahydrate, zinc (II) nitrate hexahydrate, cadmium (II) nitrate tetrahydrate.

4.4.2. Instrumentation

Metal analysis was accomplished using ICP-OES which was performed by CAF (Central Analytical Facility) at Stellenbosch University using a Thermo Scientific iCAP 6000 Series instrument. The pH measurements of aqueous solutions were determined using Corning 425 pH meter and were calibrated using stock buffer solutions having pH measurements of 4.00 and 7.00. Quantification of anions was achieved using Ion chromatography which was performed by the Central Analytical Facility (CAF) at Stellenbosch University using a Waters 432 Conductivity detector, coupled to a Waters 717 plus Auto sampler and an Agilent 1100 series binary pump.

4.4.3. Preparation of solutions

4.4.3.1. Preparation of 0.01 M mixed metal nitrate NaOAc/AcOH buffer solution

NaOAc (16.41 g, 0.200 mol) and glacial AcOH (6.670 g, 0.111 mol) was added to a 1000 mL volumetric flask. Following this, $Cu(NO_3)_2{\cdot}3H_2O$ (2.416 g, 0.100 mol), $Ni(NO_3)_2{\cdot}6H_2O$ (2.908 g, 0.100 mol), $Zn(NO_3)_2{\cdot}6H_2O$ (2.975 g, 0.100 mol), $Co(NO_3)_2{\cdot}6H_2O$ (2.910 g, 0.100 mol), $Cd(NO_3)_2{\cdot}4H_2O$ (3.085 g, 0.100 mol) and $Pb(NO_3)_2$ (3.312 g, 0.100 mol) were transferred to the same volumetric flask which was diluted to 1000 mL with distilled water. The pH reading of the solution was found to be approximately 5.05.

4.4.3.2. Preparation of saturated chloroform solution

In order to prevent leaching of the aqueous phase into the organic phase in these experiments, a saturated chloroform solution was prepared in each instance where necessary. Reagent grade chloroform was transferred into a separation funnel along with a small quantity of distilled water. The two layers were shaken vigorously and the chloroform layer was isolated and used as saturated chloroform solution.

4.4.3.3. Preparation of 0.1 M HNO_3 solution

Approximately 100 mL of reagent-grade HNO_3 solution (1 M) was diluted to 1 L with distilled H_2O in a volumetric flask. The concentration of this solution was confirmed by way of pH measurement which was found to be 1.00.

4.4.3.4. Preparation of 0.01 M mixed anion aqueous solution (anion extraction experiments)

An aqueous solution containing the anions; NO_3^-, SO_4^{2-} and Cl^-, was prepared, each at equimolar concentrations of 0.01 M. This was achieved through the addition of $CuSO_4{\cdot}5H_2O$ (1.248 g, 0.005 mol) as well as $CuCl_2{\cdot}2H_2O$ (0.4262 g, 0.005 mol) and thereafter approximately 50 mL of a stock solution of HNO_3 (0.1 M) was transferred

to a 500 mL volumetric flask, the solution was diluted to 500 mL with distilled water. The pH of the anion solution was measured and found to be approximately 2.02.

4.4.3.5. Preparation of 0.005 M mixed anion aqueous solution (anion transport experiments)

An aqueous solution containing the anions; NO_3^-, SO_4^{2-} and Cl^-, was prepared, each at equimolar concentrations of 0.005 M. This was attained by the addition of $CuSO_4 \cdot 5H_2O$ (0.6242 g, 0.01000 mol) into a 500 mL volumetric flask and diluted to about 250 mL with distilled water. Approximately 25 mL 0.1 M HCl solution (pH = 1.02) was added to the flask along with 25 mL HNO_3 (0.1 M) solution (pH = 1.01). The resulting solution was diluted to the 500 mL mark on the volumetric flask with distilled water. The pH of the final solution was measured and found to be approximately 2.09.

4.4.3.6. Preparation of aqueous receiving phase (anion transport experiments)

An aqueous solution buffered at pH of 6.50 was prepared. NaOH solution (0.100 M, 69.5 mL) was added to a 500 mL volumetric flask. A KH_2PO_4 solution (0.100 M, 250 mL) was further added to this volumetric flask. The resulting solution was diluted to 500 mL with distilled water. The pH was recorded at exactly 6.50.

4.4.3.7. Preparation of ICP samples

ICP sampling was achieved by way of a 10 × dilution, where 1 mL of aqueous phase (containing the analyte) was transferred to an ICP tube and diluted with 9 mL of 0.1 M HNO_3 solution. Prior to submission for analysis, the samples were sealed tightly using parafilm and stored in a refrigerator to prevent evaporation or any side reactions from occurring.

4.4.4. Experimental procedures

4.4.4.1. Competitive metal ion extraction studies

0.01 M solutions of ligands, **L1-L10** were prepared in separate volumetric flasks (25 mL) using saturated chloroform solution. From each of these volumetric flasks, approximately 5 mL of each 0.01 M solution was pipetted into separate sample vials. This process was repeated so that two separate 0.01 M solutions of each ligand (5 mL) were prepared. A NaOAc/AcOH buffer solution having a pH = 5.05 and containing a 0.01 M mixture (5 mL) of Cu(II), Zn(II), Ni(II), Co(II), Pb(II) and Cd(II) metal ions was contacted with each 0.01 M solution of ligand (5 mL). Each sample vial was then sealed using parafilm and shaken on a labcon-oscillating shaker at 220 rpm for 24 h.

4.4.4.2. Non-competitive metal ion extraction studies

0.01 M solutions of ligands, **L1-L6** were prepared in separate volumetric flasks (25 mL) using saturated chloroform solution. From each of these volumetric flasks, approximately 5 mL of each 0.01 M solution was pipetted into separate sample vials. This process was repeated so that 6-7 separate 0.01 M solutions of each ligand (5 mL) were prepared. A NaOAc/AcOH buffer solution having a pH = 5.05 and containing a 0.01 M mixture (5 mL) of Cu(II), Zn(II), Ni(II), Co(II), Pb(II) and Cd(II) metal ions was contacted with each 0.01 M solution of ligand (5 mL). The pH of the aqueous phase was adjusted by the addition of small drops of either concentrated NaOH or HNO_3 so as to attain six different pH values for the aqueous phases. Each vial was then sealed and shaken on a labcon-oscillating shaker at 220 rpm for 24 h.

4.4.4.3. Competitive metal ion bulk liquid membrane transport studies

0.01 M solutions of ligands, **L1-L10** were prepared in separate volumetric flasks (100 mL) using saturated chloroform solution. From each of these volumetric flasks, approximately 50 mL of each 0.01 M solution was pipetted into the bottom of the concentric cell. This process was repeated so that two separate 0.01 M solutions (50 mL) of each ligand were present at the bottom of two separate cells to ensure the experiment was done in

duplicate for each ligand. A NaOAc/AcOH buffer solution having a pH = 5.05 and containing a 0.01 M mixture (10 mL) of Cu(II), Zn(II), Ni(II), Co(II), Pb(II) and Cd(II) as their respective nitrate salts was pipetted into the middle cylindrical compartment of the cell (aqueous source phase) so that it was in contact with the membrane phase. Finally, the receiving phase, 0.1 M HNO_3 solution (30 mL) was pipetted into the space surrounding the middle compartment of the concentric cell to ensure it was only in contact with the membrane phase and not the aqueous source phase. The transport apparatus was turned on and slow stirring commenced for 24 h at 10 rpm. Thereafter, 1 mL of the aqueous source phase and aqueous receiving phase was removed and samples were prepared for ICP-OES analysis.

4.4.4.4. Competitive anion extraction studies

0.01 M solutions of the "copper-only" complexes of **L7-L10** were prepared in separate volumetric flasks (25 mL) using saturated chloroform solution. From each of these volumetric flasks, approximately 5 mL of each 0.01 M solution was pipetted into separate sample vials. This process was repeated so that two separate 0.01 M solutions of each "copper-only" complex (5 mL) was prepared. An aqueous solution containing the anions Cl^-, NO_3^- and SO_4^{2-} with a pH of 2.02 was contacted with each 0.01 M solution of the complex (5 mL). Each sample vial was then sealed using parafilm and shaken on a labcon-oscillating shaker at 220 rpm for 24 h.

4.4.4.5. Competitive anion transport studies

0.005 M solutions of the "copper-only" complexes of **L7-L10**, were prepared in separate volumetric flasks (100 mL) using saturated chloroform solution. From each of these volumetric flasks, approximately 50 mL of each 0.005 M solution was pipetted into the side of the concentric cell so that the organic membrane phase resided at the bottom of it. An aqueous solution (10 mL) containing the anions Cl^-, NO_3^- and SO_4^{2-} each at a concentration of 0.005 M with a pH of 2.09, was contacted with each 0.005 M solution of the "copper-only" complexes by being transferred in the middle compartment of the concentric cell. Thereafter, a receiving phase (30 mL) was contacted with the organic membrane phase by pipetting on the sides of the concentric cell in

order to achieve a system in which all three phases were separated from one another. The transport apparatus was turned on and slow stirring commenced for 24 h at 10 rpm.

4.5. References

1. Ritcey, G. M. *Tsinghua Sci. Technol.* **2006**, *11* (2), 137–152.

2. Kislik, V. S. *Solvent Extraction: Classical and Novel Approaches*; Elsevier, 2011.

3. Turkington, J. R.; Bailey, P. J.; Love, J. B.; Wilson, A M.; Tasker, P. A. *Chem. Commun. (Camb).* **2013**, *49* (19), 1891–1899.

4. Shim, S. L.; Yoon, I.; Park, K. M.; Jong, H. J.; Lindoy, L. F.; Nezhadali, A.; Rounaghi, G. *J. Chem. Soc. Dalt. Trans.* **2002**, *3050* (10), 2180–2184.

5. Dong, W. K.; Sun, Y. X.; Zhang, Y. P.; Li, L.; He, X. N.; Tang, X. L. *Inorganica Chim. Acta.* **2009**, *362* (1), 117–124.

6. Galbraith, S. G.; Wang, Q.; Li, L.; Blake, A.; Wilson, C.; Collinson, S. R.; Lindoy, L. F.; Plieger, P. G.; Schroeder, M.; Tasker, P. A. *Chem. - A Eur. J.* **2007**, *13* (21), 6090–6107.

7. Zhang, Y.; Cremer, P. S. *Annu. Rev. Phys. Chem.* **2010**, *61*, 63–83.

8. Forgan, R. S.; Davidson, J. E.; Fabbiani, F. P. a; Galbraith, S. G.; Henderson, D. K.; Moggach, S. A.; Parsons, S.; Tasker, P. A.; White, F. J. *Dalton Trans.* **2010**, *39* (7), 1763–1770.

9. Tasker, P. A.; Tong, C. C.; Westra, A. N. *Coord. Chem. Rev.* **2007**, *251* (13–14 SPEC. ISS.), 1868–1877.

10. Fowler, C. J.; Haverlock, T. J.; Moyer, B. A.; Shriver, J. A.; Gross, D. E.; Marquez, M.; Sessler, J. L.; Hossain, M. A.; Bowman-James, K. *J. Am. Chem. Soc.* **2008**, *130* (44), 14386–14387.

CHAPTER 5: CHAPTER SUMMARIES, CONCLUDING REMARKS & FUTURE WORK

5.1. Chapter summaries & concluding remarks

Chapter 1 provided relevant background information central to this research project beginning with the broad topic of extractive metallurgy and filtering it down within hydrometallurgy to metal solvent extraction and finally steering it towards the importance of generating stable metal complexes to extract metal ions from aqueous streams. Moreover, an introduction was given on new work executed in the field, particularly the formulation of a zwitterionic molecule capable of extracting both a metal cation and its associated anion.

Chapter 2 communicated the characterisation data of the monotopic ligand precursor, 5-tertbutyl-2-hydroxybenzaldehyde and monotopic ligands **L1**-**L6**. The precursor aldehyde was synthesised and through FT-IR (ATR) spectroscopy, ^{1}H and ^{13}C NMR spectroscopy, it was established that the product was of sufficient purity to be used in the Schiff base reaction yielding **L1**-**L6**. These ligands were then fully characterised using FT-IR (ATR), ^{1}H and ^{13}C NMR spectroscopy, melting temperature determination, mass spectrometry, elemental analysis and in the instances of free ligands **L1**-**L4** and **L6**, by SCD analysis. Two crystal complexes were successfully grown and were suitable for SCD analysis, these were **Ni[L4-2H]** and **Cu[L6-2H]**.

Chapter 3 elaborated on the synthesis and characterisation of intermediates towards producing ditopic ligands **L7**-**L10**. All intermediates, **A1**-**A3** and **B1**-**B3**, were in the end, successfully produced and the final Schiff base reaction resulted in potential zwitterionic extractants which were fully characterised using a broad range of characterisation methods. These included; FT-IR (ATR) spectroscopy, ^{1}H and ^{13}C NMR spectroscopy, melting point determination (for **L7** and **L9**), ESI-MS and micro-elemental analysis. In addition, the "copper-only" complexes of **L7**-**L10** were successfully prepared and characterised using FT-IR (ATR) spectroscopy. Lastly, the proposed ligands **L11** and **L12** were not effectively isolated and were not assessed in the solvent extraction tests.

Chapter 4 explained details relating to the solvent extraction tests performed on **L1**-**L10** as well as the "copper-only" complexes of **L7**-**L10**. In the competitive metal ion extraction experiments, all ligands displayed an

exceptional selectivity towards Cu(II) over the other metal ions. There was a slight increase in the uptake of Cu(II) by the ditopic ligands in comparison to the corresponding monotopic ligands and was justified by the incorporation of the dialkylaminomethyl groups which promoted their solubility in the organic phase. In the competitive bulk liquid membrane transport studies, all ligands continued their preference for Cu(II) ions. The cation flux rates ($molh^{-1}$) for Cu(II) under the experimental conditions employed, was low despite being transported effectively into the organic membrane phase. This implied a high formation constant for Cu(II). Ditopic ligands showed a surprising potential for the transport of Zn(II) under the experimental conditions employed. In addition, the ditopic ligands presented herein show potential to effectively separate Cu(II) ions from Zn(II) ions, this may be achieved by way of either competitive extraction to isolate Cu(II) into an organic phase or by competitive bulk membrane transport where Zn(II) is separated into a separate aqueous receiving phase.

Finally, "copper-only" complexes of ditopic ligands **L7**-**L10** were subjected to competitive anion extraction and bulk liquid membrane transport tests with the anions Cl^-, NO_3^- and SO_4^-. In both tests, the ligands showed selectivity in the increasing order of $SO_4^{2-} < Cl^- < NO_3^-$, which follows the Hoffmeister bias.

5.2. Suggestions for future work

Taking into consideration what has been observed in this research, there are numerous findings which warrant further investigation. In the context of competitive metal extraction studies, it would be insightful to perform a competitive extraction test in the absence of copper under the same conditions to identify which metal species the particular ligand would prefer second or possibly third. A similar test would be to vary the particular ligand concentration in various increments above its usual 0.01 M in order to render it in excess once all copper is extracted to identify its metal ion preference. Another revealing examination would be a time-dependent study for the competitive extraction experiments. This could reveal the time required to reach equilibrium in these tests. Furthermore, additional experiments could be conducted in which the liquid-liquid interface surface area is varied to determine its influence in extraction values. A larger library of monotopic ligands should be

generated with incremental alterations to the diamine moiety in order to put a finger on the electronic factors at play in this sequestering process.

The solubility of these extractants is another important characteristic which should be investigated, emphasis should be placed on determining the extent of solubility of these ligands in the chosen organic solvent used in the extraction tests. This may be achieved by dissolving a ligand of interest in the organic phase producing a fixed concentration for each and bringing it into contact with a solution of distilled water. The layers can be shaken for certain lengths of time. Thereafter, the water and organic layer can be isolated and the masses of ligand in each phase can be determined, this will provide a good idea as to the extent of solubility of these ligands in the organic solvent. Another crucial aspect which should be known for ligands to be successful for industrial application as extractants is the imine functionality and its sensitivity to hydrolysis at elevated temperatures and low pH values. Of course, if an extractant is more susceptible to hydrolysis it would not be suitable or applicable for industrial application, as at the low pH measurements required for leaching, the extractant would simply hydrolyse to the respective reagents from which it was derived.

Further investigation into the interaction of Zn(II) with these ditopic ligands would be interesting in order to rationalise its high transport into the receiving phase.